



**COMOTI**  
ROMANIAN RESEARCH &  
DEVELOPMENT INSTITUTE FOR  
GAS TURBINES



NATIONAL UNIVERSITY OF SCIENCE AND TECHNOLOGY  
POLITEHNICA BUCHAREST

Doctoral School of Aerospace Engineering

Engineering Sciences, Aerospace Engineering

## SUMMARY

**Research on reducing noise produced by gas turbine engines  
by modifying the blades in the leading edge and/or trailing  
edge area**

PhD Candidate: **Eng. Andrei-George TOTU**

PhD Supervisor: **Prof. dr. eng. Daniel-Eugeniu CRUNȚEANU**

Bucharest, 2026

## TABLE OF CONTENTS

<b>ABSTRACT .....</b>	<b>4</b>
<b>CHAPTER 1. INTRODUCTION .....</b>	<b>4</b>
<b>CHAPTER 2. NOISE GENERATION MECHANISMS IN ISOLATED BLADE CONFIGURATION OR CASCADES WITH APPLICATION TO AIRCRAFT TURBOMACHINERY ENGINES. INTEGRATION OF SERRATED-BLADE SOLUTIONS FOR NOISE REDUCTION .....</b>	<b>5</b>
2.1. Motivation and objectives.....	5
2.2. The mechanism of noise generation.....	7
2.3. Serrations as a passive constructive solution applied to blades.....	9
2.4. Aspects regarding the performance estimation and measurement.....	11
<b>CHAPTER 3. ASPECTS REGARDING THE MODELING OF BLADE NOISE AND NOISE REDUCTION SOLUTIONS IDENTIFIED IN THE LITERATURE .....</b>	<b>12</b>
3.1. Methods and Computational Models for Serrated Blades (Interaction Noise) ..	12
3.2. Aerodynamic implications.....	17
3.3. Configurations of interest identified in the literature.....	17
<b>CHAPTER 4. CORRELATION OF THE PARAMETERS DEFINING TURBULENCE WITH SERRATIONS. PRELIMINARY TESTS .....</b>	<b>18</b>
4.1. Correlation parameter between serrations and turbulence .....	18
4.2. Preliminary tests .....	19
<b>CHAPTER 5. PROCESSING OF EXPERIMENTAL DATA AND COMPARISON BETWEEN THEORY AND EXPERIMENT.....</b>	<b>21</b>
5.1. Introduction.....	21
5.2. Numerical and Experimental Analysis Methodology.....	23
5.3. Results.....	23
<b>CHAPTER 6. EXPERIMENTAL ANALYSIS OF INTERACTION NOISE FOR A TURBULENT JET–AIRFOILS WITH LEADING-EDGE SERRATIONS IN A 4-BLADE CASCADE CONFIGURATION.....</b>	<b>26</b>
6.1. Description of the Test Configuration.....	26
6.2. Experimental results.....	30
6.3. Serrations impact .....	34
6.4. Serrations Effects on the Radiated Acoustic Energy .....	36

<b>CHAPTER 7. DERIVATION OF SEMI-EMPIRICAL RELATIONS AND SIMULATION OF THE ACOUSTIC PERFORMANCE OF LEADING EDGE SERRATED CASCADES .....</b>	<b>37</b>
7.1. Derivation of semi-empirical laws.....	37
7.2. Leading edges serrated blades simulation in cascade configuration .....	42
7.3. Pressure fluctuations coherence (“spanwise coherence”) for the serrated leading-edge configuration. Unsteady statistics.....	46
7.4. Further development of the directivity analysis.....	49
<b>CHAPTER 8. CONCLUSIONS.....</b>	<b>50</b>
8.1. General conclusions .....	50
8.2. Thesis novelty.....	51
8.3. Personal contributions.....	51
8.4. Future perspectives.....	52
<b>PUBLICATIONS AND PROJECTS .....</b>	<b>53</b>
<b>REFERENCES.....</b>	<b>53</b>

## ABSTRACT

The present work addresses the problem of noise reduction generated by turbomachinery blades, with particular emphasis on passive solutions based on serrations and on the complex interaction between aerodynamic and acoustic phenomena. In the current context of increasingly stringent regulations regarding the acoustic impact of propulsion and energy conversion systems, understanding noise generation mechanisms and developing efficient, robust, and easily integrable solutions represent a research direction of major interest. Although aerodynamic noise associated with blades has been extensively investigated in the specialized literature, most existing analyses focus either on idealized or simplified configurations, or on experiments conducted at various scales, which do not fully capture the complexity of the interaction between turbulent flow and the actual blade geometry. In this context, the thesis aims to contribute to the advancement of knowledge through an integrated experimental and numerical approach, applied also to blades arranged in cascades, a configuration that has received relatively limited attention to date despite its practical relevance. The research was structured in a gradual manner, starting with a detailed analysis of the current state of the art in the field of aerodynamic noise and serration-based solutions, followed by the identification of optimization directions and the development of a dedicated experimental facility. This approach enabled a controlled investigation of the interaction between the flow (turbulent jet) and the blades, as well as the evaluation of acoustic performance and aerodynamic aspects for various geometric configurations. A central aspect of the study is the analysis of serrated blades both in isolated airfoil configurations and in cascades, highlighting specific features that contribute to broadening the existing knowledge base in a relatively niche research topic. Based on the experimental results and the numerical post-processing performed, relevant correlations were identified between the geometric parameters of the serrations, the characteristics of the incident turbulence, and the global acoustic pressure levels. These observations led to the formulation of experimental laws and semi-empirical relationships capable of describing the main trends in noise reduction, providing a useful framework for the preliminary assessment and design of innovative solutions. Furthermore, the development of dedicated numerical tools for the processing and representation of global parameters enabled a coherent and reproducible analysis of the data, contributing to the consolidation of a methodology applicable both in research activities and in educational and engineering contexts.

## CHAPTER 1. INTRODUCTION

The reduction of noise generated by aerodynamic systems represents one of the major challenges of modern engineering, particularly in fields such as aeronautics, turbomachinery, and energy conversion using systems that incorporate aerodynamically profiled bladed elements. The growth of air traffic, the expansion of wind turbine deployment, and the continuous development of ventilation systems as well as propulsion systems (in general) have led to sustained concern regarding the limitation of acoustic impact on the environment and on quality of life. In this context, aerodynamic noise is no longer regarded merely as an inevitable side effect, but rather as a performance criterion that must be addressed from the earliest stages of design. The phenomenon of noise generation in the case of blades (or aerodynamically profiled elements placed in a flow) is closely linked to the structure of the flow (the presence of turbulent formations) and to the manner in which it interacts with solid surfaces. This interaction leads to pressure fluctuations distributed in space and time, which propagate in the form of acoustic waves. Although the fundamental mechanisms are known and theoretically described, the complexity of the phenomenon increases significantly under real operating conditions, where blade geometry, three-dimensional effects, and the presence of other components influence both the aerodynamic behavior and the acoustic response.

The specialized literature reflects a sustained interest in passive noise reduction solutions, due to their constructive simplicity and reduced impact on overall performance (at least in theory). Among these, serrations (generally defined as local geometric modifications in the form of cut-outs of various shapes) applied to blade edges (leading or trailing edge) have proven effective in numerous studies, being inspired both by biological observations and by theoretical and experimental analyses. However, most of the reported results are based on experiments conducted at reduced scale, on isolated blades or in simplified configurations, which limits the generalization of conclusions and their direct applicability to real systems. An insufficiently explored aspect concerns the acoustic behavior of blades with modified geometry integrated into a cascade, where blade-to-blade interaction introduces additional mechanisms of noise generation and modification (notably destructive interference effects). Under these conditions, solutions validated for isolated blades may not lead to the same benefits, and certain effects may even become dominant. This gap in the specialized literature constituted one of the main motivations of the present thesis.

The present work aims to address this issue through a coherent research effort that combines literature analysis, experimental development, and numerical modeling. Through the design and realization of a dedicated experimental setup, various blade configurations were investigated, with emphasis on the evaluation of acoustic and aerodynamic performance under controlled conditions. The conducted studies allowed not only the validation of existing solutions, but also the identification of behaviors specific to blades arranged in a cascade, contributing to a deeper understanding of the phenomena involved. In addition, the definition of experimental (semi-empirical) relationships based on the obtained data sought to provide a useful tool for the rapid evaluation of such solutions. The development of codes (computational algorithms) for the processing and representation of relevant global parameters complements this approach, facilitating the integrated analysis of the results and opening perspectives for further applications in research, education, and applied engineering.

## **CHAPTER 2. NOISE GENERATION MECHANISMS IN ISOLATED BLADE CONFIGURATION OR CASCADES WITH APPLICATION TO AIRCRAFT TURBOMACHINERY ENGINES. INTEGRATION OF SERRATED-BLADE SOLUTIONS FOR NOISE REDUCTION**

### **2.1. Motivation and objectives**

As cities become increasingly congested, aircraft noise has become a highly topical issue, given that airports are no longer isolated. Among the main noise sources of an aircraft, the propulsion system makes a significant contribution, particularly as a result of the development of turbofan engines with very high bypass ratios, intended to reduce specific fuel consumption. Under these conditions, the secondary flow, which conveys a large mass flow rate of air, becomes one of the dominant noise sources. Azimi [1] highlights the correlation between the relative contribution of noise sources and the adopted technological solution: for engines with a low bypass ratio, fan noise is comparable to jet noise, whereas for high bypass ratios, the fan becomes the main source of acoustic radiation, characterized by a dominant frequency associated with the angular velocity, the Blade Passing Frequency (BPF) [2]. Chaytania [2] shows that the frequency range of interest for noise reduction lies between 0.5 and 3 BPF, corresponding to the main operating regimes of the engine. The main noise sources of turbofan engines are presented in Figure 1.

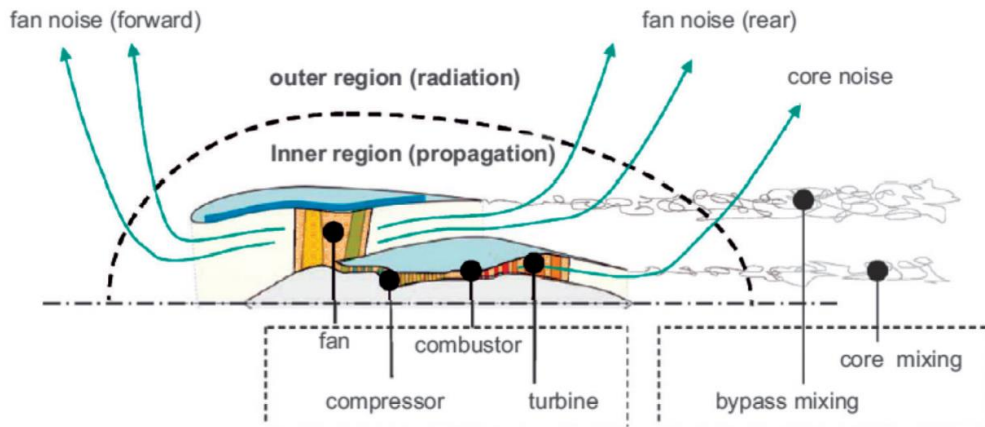


Figure 1. Identification of noise sources for bypass gas turbine engine [1]

The relative contribution of noise sources (when considering the bypass gas turbine engine as an assembly composed of multiple components) is not the same throughout all phases of aircraft operation. Specialized literature indicates that the noise produced by the fan during the takeoff phase is at a level comparable to the noise generated by the jet. During the approach and landing phase (“approach”), the predominant noise component produced by the propulsion system is generated by the fan (Figure 2).

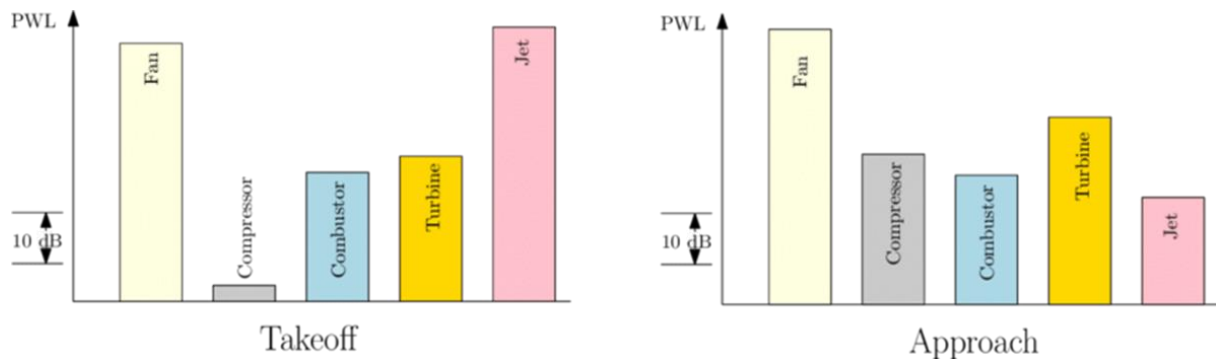


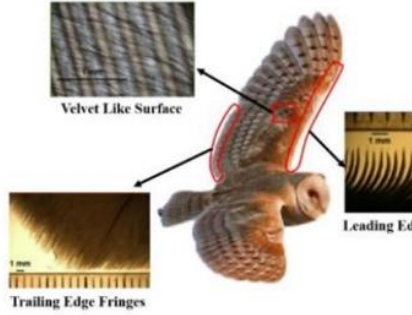
Figure 2. Contribution to noise generation of the various components for a modern bypass engine [2]

The motivation of the study is further supported by European directives on noise emissions, which aim to ensure an improved living environment. At the level of the European Union, these directives are also transposed into national legislation, an example being Directive 2002/49/EC on the assessment and management of environmental noise, similar to Law No. 121 of 3 July 2019 [RO]. Other relevant regulations address the limitation of aircraft noise and operational restrictions in areas adjacent to airports, such as Regulation No. 216/2008, Regulation No. 748/2012, Regulation No. 598/2014, or Directive 2006/93/EC.

Within the HORIZON 2020 programme, the noise issue was identified as a priority direction, leading to the development of applied projects focused on reducing the acoustic impact of aviation. Relevant examples include the ANIMA, ARTEM, or RUMBLE projects, which target the identification of new solutions, the optimization of existing ones, and the definition of procedures for limiting aircraft noise.

The modification of the leading edge or trailing edge for the reduction of rotor–stator interaction noise represents a relatively recent solution, still only sparsely addressed in the specialized literature. These solutions are inspired by adaptations observed in nature, such as the feather structure of owls enabling silent flight [3] or the protuberances on the flippers of certain whale species [4], illustrated in Figure 3. The effective integration of these bio-inspired concepts into aero-engine designs can contribute significantly to reducing the acoustic impact of aviation. The present thesis focuses on the use of serrated blades for reducing rotor–stator interaction noise, as well as blade self-

noise, through the identification of the physical mechanisms involved and the optimization directions that enable solution scalability. Previous studies have reported noise level reductions of approximately 6–7 dB for serrations applied at the leading edge [5] [6] [7] and of 1–3 dB for trailing-edge serrations [8] [9], while combining the two solutions could lead to additional reductions in the overall sound pressure level, as illustrated in Figure 4.



(a) owls adaptation [3]

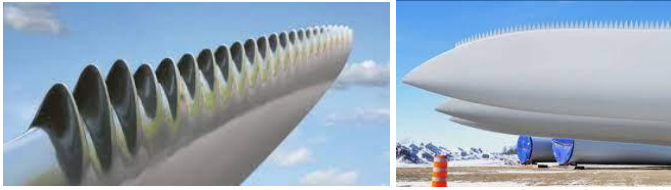


(b) humpback whales adaptation [4]

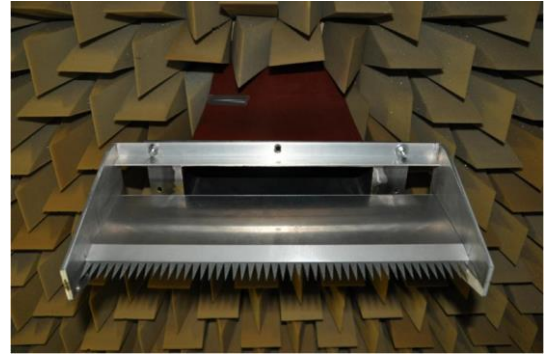
Figure 3. Solutions for improving aerodynamic and acoustic performance found in nature



(a) modified leading edge [6]



(b) wind turbine leading/trailing edge [10] [11]



(c) flat plate serrated trailing edge [7]

Figure 4. Solutions for improving aerodynamic and acoustic performance encountered in engineering

## 2.2. The mechanism of noise generation

As noted by Chaitanya [12], airfoils placed in a turbulent flow constitute efficient sources of noise generation, by converting turbulent rotational motion into acoustic emission, predominantly in the trailing-edge region. Lyu [5] and Brooks [13] show that the noise of an aerodynamic profile can be divided into self-noise and interaction noise with the turbulence of the incident flow, the sources of self-noise being associated with fluid–surface interaction and separations in the trailing-edge region, as illustrated in Figure 5 [13] [14]. The mechanisms of blade noise generation have been studied since the 1950s, through fundamental contributions by Powell, Ffowcs Williams, Hall, Chase, Paterson, Howe, and Brooks, which form the basis of the aeroacoustic theories used today.

Aerodynamic noise occurs when a non-uniform and unsteady flow interact with the solid surface of an aerodynamic profile, a phenomenon known as aerofoil–gust interaction (AGI) [15]. This type of noise is frequently encountered in aerospace applications such as rotor blades, turbofan engines, high-lift devices, helicopter blades, or wind turbines, where the flow turbulence is imposed by the wind and has a difficult-to-predict character [15] [16]. The acoustic pressure field for a two-dimensional aerodynamic profile placed in a turbulent flow is shown in Figure 6, highlighting dipole-



type acoustic source behavior, in agreement with the classical theories developed during the 1950s–1970s.

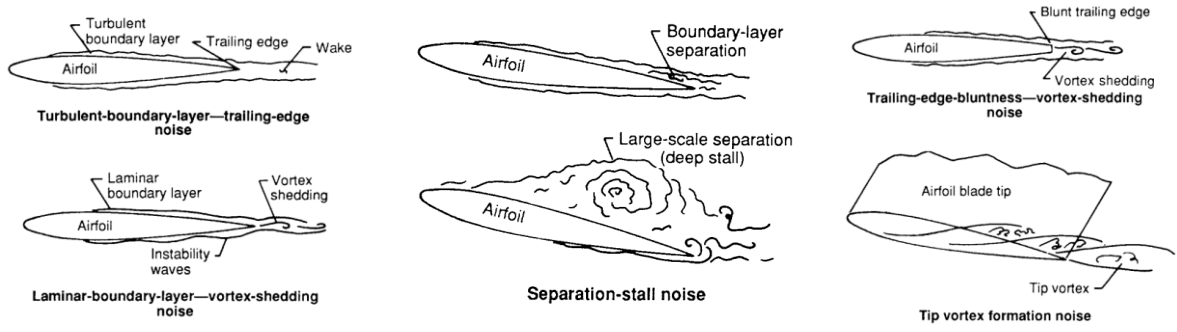


Figure 5. Flow over an airfoil that led to the generation of self-noise [13]

Lyu [5] shows that fluid–blade interaction noise, characteristic of wind turbines, is of high level, exhibiting large amplitudes at low frequencies as well as broadband components, and can be generally assimilated to AGI-type noise. A relevant example is the interaction of the wake originating from the fan of a turbofan engine with the blades of the downstream stages, which generates noise specific to the leading edge.

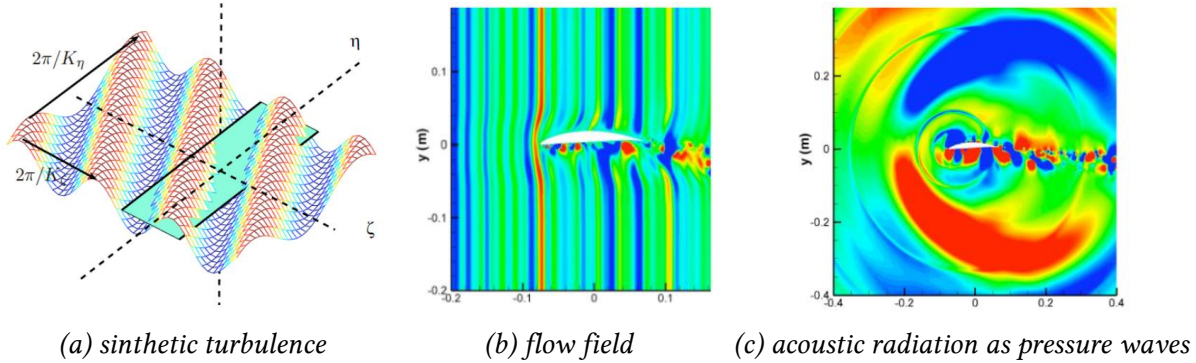


Figure 6. Velocity and pressure fields resulting from the action of a turbulent flow [17]

In the case of open-rotor configurations with counter-rotating propellers, the interactions between stages lead to significant broadband acoustic emissions, which are responsible for a large fraction of the noise generated by these propulsion systems [5]. As illustrated in Figure 7, the interpenetration of flow structures originating downstream of the two stages generates a pressure field with high fluctuations, influencing the propagation front of the acoustic waves. The application of serrations on the trailing edge can promote a more efficient diffusion of pressure fluctuations, leading to a reduction of far-field noise levels.

Trailing-edge noise is an aerodynamic noise resulting from the scattering of pressure fluctuations on a solid surface and represents a major noise source, characterized by both high-amplitude tonal components and broadband noise. This type of noise is encountered in wings, propellers, fans, compressors, and axial turbines, as well as in wind turbines [16].

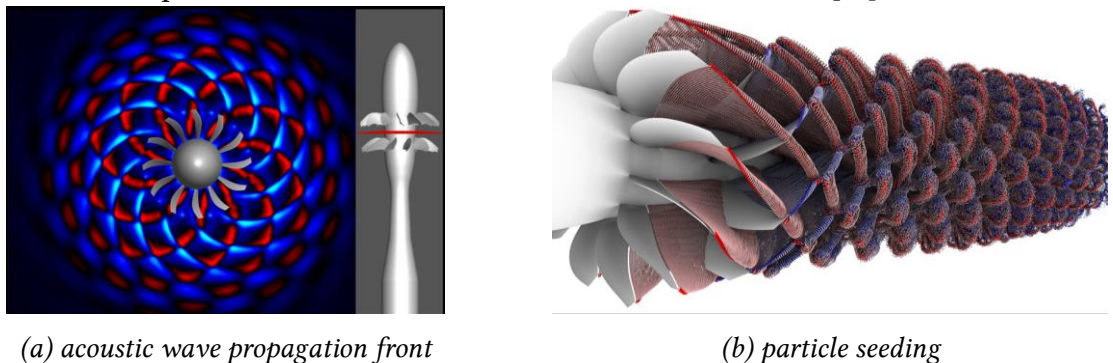


Figure 7. Interaction between the stages of the open-rotor configuration [18]



### 2.3. Serrations as a passive constructive solution applied to blades

Serrations are tooth-like structures integrated into the geometry of a flat plate or an aerodynamically profiled blade (airfoil), defined by a variation law in the spanwise direction, amplitude, and pitch. In the specialized literature, these geometric elements are denoted differently depending on the adopted approach, with the amplitude expressed, for example, by  $h$  or  $A$ , and the pitch by  $p$  or  $\lambda$ , as illustrated in Figure 8. Based on these quantities, dimensionless parameters are defined and used to describe the aerodynamic and acoustic behavior, with the nondimensionalization frequently including the chord, the span, or parameters of the incident turbulence.

The application of serrations represents a passive noise-reduction solution that does not require additional actuation systems; however, its efficiency is limited to certain operating conditions, being dependent on the flow regime and on the characteristics of the turbulent incoming flow. For this reason, geometric optimization is essential in order to achieve benefits over as wide a range of operating conditions as possible. Experimental and theoretical studies have shown that the application of serrations in the leading edge region, inspired by the structure of whale flippers, can lead to improvements in aerodynamic performance, especially at high angles of attack [4] [5] [19]. Ito [20] demonstrates experimentally, through smoke visualizations, that the presence of sawtooth-type serrations leads to an improvement of the flow field for an airfoil tested at low Reynolds numbers. From an acoustic standpoint, correlating the serration parameters with those of the incident turbulence can result in significant reductions of the noise level within frequency bands of interest for the designer [5] [12] [21].

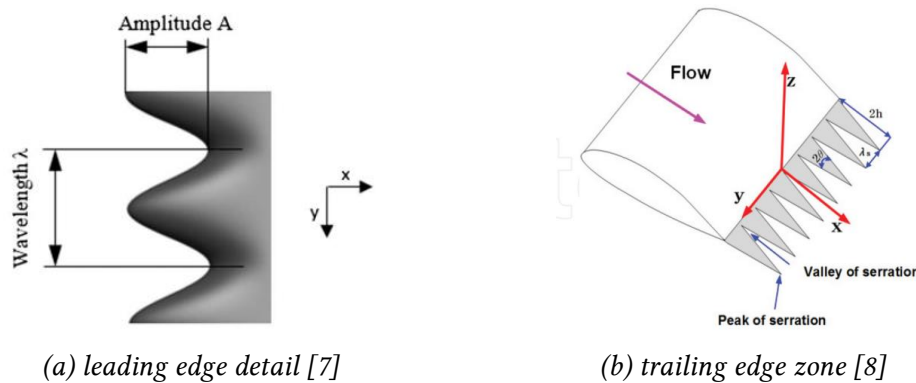
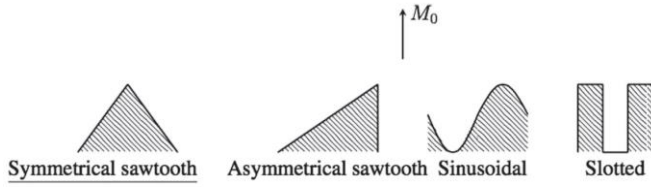


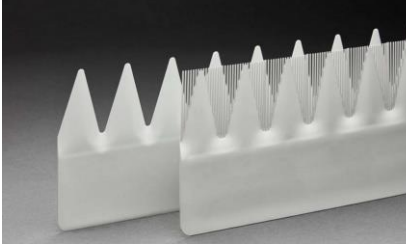
Figure 8. Geometric parameters defining the serration

The idea of adapting solutions observed in nature is not easy to implement. Research efforts (ranging from theoretical to experimental studies) initially focused on simple solutions that are easy to model and to integrate into the complex equations associated with the studied phenomenon. In this regard, there is an extensive body of experimental work conducted on passive solutions in the form of symmetric sawtooth trailing-edge serrations [6] [14] [22]. Other configurations that have begun to be investigated include asymmetric sawtooth serrations, sinusoidal serrations, cut-outs (“slots”), etc. Howe’s theory [23], which laid the foundation for this noise-reduction approach using serrations, is rather limited in the sense that difficulties arise when evaluating the integral relations if complex shapes are employed. Nevertheless, several works have been identified that aim to overcome these limitations of the classical models (Howe [23], Amiet [24] [25] [26], Curle [27], or Lighthill [28]).

Figure 9 highlights several 2D and 3D trailing-edge serration solutions integrated into flat plates or airfoils. It can be observed that, compared to the original theory, researchers have introduced variations in shape or even proposed entirely new geometries. In such cases, only experiments (also mostly at reduced scale) are able to capture the behavior of these solutions. Some researchers preferred to apply or add a serrated portion at the trailing edge [22] [29] [30], even though this slightly modifies the airfoil chord, while other authors chose to design airfoils that fully incorporate three-dimensional serrations [31].



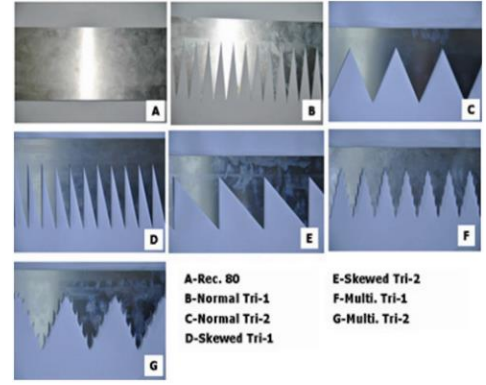
(a) general 2D shapes [16]



(c) sinusoidal serrations (3D) [31]



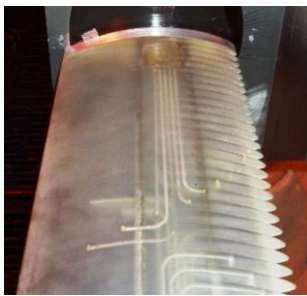
(d) triangular serrations („slots”) [6]



(b) various triangular shapes for serrations [8]

Figure 9. Trailing edge triangular serrations shapes

Ryi [8] experimentally shows that the frequency of the vortex shedding phenomenon generated by serrations on wind turbine airfoils depends strongly on their geometric parameters, with the most pronounced variations being observed along the spanwise direction. Gruber [6] extends regular solutions by using serrations defined by random functions, with normally distributed amplitudes, allowing correlation between the chord of the original airfoil and the mean chord of the modified solution. Trailing-edge serrations are easier to manufacture and have been frequently studied on flat plates or thin airfoils, whereas for three-dimensional serrations applied at the leading edge, an experimental intensification of acoustic sources has been observed in regions of minimum amplitude [12]. Chaytania [2] highlights that the noise of an airfoil in a turbulent flow is dominated by the leading-edge contribution at low frequencies and by the trailing-edge contribution at high frequencies, and that the use of a flat plate can lead to an overestimation of noise reductions compared to the case of a real airfoil. To increase the effectiveness of leading-edge serrations, advanced geometries are proposed (Figure 10), such as the superposition of multiple sinusoidal frequencies, truncated triangular serrations, or the introduction of channels in regions of maximum acoustic source intensity [12].



(a) low amplitude LE serrations [6]



(b) high amplitude le serrations [21]



(c) 3D printing modular serrated LE edge [7]



(d) full blade serrations [19]

Figure 10. Various leading edge serrations

## 2.4. Aspects regarding the performance estimation and measurement

Chaitanya et al. [21] show that the analysis of serration effectiveness must include the identification of the noise-reduction mechanism, the sensitivity to geometric and turbulence parameters, the transition from two-dimensional geometries to real three-dimensional airfoils, and the separation of effects on self-noise and interaction noise. Most experimental studies are based on sinusoidal serrations applied at the leading edge, with the analysis of interaction noise being founded on the classical theories developed by Sears, Amiet, and Howe [5] [9] [13] [23] [24] [25] [26] [32] [33]. Analytical models, such as those of Howe or Amiet, rely on simplifying assumptions (two-dimensional flow, frozen turbulence, infinite span), which limits their range of applicability and may lead to an overestimation of noise reduction [6] [34].

The literature reports the development of theoretical and semi-empirical models for flat plates and serrated airfoils, such as those proposed by Lyu [5] [9], Brooks [13], Biedermann [7], Chaitanya [2], and Ryi [8], which explicitly include serration and turbulence parameters but remain valid only under specific flow conditions. Models dedicated to AGI-type noise, such as RDT (Goldstein) [15], were experimentally compared by Tian [10], highlighting differences between theoretical predictions and measured spectra. In general, analytical models provide a detailed description of the physical mechanisms, while empirical models are more robust experimentally but limited in their domain of applicability [6] [34].

Experimental results indicate that three-dimensional effects are significant, with the boundary layer in the trailing-edge region being more energetic than in the case of a flat plate [21]. Liu [35] and Leon [22] experimentally demonstrate that trailing-edge serrations modify the wake structure and reduce the intensity of turbulent formations, without significantly altering the overall aerodynamic behavior. Despite the progress achieved, there is still no complete model that fully describes the phenomenon, which is why current approaches combine simplified analytical models, numerical simulations, and experimental validation [5]. Reproducing interaction noise specific to turbomachinery requires the use of artificially generated turbulence by means of grids, the structure of the resulting flow field being illustrated in Figure 11.

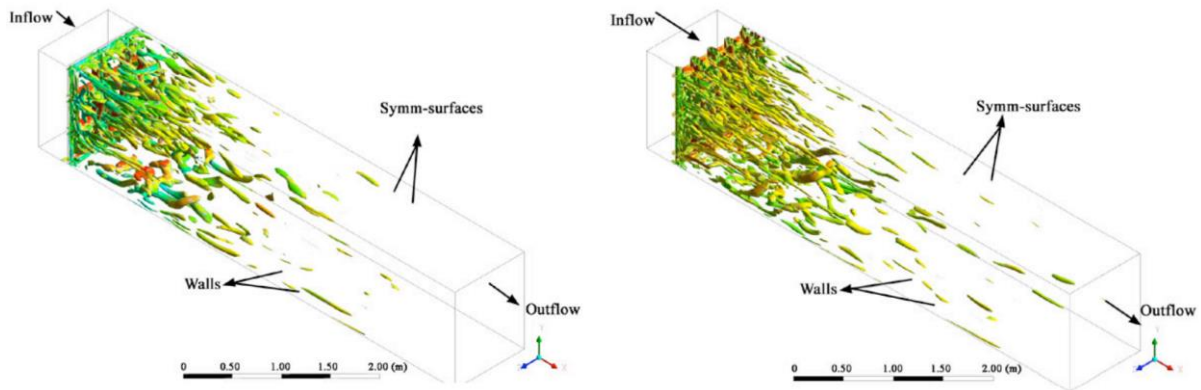


Figure 11. Turbulence generated by the grid placement (left – grid 1; right – grid 2) [39]

Liu [39] shows experimentally that turbulence generated by a grid can be considered isotropic, in accordance with the assumptions of analytical models, only at a downstream distance of approximately 2–4 m, the differences between measured parameters and numerically obtained ones being generally on the order of 15–20%, with better correlations reported in [6], [40], [41], [42]. An alternative method for turbulence generation is the use of a rod placed upstream of the airfoil, which produces quasi-periodic vortices described by von Kármán's theory [43] [44] [45], leading to unsteady aerodynamic forces and to acoustic emissions with a dominant tonal component superimposed on broadband noise [44].

To correlate acoustic effects with aerodynamic implications, Leon et al. [22] integrate acoustic measurements performed with circular microphone arrays within wind-tunnel experiments. Tong [34] emphasizes, however, that despite the large number of existing studies, the mechanisms leading to noise reduction through serrations—particularly at the leading edge—are not yet fully understood, most results being obtained experimentally under homogeneous and isotropic turbulence conditions, with significant difficulties in measuring the strongly unsteady flow field.

## CHAPTER 3. ASPECTS REGARDING THE MODELING OF BLADE NOISE AND NOISE REDUCTION SOLUTIONS IDENTIFIED IN THE LITERATURE

### 3.1. Methods and Computational Models for Serrated Blades (Interaction Noise)

With the development of bladed machines (referring here to turbomachinery), questions began to arise regarding various characteristics and dependencies of the flow in relation to measurable phenomena. One of the concerns that emerged in the early 1950s was the determination of the acoustic spectrum generated by aerodynamic effects. In this context, a number of authors initiated investigations using both theoretical and experimental approaches (among whom Curle, Lighthill, Phillips, Proudman, and to some extent, by analogy, Stratton can be mentioned) [27]. The most notable works that form the basis for describing the mechanisms by which aerodynamic noise is generated—distinct from noise generated by the vibration of a solid placed in a medium—have been identified as those of Curle and Lighthill. Starting from the Navier–Stokes equations and the conservation of momentum in a form proposed by Reynolds, the transition was made from the exact equation of fluid motion (Equation (1)) to relation (2) by adding source-type terms (the mass source  $Q(x,t)$  per unit volume, introduced at a given time at position  $x$ ) [27] [28]

$$\frac{\partial^2}{\partial t^2} - a_0^2 \nabla_\rho^2 = \frac{\partial^2}{\partial x_i \partial x_j} (T_{ij}) \quad (1)$$

where  $T_{ij} = \rho v_i v_j + p_{ij} - a_0^2 \rho \delta_{ij}$ ,  $\rho$  is the density,  $p_{ij}$  is the pressure tensor component,  $a_0$  is the speed of sound and  $v_i$  is the velocity component on  $x_i$  ( $i = 1,2,3$ ) direction.

Starting from relation (2), Curle [27] attempts to further develop Lighthill's theory and focuses on the differences between the acoustic intensities generated by sources with different characteristics (dipoles versus quadrupoles). Through his analysis, he arrives at the same relation obtained by Lighthill for quadrupoles (also known as Lighthill's eighth law), as well as at a similar relation for dipole-type sources [27].

$$\rho - \rho_0 = \frac{1}{4\pi a_0^2} \frac{\partial^2}{\partial x_i \partial x_j} \int v \frac{T_{ij} \left( y, t - \frac{|x-y|}{a_0} \right)}{|x-y|} dy \quad (2)$$

This similarity between the two types of sources is mentioned in relation (3). The relation is useful for evaluating, at least quantitatively, the acoustic effects corresponding to different specific sources. For example, for airfoils, the suction side represents a dipole-type source, while the fluctuating flow in the shear layer corresponds to a quadrupole-type acoustic source, as also noted by Turner [46].

$$\frac{I_Q}{I_B} \sim \left( \frac{U_0}{a_0} \right)^2 \cdot f(R) \quad (3)$$

Starting from Curle's work, Amiet [25] attempts to further develop the general relations formulated in the 1950s and to apply them to a simplified aerodynamic profile (a flat plate). He also identifies that the environment in which airfoils are placed is not undisturbed; however, the turbulence can be considered "frozen turbulence," whose parameters describing the fluctuating behavior are constant along the three propagation directions (constant wavenumbers). In this way, by also employing various mathematical procedures, he succeeds in formulating a law for the PSD ("Power Spectral Density") using a turbulence description specific to the von Kármán spectral model, which can subsequently be converted into acoustic pressure level (for example, relation (4)).

$$SPL_{1/3} = 10 \lg \left[ \frac{Ld}{z^2} M^5 \frac{\overline{u^2}}{U^2} \frac{\widehat{k_x^3}}{(1 + \widehat{k_x^2})^{7/3}} \right] + 181.3 \quad (4)$$

Obviously, "complete" theories are based on simplifying assumptions. The same applies to Amiet's theory which, when applied to blades having an airfoil section, requires corrections. One such correction, for example, identified by Tian [10], is given by relation (5).

$$SPL [dB] = \frac{9}{50} \frac{\frac{e}{c}}{\left(\frac{e}{c}\right)_{ref}} \frac{f}{U} \frac{\left(\frac{\Lambda}{c}\right)_{ref}}{\frac{\Lambda}{c}} \quad (5)$$

Liu [39] demonstrates experimentally that turbulence generated using a grid can be considered isotropic, in accordance with the assumptions of analytical models, only at a distance of approximately 2–4 m downstream, the differences between measured parameters and those obtained numerically being generally on the order of 15–20%, with better correlations reported in [6], [40], [41], [42]. An alternative method for turbulence generation is the use of a rod placed upstream of the airfoil, which produces quasi-periodic vortices described by von Kármán theory [43] [44] [45], leading to unsteady aerodynamic forces and to acoustic emissions with a dominant tonal component superimposed on broadband noise [44].

For correlating acoustic effects with aerodynamic implications, Leon et al. [22] use circular microphone arrays integrated into wind tunnel experiments. However, Tong [34] emphasizes that the mechanisms leading to noise reduction through serrations, especially at the leading edge, are not yet fully understood, most results being based on experiments conducted under homogeneous and isotropic turbulence conditions, with significant difficulties in measuring the strongly unsteady flow field. As previously mentioned, the turbulence associated with the flow is considered isotropic and can be described by wavenumbers associated with the directions of propagation. Relation (6) presents a commonly used formulation for the turbulence convecting upstream toward the serrated LE.

$$w(x', y', t) = \int \int_{-\infty}^{\infty} \tilde{w}(k_1, k_2) e^{i(k_1(x' - Ut) + k_2 y')} dk_1 dk_2 \quad (6)$$

This formulation of turbulence can also be written in other forms, as presented by Lyu [5] or Amiet [24], [25], [26], the calculation procedure following a Fourier-type decomposition of the gust into simple plane waves of the form given in (7)

$$w_i = w_{ia} e^{-i(\omega t - k_1 x' - k_2 y')} \quad (7)$$

The calculation is further based on solving a second-order differential equation for the velocity potential function, which represents a wave propagation equation. Solving this equation using the formulation given in (7) leads to the derivation of a system of equations with a matrix formulation of the type shown in relation (8), where A and B are two diagonal matrices, the problem being reduced to a system of PDEs that is solved iteratively.

$$D\Phi = A\Phi + B \frac{\partial \Phi}{\partial x} \quad (8)$$

where  $\Phi = (\dots \Phi_{-n'}(x, z), \Phi_{-n'+1}(x, z), \dots \Phi_{n'-1}(x, z), \Phi_n(x, z), \dots)^T$

and A and B matrices can be written as

$$A_{ml} = (k_{2m}^2 - k^2)\delta_{ml}, B_{ml} = \begin{cases} 4\sigma \frac{m+l+\frac{k_2\lambda}{\pi}}{\lambda(l-m)}, & m-l = \text{even} \\ 0, & m-l = \text{odd} \end{cases} \quad (9)$$

with  $\delta_{ml}$  – Kroneker symbol, m and l are the modes corresponding to the row and column indices of the matrix. The fundamental equation of the model developed by Lyu [5] is written in (10), where the acoustic pressure is expressed for the mid-span plane of the blade.

$$S_{pp}(x, \omega) = (2\pi dU) \left( \frac{\rho_0 \omega x_3}{2\pi c_0 s_0^2} \right)^2 \sum_{m=-\infty}^{\infty} \frac{\Phi_{\omega\omega}(\omega|U, 2m\pi/\lambda)}{|\gamma_d(\omega|U, 2m\pi/\lambda)|^2} \left| \mathcal{L}\left(\omega, \frac{\omega}{U}, \frac{2m\pi}{\lambda}\right) \right|^2 \quad (10)$$

It should be noted in relation (11) that the acoustic pressure depends on the spectrum of the incident turbulence (denoted here by  $\Phi_{\omega\omega}$ ). Several models exist, but the most commonly used is the von Kármán spectrum, which in Amiet's formulation [25] is written according to (7). This spectrum can also be described using experimentally measured quantities (such as turbulence intensity and a characteristic length parameter [17]). Lyu et al. [5] solve relation (11) for the experimental conditions used by Narayanan [40]. Since the theory is developed starting from Amiet's relations, differences in acoustic pressure are expected in the low-frequency range. Because the computation is performed in the mid-span plane, it can be considered a more two-dimensional than three-dimensional analysis; therefore, for isotropic turbulence, one may use the relation mentioned by Polacsek et al. [17] to extend the result from the analyzed plane (2D) to a point located anywhere in space (at a  $R_{\text{obs}}$  radius) using (11).

$$S_{pp}^{3D}(\omega) = S_{pp}^{2D}(\omega) \cdot \frac{kl_y(\omega)L}{2\pi R_{\text{obs}}} \quad (11)$$

where  $l_y$  is a correlation between the blade length L and the von Kármán spectrum, and k is a parameter described in [17] as a combination of the wavenumbers, the flow velocity, and the serration angle. The modification of the trailing edge by means of serrations is described analytically by Howe [23], who starts from the expression of the acoustic pressure in the far field formulated as a Fourier transform and rewrites it using Green's functions, obtaining a relation for the acoustic spectrum as a function of the serration parameters, expressed by equation (12). In the limit in which the serration amplitude (h – semi-amplitude) tends to zero, equation (12) reduces to the spectrum corresponding to a blade with a straight trailing edge. Howe solves equation (12) for various combinations of serration amplitudes and wavelengths, at a constant ratio between the serration amplitude and the thickness of the turbulent boundary layer. The same relations are also solved by Al Tlua [14] using a MATLAB algorithm, the obtained results being identical, with the author additionally performing a comparison between triangular and sinusoidal serrations applied at the trailing edge.

$$\Psi(\omega) = \left(1 + \frac{1}{2}\epsilon \frac{\partial}{\partial \epsilon}\right) f\left(\frac{\omega\delta}{U_c}, \frac{h}{\lambda}, \frac{h}{\delta}; \epsilon\right), \quad (12)$$

$$f\left(\frac{\omega\delta}{U_c}, \frac{h}{\lambda}, \frac{h}{\delta}; \epsilon\right) = \frac{1}{\left\{\left(\frac{\omega\delta}{U_c}\right)^2 \left[1 + \left(\frac{4h}{\lambda}\right)^2 + \epsilon^2\right]\right\}} \cdot \left(1 + \frac{64 \left(\frac{h}{\lambda}\right)^3 \left(\frac{\delta}{h}\right) \left(\frac{\omega\delta}{U_c}\right)^2 \left\{\cosh\left\{\frac{\lambda}{2\delta} \sqrt{\left[\left(\frac{\omega\delta}{U_c}\right)^2 + \epsilon^2}\right]\right\} - \cos\left(\frac{2\omega h}{U_c}\right)\right\}}{\sqrt{\left[\left(\frac{\omega\delta}{U_c}\right)^2 + \epsilon^2\right] \left\{\left(\frac{\omega\delta}{U_c}\right)^2 \left[1 + \left(\frac{4h}{\lambda}\right)^2 + \epsilon^2\right]\right\} \sinh\left\{\frac{\lambda}{2\delta} \sqrt{\left[\left(\frac{\omega\delta}{U_c}\right)^2 + \epsilon^2}\right]\right\}}}\right)$$

For the terms that were not described in this chapter, related to equation (12), the additional relations suggested by Moreau et al. [38] can be used, where all the experimental constants are clarified, as well as the relations corresponding to the thickness of the turbulent boundary layer (equations (13)).

$$\begin{aligned} \delta &= 8\delta^* \\ \frac{\delta}{c} &= \frac{0.37}{Re_c^{1/5}} \end{aligned} \quad (13)$$

Al Tlua [14] also identifies in the literature a more complete relation (relation (14)) for the thickness of the turbulent boundary layer, similar to the second one written in (14).

$$\delta = \frac{0.37c \left[1 + \left(\frac{Re_c}{6.9 \cdot 10^7}\right)^2\right]^{1/10}}{Re_c^{1/5}} \quad (14)$$

Lyu [9] solves the same problem of triangular serrations placed at the trailing edge and obtains a relation similar to that for triangular serrations placed at the leading edge. The meaning of the terms in relation (15) is the same as those in (10), the two formulations being quite close.

$$S_{pp}(x, \omega) = \left(\frac{\omega x_3 c}{4\pi c_0 s_0^2}\right)^2 2\pi d \sum_{m=-\infty}^{\infty} \left|\mathcal{L}\left(\omega, \frac{\omega}{U}, \frac{2m\pi}{\lambda}\right)\right|^2 \Pi(\omega, 2m\pi/\lambda) \quad (15)$$

Lyu et al. [9] perform a comparative analysis between Howe's model (relation (13)) and their own model (relation (15)), identifying a fairly good similarity between the two approaches. From the two plots, it can be observed that the spectrum obtained using Howe's method [23] overestimates the noise reduction. At the time of publication, Howe obtained a reduction of at least  $10 \cdot \log[1 + (4h/\lambda)^2]$  dB, which would lead to values exceeding 10 dB under certain conditions. Over the years, various authors have shown that noise reduction does indeed occur when using such serrations, but it is usually less than half of the values predicted by the aforementioned relation. Al Tlua [14] also analyzes the types of serrations mentioned by Lau [15], succeeding in identifying analytical relations for almost all variants: straight trailing edge (relation (16)), triangular trailing edge (relation (17)), slotted trailing edge (relation (18)), and sinusoidal trailing edge (relation (19)).

$$\Psi_{drept}(\omega) = \frac{\left(\frac{\omega\delta}{U_c}\right)^2}{\left[\frac{\omega\delta}{U_c} + \epsilon^2\right]^2} \quad (16)$$

where  $U_c = 0.77U$  in the convection velocity,  $C_m = 0.1553$  and  $\epsilon = 1.33$ .



$$\Psi_{\text{triunghi}}(\omega) = 8 \left(\frac{h}{\delta}\right)^2 \left(\frac{\omega h}{U_c}\right) \sum_{n=-\infty}^{\infty} \frac{\left[1 - \cos\left(\frac{2\omega h}{U_c}\right) / \cos(n\pi)\right] \left[\left(\frac{\omega h}{U_c}\right)^2 + \left(\frac{2n\pi h}{\lambda}\right)^2\right]}{\left[(n\pi)^2 - \left(\frac{2\omega h}{U_c}\right)^2\right]^2 \left[\left(\frac{\omega h}{U_c}\right)^2 + \left(\frac{2n\pi h}{\lambda}\right)^2 + \left(\frac{\varepsilon h}{\delta}\right)^2\right]^2} \quad (17)$$

$$\Psi_{\text{slot}}(\omega) = \sum_{n=-\infty}^{\infty} \Theta \Theta^* \frac{\left[\left(\frac{\omega h}{U_c}\right)^2 + \left(\frac{2n\pi\delta}{\lambda_1 + \lambda_2}\right)^2\right]}{\left[\left(\frac{\omega h}{U_c}\right)^2 + \left(\frac{2n\pi\delta}{\lambda_1 + \lambda_2}\right)^2 + (\varepsilon^2)^2\right]^2} \quad (18)$$

$$\text{where } \Theta(K, \lambda_1, \lambda_2, h) = n^{-1} \left[ \left( e^{\frac{2in\pi\lambda_1}{\lambda_1 + \lambda_2}} - 1 \right) e^{iK_1 h} + \left( 1 - e^{-\frac{2in\pi\lambda_1}{\lambda_1 + \lambda_2}} \right) e^{-iK_1 h} \right]$$

$$\Psi_{\text{sin}}(\omega) = \left(\frac{\omega h}{U}\right) \sum_{n=-\infty}^{\infty} J_n^2\left(\frac{\omega h}{U}\right) \frac{\left(\frac{\omega\delta}{U}\right)^2 + \left(\frac{2n\pi\delta}{\lambda}\right)^2}{\left[\left(\frac{\omega\delta}{U}\right)^2 + \left(\frac{2n\pi\delta}{\lambda}\right)^2 + \varepsilon^2\right]^2} \quad (19)$$

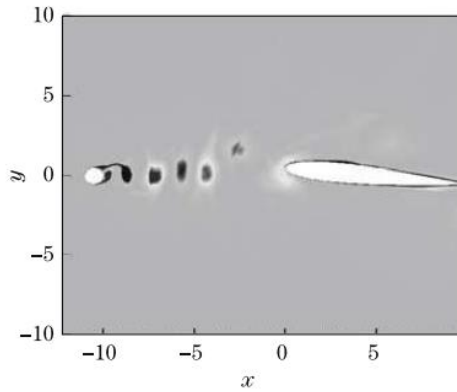
Using both the above relations for the normalized spectra (relations (16) to (19)) and relations (10) and (15), a transformation of the type given by relation (20) is applied.

$$OASPL_{\text{norm}} = 10 \lg \left( \int_{\omega_{\min}}^{\omega_{\max}} \Psi(\omega) d\omega \right) \quad (20)$$

Ryi and Choi [8] also investigate noise reduction through trailing-edge modification, but their application targets wind turbine rotor airfoils. They employ an experimental setup consisting of a wind tunnel placed inside an anechoic chamber to characterize a wind turbine blade with constant chord (350 mm) and no twist, using six different serration types. The outcome of these experiments is the derivation of an empirical law for the reduction of the acoustic pressure level achieved by these methods. The model is composed of six relations, leading to a function for estimating trailing-edge noise reduction, given by relation (21):

$$SPL_{\text{serBF}} = 3.5 - 8[\log(St^*) + 0.3]^2 - \left[ \log\left(\frac{\lambda_s}{h}\right) + 0.4 \right]^2 \quad (21)$$

As noted by Teruna et al. [43], rods are very effective elements for generating tonal components, mainly due to the fact that they produce essentially the same fluctuation along their entire span/length (Figure 12).



[44] axial section view (2D)



[50] turbulent structures (3D)

Figure 12. Rod–airfoil interaction

Liu et al. [51] attempt to characterize the behavior of several grids integrated into their experimental setup using numerical analysis. Gruber [6] employs both experimental and theoretical approaches, using the von Kármán model [5] as a reference (Equation (22)). A similar approach is adopted by Chaitanya [21], who conducts experiments at several incident flow velocities. This relation has also been identified using different notations by various authors (Biedermann [7], Polacsek [17], or Hales [52]).

$$\Phi_{ww}(k_1, k_2) = \frac{4\overline{u^2}}{9\pi k_e^2} \frac{\widehat{k_1^2} + \widehat{k_2^2}}{(1 + \widehat{k_1^2} + \widehat{k_2^2})^{7/3}} \quad (22)$$

$$\text{where } k_e = \frac{\sqrt{\pi}\Gamma(5/6)}{L_t\Gamma(1/3)}, \widehat{k_1} = \frac{k_1}{k_e}, \widehat{k_2} = \frac{k_2}{k_e}$$

The nondimensionalized turbulence spectrum, denoted by Lyu et al. [33] as  $\Pi_l(\omega, k_2)$ , can also be characterized using the Liepmann model, which is written according to Equation (23). As in the case of the von Kármán spectrum, the formulations are similar, with the notation being slightly adapted from one author to another (Amiet [24] [25], Biedermann [7], Chaitanya [2]).

$$\Pi_l(\omega, k_2) = \frac{3TI^2L_t^2}{4\pi} \frac{L_t^2(k_1^2 + k_2^2)}{(1 + L_t^2(k_1^2 + k_2^2))^{5/2}} \quad (23)$$

where  $TI$  and  $L_t$  represent the turbulence intensity and the ILS (“integral length scale”), parameters that are most often determined experimentally.

### 3.2. Aerodynamic implications

Tong et al. [34] numerically analyze a stator blade with a NACA 65(12)-10 airfoil, showing that leading-edge serrations behave similarly to a delta wing, generating lateral vorticity regions that influence the streamwise flow. In the presence of an upstream rod, the noise reductions are significant, on the order of 11–16 dB over a wide range of Strouhal numbers, with important changes also observed in the RMS coefficients, while the mean aerodynamic values remain relatively constant.

Teruna et al. [43] employ LBM-based aeroacoustic simulations to evaluate blades with symmetric and cambered airfoils, analyzing simple serrations, porous solutions, and combinations thereof at the leading edge. The results show that porous solutions promote undesired lateral flows and lead to a degradation of aerodynamic performance, including through communication between the pressure side and the suction side.

Ito [53] experimentally demonstrates that small-amplitude serrations applied at the leading edge of a NACA63-414 stator blade delay flow separation on the suction side at low Reynolds numbers, without significant changes in the global aerodynamic coefficients, with higher tooth densities exhibiting more favorable aerodynamic behavior. Polacsek [17] numerically and experimentally validates the effects of serrations through the analysis of local pressure coefficient distributions, highlighting atypical pressure-field behaviors, particularly on the pressure side, associated with modifications of the leading-edge geometry.

### 3.3. Configurations of interest identified in the literature

Throughout the present work, various sources have been mentioned in which a wide range of blade variants have been presented. The simplest geometry is the flat plate placed in a flow, for which the theoretical solution for obtaining the pressure and velocity fields was derived analytically as early as the 1950s. This solution has been validated by several authors over time and adapted so as to allow comparison with more complex models associated with serrated blades. The theoretical development

(from an analytical standpoint) of blades with serrated leading or trailing edges was carried out starting from the flat-plate model, in which the law of variation of the regions of interest was modified. Important contributions have also been identified on the experimental side, such that various authors have obtained either empirical or semi-empirical laws that couple the parameters of the incident-flow turbulence with the serration parameters in order to achieve an optimal noise reduction. In the extended version of the work, a subset of the relevant geometries analyzed over time is summarized, together with several testing conditions required for a comparative analysis (two-dimensional or three-dimensional configuration, broadband turbulence generated by a grid, or tonal components generated by a rod placed upstream).

## CHAPTER 4. CORRELATION OF THE PARAMETERS DEFINING TURBULENCE WITH SERRATIONS. PRELIMINARY TESTS

### 4.1. Correlation parameter between serrations and turbulence

For generating the fluctuating component in the flow, either a rod can be used (to obtain a tonal component) or a grid (to obtain broadband noise). In the 1:1 configuration (inside a stage installed on the engine), the properties of the incident fluid at the blade are those corresponding to the rotor wake. Thus, the reference parameter, as commonly used for serrated solutions, is represented by a function that includes as variables the turbulent kinetic energy (TKE) and the turbulent energy dissipation rate (TED). The ILS parameter can be determined numerically using a function defined later in the post-processing stage, a function written according to (24).

$$\Lambda = C_\mu^{3/4} \frac{k^{3/2}}{\epsilon} \quad (24)$$

where  $C_\mu=0.09$ . The same parameter can also be written in the form (25), starting from the Smith  $k-l$  and the Menter  $k-\omega$  SST turbulence models [66].

$$\Lambda = \frac{C_{Re}}{C_\mu} \frac{k^{1/2}}{\omega} \approx \frac{C_{Re}}{C_\mu} l \quad (25)$$

At the same time, the relation  $\Lambda = 0.21 L_w$  [66] can also be written, where  $L_w$  represents the size of a vortex (“Gaussian wake width”). A review of the literature shows that the parameter  $\Lambda$  varies between 0, in the vicinity of the blade extremities, and approximately 10 mm in two distinct regions associated with the vortices generated at the hub and at the tip of the rotor blade. A correlation between  $\Lambda$  and the serration wavelength  $\lambda$  is required, most experimental studies indicating that the optimal wavelength is approximately four times larger than  $\Lambda$ . At the same time, the serration amplitude must be limited, values larger than 10% of the chord providing no significant acoustic benefit and negatively affecting the aerodynamic flow. For the geometry analyzed, a serration is sought that preserves the incidence of the reference blade and is correlated with the characteristics of the turbulence, while maintaining the original airfoil chord length in section. The transition from a straight leading-edge blade to a twisted blade with variable wavelength and amplitude is complex and must account for the streamlines in order to avoid aerodynamic penalties; parametric approaches in this direction are reported in [66].

Turbulence generation can be achieved either by rods, which predominantly induce tonal components useful for the analysis of frequencies of interest (typically multiples of the BPF), or by grids, which lead to a more uniform broadband spectrum, both methods being considered in subsequent investigations. Numerous experimental facilities based on convergent ducts with grids and, in some cases, additional rods are reported in the literature [44] [41] [6] [49] [43] [51] [16] [68]. Based on these examples, a convergent duct was designed to provide exit velocities exceeding 50 m/s,

using the air supply of the COMOTI anechoic chamber (Măgurele, RO). The dimensions of the outlet section were established by scaling, at 150 mm × 75 mm, and the shape of the convergent part was chosen so as to avoid flow separation, allow the insertion of turbulence-generating elements and measurement instrumentation, be manufacturable by 3D printing, and ensure adequate mechanical strength.

The identification of the “optimal” convergent-duct–turbulence-grid combination starts from establishing the dimensions of the blades to be placed in the flow. Since the flow duct has dimensions of 150 mm × 75 mm, in a cascade-type configuration blades with a span of 75–150 mm could be introduced (Figure 13), the limitation being given by the ratio between chord and blade spacing,  $\sigma$  (which is usually between 0.8 and 1.2). For  $\sigma \approx 1.1$ , five blades can be introduced (three central and two forming the flow channel) with a chord of 50 mm. Taking into account existing experiments reported in the literature, where the maximum amplitude is recommended not to exceed 20% of the chord, the amplitude-to-wavelength ratio should lie in the interval [1..2], and the wavelength-to-ILS ratio (optimal around 4), it follows that, at this scale, a target value of  $\Lambda = 2.5$  mm is sought.

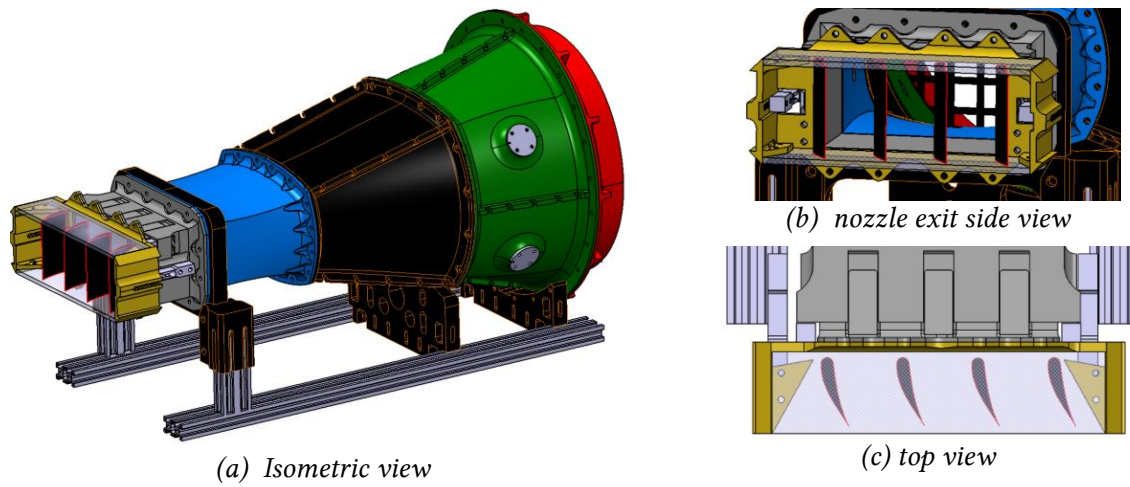


Figure 13. Cascade configuration

The process of determining the mesh size of the grids is an iterative one, starting from values identified in literature (at least in terms of order of magnitude). Two grid placement locations were also selected: one at 75 mm from the coupling region with the convergent duct and another at 200 mm upstream of the inlet, in order to assess whether the turbulent phenomena dissipate or not over the total length of approximately 600 mm between the inlet and the outlet.

## 4.2. Preliminary tests

The experimental setup was coupled to a centrifugal fan and placed inside the anechoic chamber. The air supply ducting was flexible, thus facilitating the relocation of a major noise source (the fan blades) to as large a distance as possible and at a favorable angle. The fan was shielded by a sliding door placed 10 m outside the anechoic chamber, and the anechoic chamber door was closed as much as allowed by the air ducting. The setup was positioned diagonally so that the air ducting was as straight as possible. Two microphones were placed at a radius of 1 m: the first approximately along the flow direction (at ~10 degrees relative to the longitudinal axis of the nozzle), and the second at 90 degrees relative to the axis. Regarding the tested configurations, a combination of printed blades and printed grids was implemented to demonstrate the noise reduction capabilities of such blades (with serrations). Figure 14 presents the testing variants at the nozzle exit.

In addition to the acoustic recordings, flow velocity measurements were performed at the exit of the bladed cascade. These were carried out using a Pitot tube, the measured velocities being close in value, while a slight influence of the reduction of the exit cross-section due to the placement of the

lateral blades was nevertheless observed. The measurements were performed between the central blades, along the flow direction dictated by the placement of the blades in the cascade at an angle of 15 degrees (the measured velocity therefore corresponds to the maximum value obtained for that configuration).

The preliminary tests were divided into three series/campaigns. In the first series, the objective was to highlight the self-noise of the blades, as well as the noise generated exclusively by the jet (with and without the plates supporting the blades). The spectra contain a significant amount of parasitic noise, the predominant component (at  $\sim 786$  Hz and its first harmonic) originating from the fan and propagating through the air ducting. The jet exiting the nozzle also produces noise around the frequency of 1000 Hz, the interaction noise being broadband in nature (the noise reduction mechanism being best identified above 1500 Hz). Other peaks appearing at high frequencies (above 5 kHz, but not only) may originate from sealing imperfections.

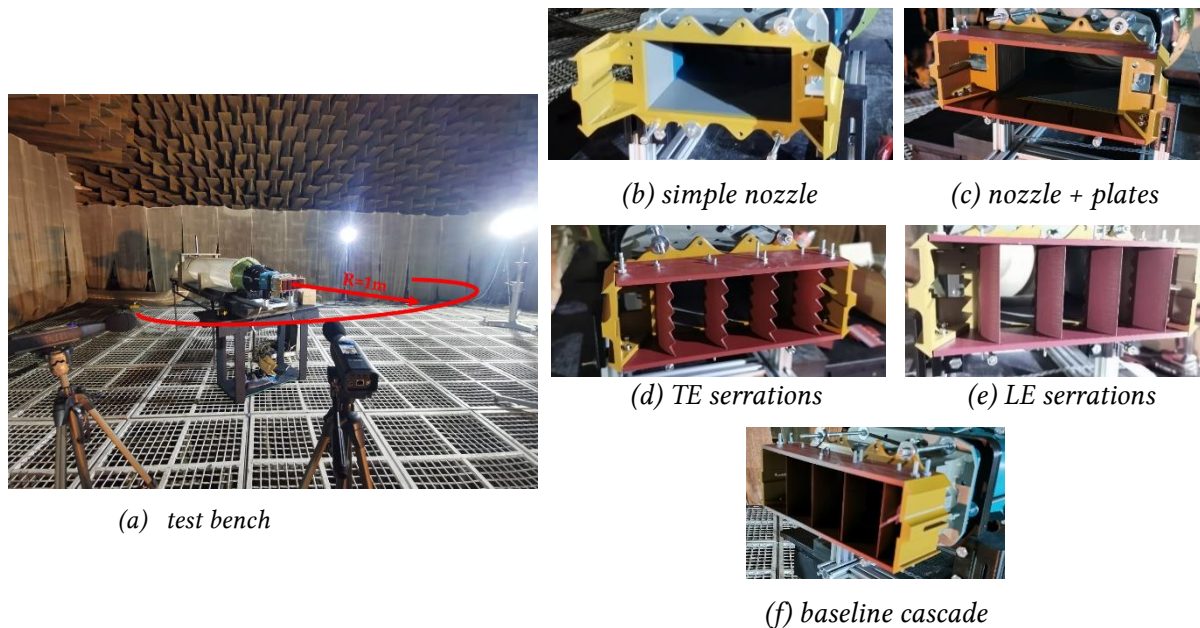


Figure 14. Tested configurations

The second series of tests was based on placing a grid (with 20 mm mesh size and 4.5 mm thickness) upstream of the bladed sector ( $\sim 300$  mm). In addition to the jet noise, a reduction in the overall sound pressure level of approximately 1.5 dB was observed for blades with leading-edge serrations compared to the baseline blades (with straight leading edge). For blades with trailing-edge serrations, a reduction of less than 1 dB in the overall noise level was recorded (Figure 15).

Placing the grid in position 1 (more than 500 mm upstream of the blades) did not lead to the generation of high-intensity turbulence; therefore, the recorded spectra are not close to those obtained with the turbulence source placed nearer to the nozzle exit. Nevertheless, for blades with trailing-edge serrations, a decrease in the sound pressure level is observed in the 2–5 kHz range (recorded by both microphones). This reduction (even up to 15 dB at certain frequencies) may be a particular feature of the directivity of such solutions and requires further investigation. Overall, it was observed that, in order to maintain the fluctuating character of the flow, the turbulence-generation mechanism must be placed close to the blade, since the generated vortices dissipate very rapidly within the fluid mass.



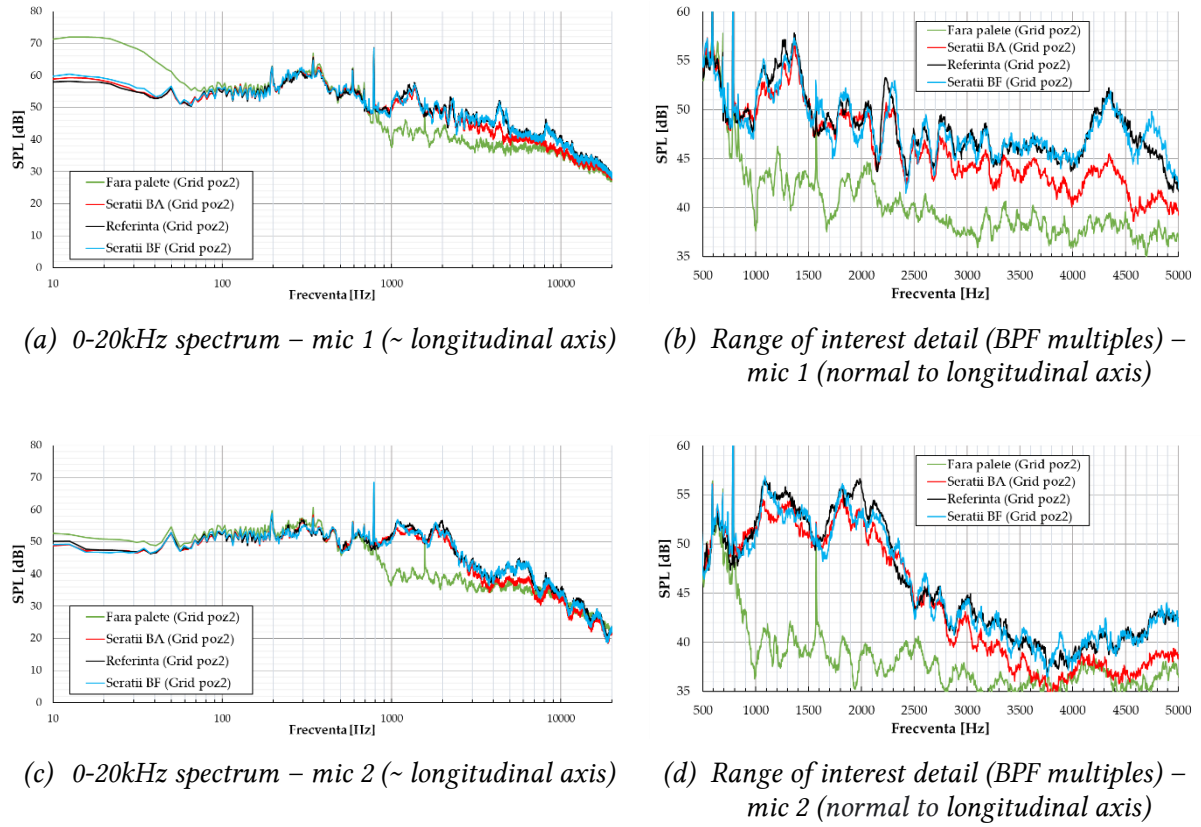


Figure 15. Interaction noise (grid-generated turbulence, position 2 – blade cascade)

## CHAPTER 5. PROCESSING OF EXPERIMENTAL DATA AND COMPARISON BETWEEN THEORY AND EXPERIMENT

### 5.1. Introduction

The study of serrated blades and their impact on noise has been a topic of interest since the 1950s [69], due to their influence on noise, turbomachine efficiency, and the environment. Modifications applied at the leading edge or trailing edge have demonstrated potential in reducing noise generated by fans, turbines, and propellers [70]–[76], by enhancing fluid mixing and reducing turbulence, which is the main source of mixing noise. In addition, serrations can improve aerodynamic performance, leading to more favorable lift-to-drag ratios and reduced energy losses [78], while advanced solutions such as permeable regions or metamaterials have also shown promising results [79]. The reduction of noise pollution associated with aerodynamic components is particularly important in urban areas, which is why these solutions are relevant for the development of more sustainable technologies [14], [80], [81].

With regard to the behavior of blades in isolated configurations versus cascades, Lewis et al. [82] show that the developed mathematical models can satisfactorily reproduce experimentally measured spectra, with general formulas being identified both for isolated airfoils and for blade cascades [78], [82], [83], as well as for jet mixing noise [80], [84], [85]. Turbulence, a chaotic and difficult-to-predict phenomenon, plays an essential role in turbomachine performance, influencing energy losses and overall efficiency [69], [70], [82], [85] [86] [87] [88]. For this reason, understanding and correctly modeling turbulence are essential not only in aviation, but also in fields such as wind energy, meteorology, or fluid transport [89] [90] [91].

Mathematical turbulence models, although they cannot directly solve the Navier–Stokes equations in turbulent regimes, allow the description and prediction of flow behavior for different

types of turbulence, such as isotropic, two-dimensional, boundary-layer, or high-speed turbulence [78], [79], [81], [82], [84], [85], [92], [93]. In this work, a comparative analysis of these models and turbulence scales is carried out, with emphasis on the accuracy of predictions relative to experimental data obtained under real conditions. The physical reproduction of turbulence involves both numerical simulations and experimental testing, with model selection being performed based on predictive accuracy, generalization capability, and computational efficiency [82], [94], [95]. In turbojet and turbofan engines, turbulence is an omnipresent phenomenon that directly influences system performance and efficiency. The turbulence scale is determined through mathematical models and numerical simulations and can be interpreted both as an indicator of turbulence intensity and as a characteristic length associated with turbulent motions, representing the distance traveled by a fluid particle between successive interactions.

Within experimental studies, turbulence characterization is carried out through the combined use of multiple measurement instruments, such as hot-wire anemometers and other probes for determining velocity and associated fluctuations [70] [78] [96] [97], Pitot tubes for evaluating pressure and mean velocity [14], pressure sensors for measuring local variations within the duct and on surfaces [97] [61], as well as advanced optical systems such as PIV or Schlieren setups for flow visualization [93] [55] [98]. The correlated use of these methods enables the determination of relevant turbulent parameters, such as velocity and pressure fluctuations ( $u'$ ,  $p'$ ), turbulent kinetic energy and dissipation rate ( $K$  and  $\epsilon$ ), their characteristic frequencies, and the integral length scale of turbulent structures ( $\Lambda$ ) [82] [88] [99].

$$\begin{aligned}
 TI &= \sqrt{\frac{\overline{u'^2}}{U_0^2}} \\
 \overline{u'^2} &= \int_{-\infty}^{+\infty} S_{uu}(f) df \\
 \Lambda &= \frac{U_0 S_{uu}(f=0)}{2\overline{u'^2}}
 \end{aligned} \tag{26}$$

where  $TI$  is the turbulence intensity and  $S_{uu}$  is the longitudinal turbulent velocity spectrum. In order to artificially generate turbulence in an experimental setup, various methods can be used, such as perforated plates (orifice plates, circular grids) [100] [101] [102], rectangular grids [78] [86] [88], rotating vanes or active grids [103], bars/rods [50] [104] [45], or pulsating air jets [105]. These devices can be used to perturb the fluid flow and to create turbulence in a controlled manner. Numerical simulations are also employed to model and induce artificial turbulence in experimental configurations. Turbulence scales describe the transfer of energy and the role of viscosity across different sizes of turbulent motions and constitute an essential theoretical framework for the interpretation of aeroacoustic phenomena. The Von Kármán scale [78] [88] [99] [106] [107] [108] is frequently used to describe energy transfer between large turbulent structures and how these generate fluctuating pressure fields responsible for tonal and “whistling”-type acoustic emissions in applications such as wings, propellers, or helicopter blades. The Liepmann scale [78] [99] [107] is associated with the interaction between turbulence and viscosity and is relevant for leading-edge noise, where oscillatory pressure variations can be modeled as dipole-type acoustic sources. The Taylor scale [109] [110] represents an intermediate scale at which kinetic energy transfer is significantly influenced by viscosity and is associated with the dispersion of turbulent structures in the leading-edge region, contributing to broadband noise characteristic of high-speed flows. The Obukhov–Corrsin scale [111] [112] extends the analysis by including thermal effects and is relevant for flows with temperature gradients, where density fluctuations can generate “rumble”-type acoustic emissions, particularly in the trailing-edge region. At the smallest dimensions, the Kolmogorov scale



[109] describes energy dissipation at the molecular level and is associated with low-intensity continuous noise occurring in regimes close to stall. In addition to these fundamental scales, the literature also mentions other relevant models, such as Batchelor [112], Ozmidov [111], Monin–Obukhov [113], Corrsin [114], Kraichnan [107], and Kaimal and Davenport [115], which are mainly used for large-scale applications or under complex atmospheric conditions.

In the Von Kármán model, the characteristic turbulence length scale refers to the typical size of turbulent structures in a fluid medium, such as vortices. Turbulence energy in the Von Kármán spectrum is usually expressed as spectral density [106], with units of energy per unit frequency or wavenumber. These units may vary depending on the context of the spectral analysis of turbulence. Turbulence spectra can be calculated using specialized signal spectral analysis functions, in order to visualize the distribution of turbulent energy as a function of frequency or wavenumber, by applying the Von Kármán interpolation formula and the following equation, which can be used [108]:

$$E(k) = \frac{55}{9\sqrt{\pi}} \frac{\Gamma\left(\frac{5}{6}\right) \overline{u'^2}}{\Gamma\left(\frac{1}{3}\right) k_e} \frac{\left(\frac{k}{k_e}\right)^4}{\left[1 + \left(\frac{k}{k_e}\right)^2\right]^{\frac{17}{6}}} \quad (27)$$

where  $k$  it is the magnitude of the vector containing the wavenumbers,  $\Gamma(\cdot)$  is the Gamma function and  $k_e = \frac{\sqrt{\pi}}{\Lambda_f} \frac{\Gamma\left(\frac{5}{6}\right)}{\Gamma\left(\frac{1}{3}\right)}$  is the smaller vortex scale. The one-dimensional longitudinal von Kármán turbulence spectrum, obtained by integrating the energy spectrum, is given by:

$$\Phi_{uu}(k_x) = \int_{-\infty}^{\infty} \int_{-\infty}^{\infty} \frac{E(k)}{4\pi k^2} \left(1 - \frac{k_x^2}{k^2}\right) dk_z dk_y = \frac{2}{\sqrt{\pi}} \frac{\Gamma\left(\frac{5}{6}\right) \overline{u'^2}}{\Gamma\left(\frac{1}{3}\right) k_e} \left[1 + \left(\frac{k_x}{k_e}\right)^2\right]^{-\frac{5}{6}} \quad (28)$$

## 5.2. Numerical and Experimental Analysis Methodology

The experimental setup was coupled to a centrifugal fan rated at 9800 Pa and 7.5 kW and installed inside an anechoic chamber designed in accordance with ISO 3745 [55], featuring an absorption coefficient of 99% in the 150 Hz–20 kHz frequency band. The air supply source was positioned outside the chamber and connected via a flexible hose, while the test section was placed diagonally in order to minimize duct curvature. Acoustic measurements were performed using two Class 1 sound level meters, positioned at a distance of 1 m from the source, one approximately axial and the other at 90°, with raw signals acquired at 50 kS/s. Similar but more complex experimental configurations for blade cascades are reported in [88] [58], while propagation corrections and reflection effects are discussed in [117] and [118].

The tests included combinations of serrated blades and 3D-printed grids, the blades being equipped with rounded triangular serrations with an amplitude equal to 20% of the chord. The turbulence grids were placed in two distinct positions within the convergent section, in order to control the flow characteristics. Correlation of the experimental results with theoretical models required determination of the flow velocity, which was carried out using an L-type Pitot tube, with measurements performed taking into account the cascade configuration and the blade installation angle. The values measured along the blade span were averaged for each of the five analyzed cases.

## 5.3. Results

The preliminary tests were structured into three series, the first being dedicated to identifying the self-noise of the blades and the noise generated exclusively by the jet, with and without the supporting plates. The obtained spectra indicate the presence of significant unwanted noise,

dominated by a tonal component around the frequency of 786 Hz and its first harmonic, associated with the rotor and propagated through the air duct. The jet contributes additional noise around 1000 Hz, while the interaction noise exhibits a broadband character, the reduction mechanism being more evident at frequencies above 1500 Hz, whereas high-frequency peaks can be associated with imperfect sealing.

The second test series included the placement of a turbulence grid upstream of the blades, which led to a reduction of the global sound pressure level of approximately 1.5 dB for blades with a serrated leading edge, compared to those with a straight leading edge, while for trailing-edge serrations the reduction was below 1 dB, the results being illustrated in Figure 16. A detailed quantitative evaluation of the efficiency of the two treatments could be carried out using logarithmic-type relations based on acoustic power levels and the Strouhal number, such as those proposed in [88] and [70]. For a correct interpretation, the acoustic spectra were transformed from RMS to PSD, taking into account the Hanning window, the spectral resolution ( $\Delta f$ ), and the square of the RMS pressure. In agreement with observations reported in the literature, the von Kármán spectrum exhibits limitations in the high-frequency range, where the transition from the  $-5/3$  slope to an exponential decay is not correctly captured [88]. This deficiency can be corrected by applying the correction proposed by Pope [108], which adjusts the dissipation range by modifying the energy spectrum.

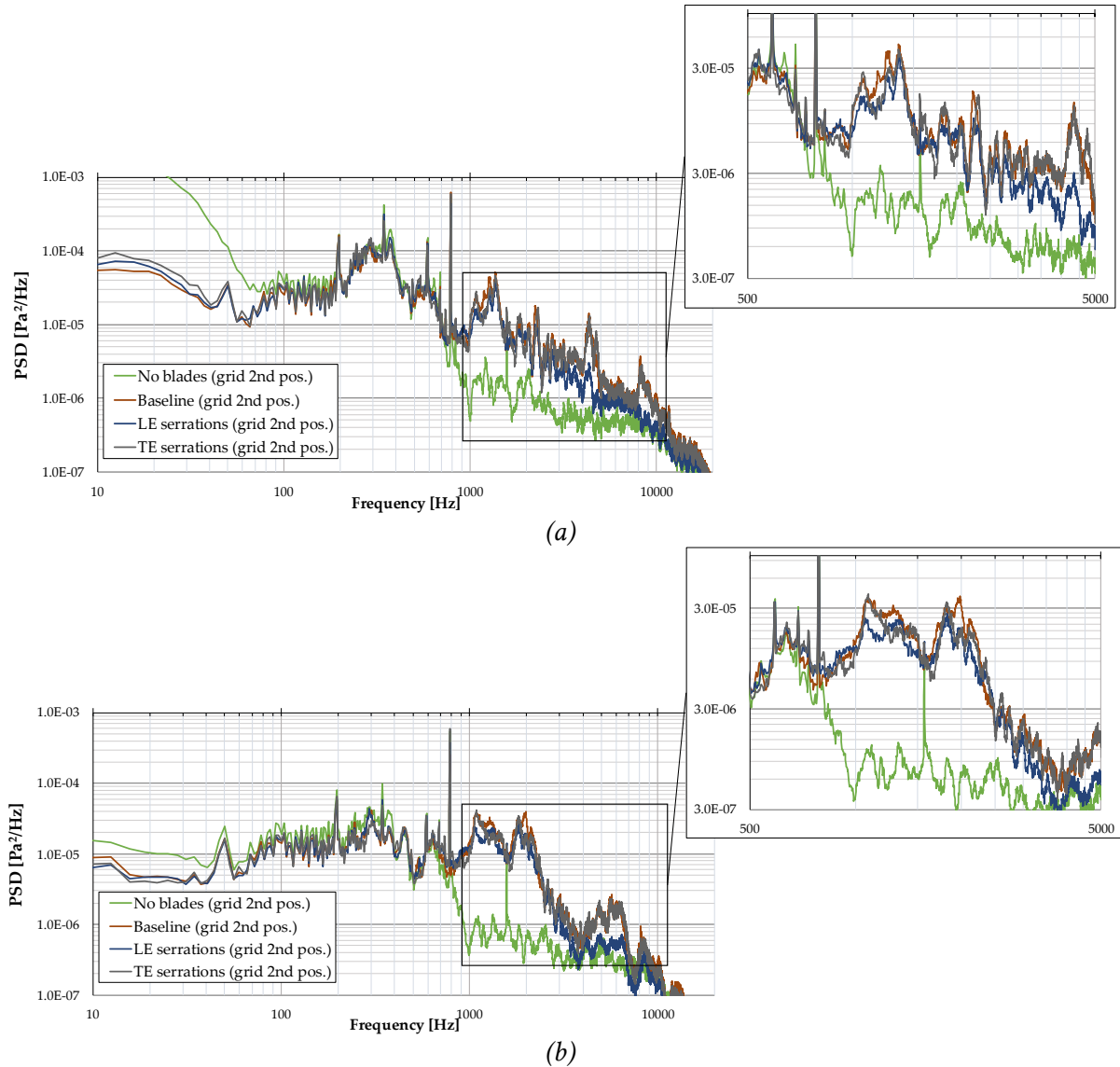


Figure 16. Interaction noise: (a) 0-20kHz spectrum+ details (BPF multiples) - Mic 1 (10 deg relative to axial direction); (b) 0-20kHz spectrum+ details (BPF multiples) - Mic 2 (normal to axial direction).

Placing the grid in the first position (at more than 500 mm upstream of the blades) did not lead to the generation of high-intensity turbulence; therefore, the spectra recorded in Figure 16 are not comparable to those obtained with the turbulence source positioned closer to the outlet. Nevertheless, a decrease in the sound pressure level in the 2–5 kHz range (recorded by both microphones) can be observed for blades with trailing-edge serrations. This reduction (up to 15 dB at certain frequencies) may be a particular feature related to the directivity of such solutions and should be further investigated. Overall, it was observed that, in order to preserve the fluctuating character of the flow, the turbulence-generating mechanism should be placed close to the blade, as the generated vortices dissipate very rapidly within the fluid mass.

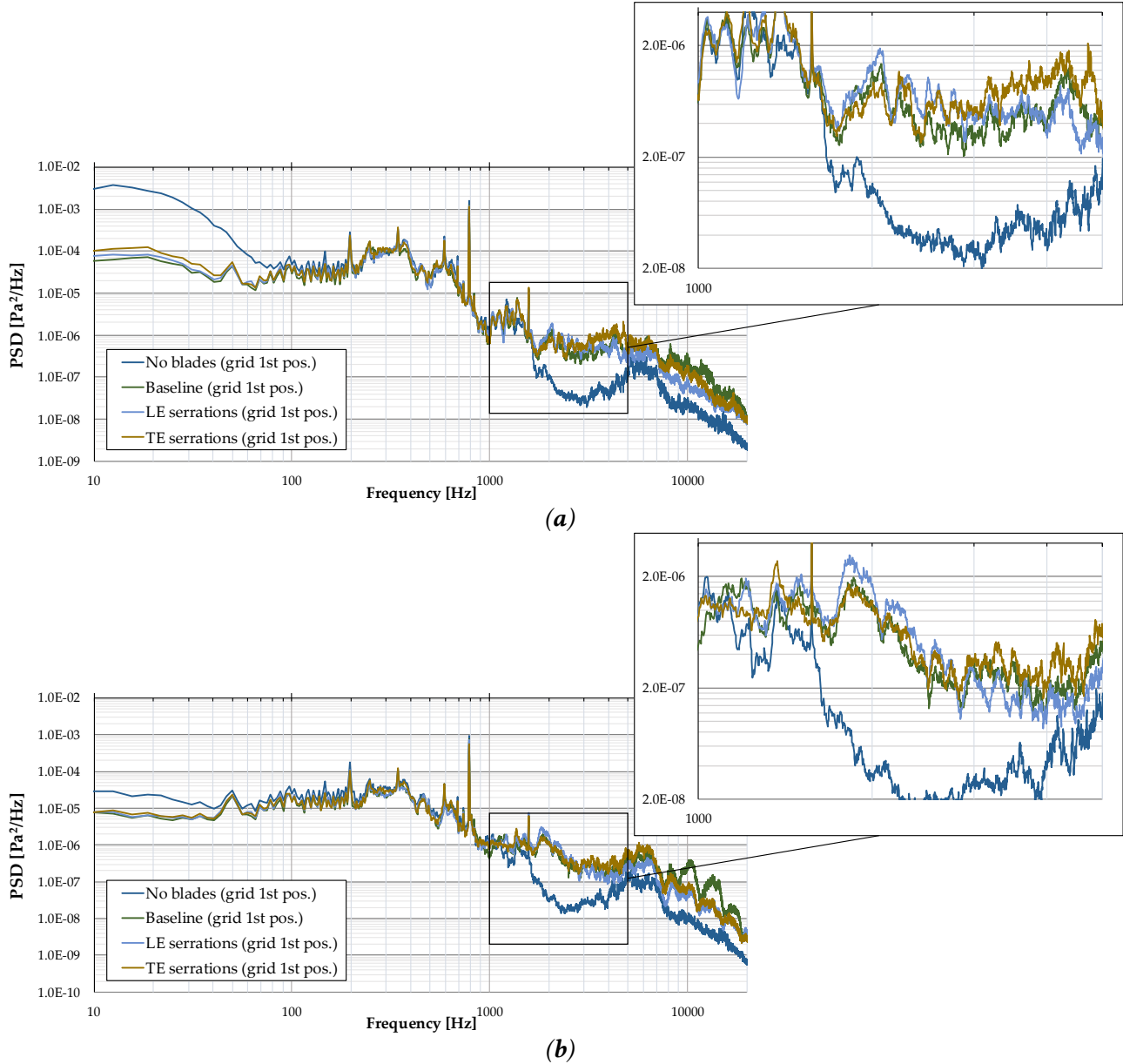


Figure 17. Interaction noise: (a) 0-20kHz spectrum+ details (BPF multiples) - Mic 1 (10 deg relative to axial direction); (b) 0-20kHz spectrum+ details (BPF multiples) - Mic 2 (normal to axial direction).

The presentation of OASPL (Overall Sound Pressure Level) is preferred, as it provides a global measure of sound intensity in dB. In contrast, PSD (Power Spectral Density) examines only the distribution of power across frequencies, without accounting for the cumulative acoustic effect. A comparative representation of the global acoustic pressure levels, derived from the corresponding spectra, is presented in Figure 18. The tonal components, including the first tone at 780 Hz (Figure 17), were filtered out.

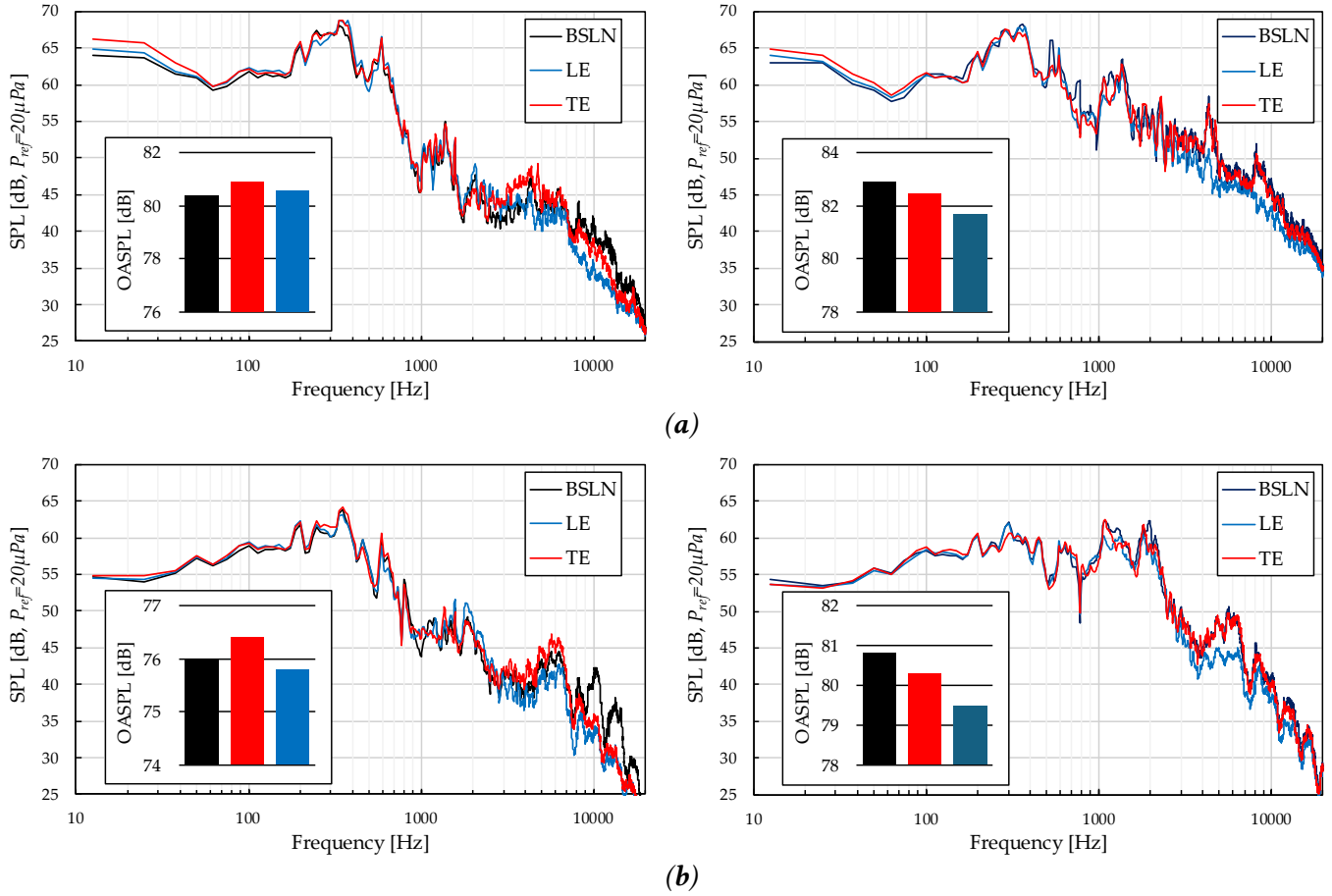


Figure 18. Acoustic pressure level spectrum (left – grid at the first position; right – grid at the second position): (a) 10 degrees relative to the axis of the rig; (b) perpendicular to the axis of the rig.

It can be observed that placing the grid in the first position alters the global values (this was also evident numerically in the power spectra, where the interaction was not well represented). In contrast, a reduction of approximately 1.5 dB (OASPL) was observed for the grid-leading-edge interaction noise in both measurement directions. Trailing-edge noise was less attenuated; however, such serrations exhibited a similar impact over the entire frequency range. The optimal operating range for serrations applied at the leading edge, for the tested combinations, appears to be in the mid-frequency band (2000–5000 Hz). The difference in global levels observed in Figure 18 may be a characteristic of directivity, which will be further addressed in future work through the use of microphone array configurations.

## CHAPTER 6. EXPERIMENTAL ANALYSIS OF INTERACTION NOISE FOR A TURBULENT JET-AIRFOILS WITH LEADING-EDGE SERRATIONS IN A 4-BLADE CASCADE CONFIGURATION

### 6.1. Description of the Test Configuration

In aeronautical applications, blade cascades are characteristic of fans and compressors in gas turbine engines, where the interaction between incident turbulence and the leading edge, as well as flow separation in the trailing-edge region, generates tonal and broadband noise [6] [44] [41] [49] [43] [119] [16] [68]. Acoustic pressure levels can reach high values in the vicinity of the source and contribute significantly to the perceived noise during phases close to takeoff. International regulations impose cumulative noise reductions on the order of 10–15 dB relative to reference levels from the

2000s for the certification of new aircraft configurations, in accordance with ICAO standards [120] [121] [122] [123]. Noise reduction in blade cascades can be achieved through active solutions, which are effective but complex, or through passive solutions, such as integrated acoustic treatments, leading- and/or trailing-edge profiling using serrations, or bio-inspired geometries, which offer scalability advantages without major penalties in mass or performance [6] [7] [43] [55] [124] [125] [126] [127] [142]. In this context, cascade acoustic tests are essential for evaluating the spatial and spectral distribution of the acoustic field and for validating passive solutions, through the use of microphone arrays and beamforming techniques. These methods allow the identification of modifications in acoustic lobes and SPL reductions on the order of 2–6 dB in the mid- and high-frequency ranges, or even higher for tonal components [55] [60] [62] [66].

The experimental setup used is the same as in previous studies, as shown in Figure 19, and includes an air supply with a convergent section installed in an anechoic chamber. In the present tests, a grid was introduced along the flow path to generate controlled turbulence with well-defined global parameters [128]. Several blade variants were designed and manufactured, with a mean chord of 50 mm and a span of 75 mm, featuring a chord variation of  $\pm 10\%$ , generating a sinusoidal leading-edge geometry defined by “teeth,” with the pitch determined by their number. The acoustic field was measured using an array of 13 microphones arranged over a  $180^\circ$  circular sector, with the possibility of rotating the measurement plane, following a methodology similar to those used in modern research facilities [130] [131] [132].

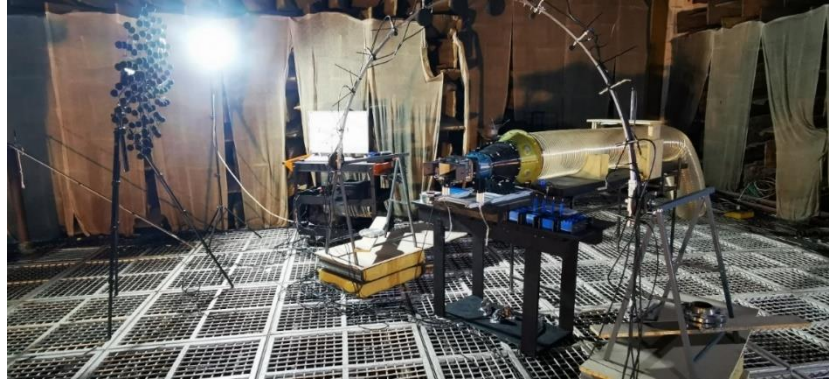


Figure 19. Experimental setup for testing blade cascades

The blades tested were mounted at the nozzle exit between two plates that set the installation angle within the cascade (Figure 20). Four pairs of plates were used, corresponding to incidence angles of  $0^\circ$ ,  $5^\circ$ ,  $10^\circ$ , and  $15^\circ$ , respectively. For preliminary recordings prior to the actual tests, the acoustic spectrum of the turbulence grid was captured using an aerodynamically profiled microphone, as well as a surface-mounted microphone (Figure 21).

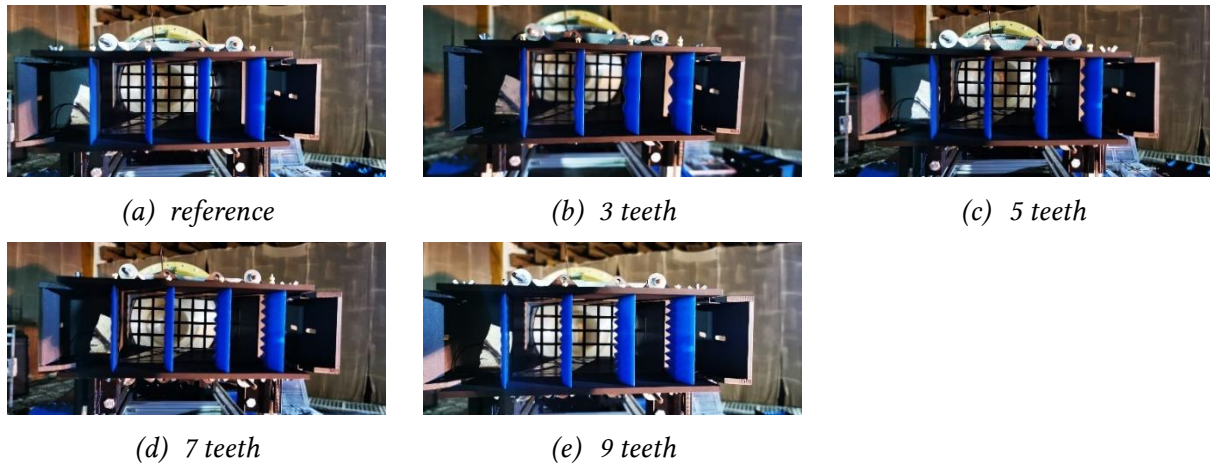


Figure 20. Blade cascades





Figure 21. Microphones placement for identifying turbulence parameters (left – aerodynamically profiled microphone, right – surface-mounted microphone)

The characterization of turbulence parameters was carried out using an indirect approach, based on acoustic measurements performed downstream of a turbulence-generating grid, which allow the extraction of information regarding the spectral content of the acoustic pressure associated with the local interaction between the turbulent flow and the channel walls. The experiments were conducted in a test duct with constant cross-section, at a mean flow velocity of 50 m/s, the grid being used to generate coherent turbulent structures.

Downstream of the grid, two types of microphones were employed: a surface-mounted microphone, installed in the channel wall, to measure pressure at the fluid–solid interface, and an aerodynamically profiled microphone, inserted into the flow, to directly capture the noise generated by vortical structures. The signals were acquired at 50 kHz and processed using the Fourier transform in order to determine acoustic pressure spectra and power spectral density. For the estimation of turbulence parameters, a semi-empirical approach was adopted, grounded in classical models from the aeroacoustics literature. The corresponding analytical relations and mathematical developments are presented in detail in the extended work, while here the applied methodology and the physical interpretation of the results are described.

The method starts from the observation that the acoustic pressure radiated by convective turbulent structures directly reflects both the intensity of velocity fluctuations and the size of coherent structures in the flow. From a spectral point of view, this behavior manifests as an increase in energy at low frequencies, followed by a decay at higher frequencies, governed by a characteristic frequency associated with the integral turbulence scale, in agreement with classical models of dipole-type acoustic sources. The theoretical model was adjusted based on the spectra obtained experimentally from the surface microphone signal, through a curve-fitting procedure that minimizes the difference between the measured and the estimated spectra over a relevant spectral range. As a result of this process, global parameters characterizing the relative turbulence intensity and the size of coherent structures were determined.

The spectral content of the acoustic signals was analyzed by estimating the power spectral density, using a standard segmentation and spectral averaging method. The analysis was applied both to the pressure signal measured at the wall and to the signal recorded directly in the flow, allowing the identification of differences induced by the relative positioning with respect to the turbulent structures. The use of power spectral density expressed in physical units enables a direct energetic interpretation and a coherent correlation with theoretical models of turbulent flow.

On the raw spectral data recorded by the two microphones, the following processing steps were applied: segmentation into Hann windows with 50% overlap, application of FFT to each window and averaging of the spectral energy, normalization of the result by the window energy (dedicated codes using structures similar to the MATLAB “pwelch” function are attached in the work), construction of the frequency vector, and representation of the acoustic pressure level (SPL) distribution. The estimation of turbulence parameters based on the measured acoustic signal can also be performed through the analysis of the autocorrelation function of the acoustic pressure, a method frequently used in aeroacoustics studies of turbulent flows. This approach is based on the assumption that the pressure fluctuations recorded near the source are directly correlated with velocity

fluctuations in the turbulent flow, and that the temporal structure of the signal reflects the spatial organization of vortical structures. The analysis of the autocorrelation function allows the extraction of two relevant global parameters: the characteristic length of turbulent structures and the relative turbulence intensity. The characteristic length is associated with the average size of coherent structures and is obtained by integrating the autocorrelation function over a finite time interval, chosen so as to capture signal decorrelation. Turbulence intensity is estimated indirectly, by correlating the energetic level of the acoustic signal with this characteristic length, using simplifying assumptions regarding pressure wave propagation.

Applying the method to both the signal measured at the wall and the signal recorded directly in the flow enables a comparison of turbulence parameters at two distinct positions within the flow field. This comparison provides additional information on the evolution, attenuation, and reorganization of turbulent structures after passing through the turbulence-generating elements. The method offers the advantage of relatively simple implementation and a direct connection with measurable physical quantities, making it suitable for the global characterization of turbulence in aeroacoustic experiments.

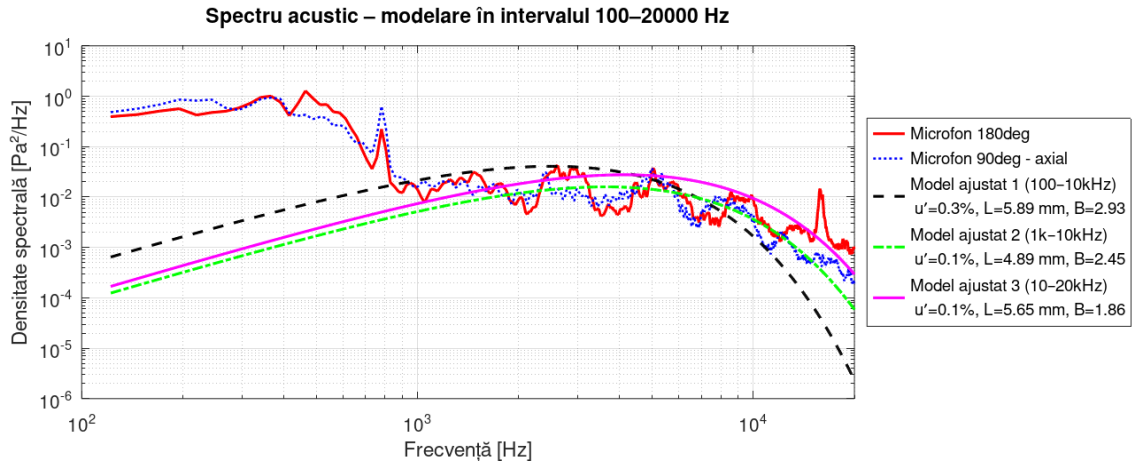
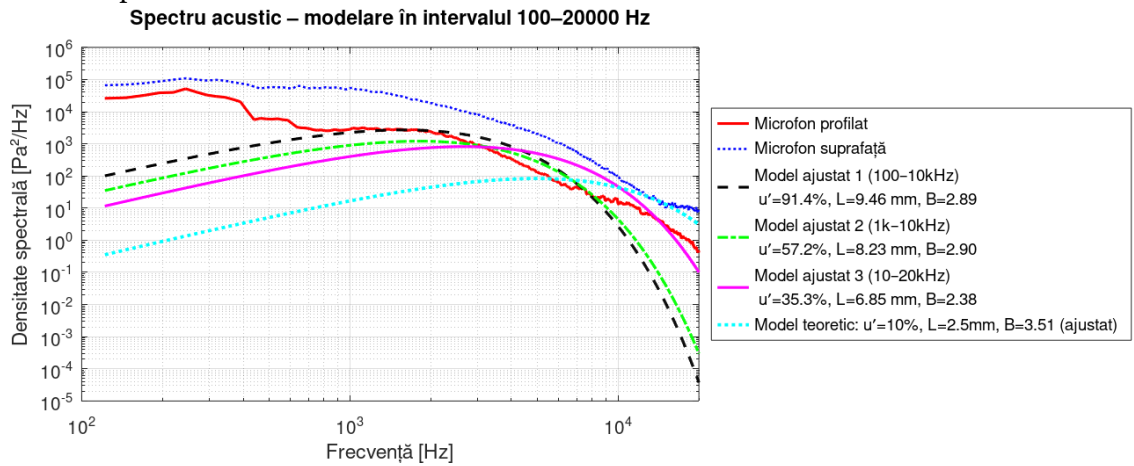


Figure 22. Superposition of the recorded and correlated spectra (curve fitting)

By comparing the methods used, the smaller values of the turbulence parameters are more plausible, since the PSD/autocorrelation methods integrate the acoustic pressure signals in the energy domain and are based on relations specific to plane waves ( $S_{uu} = S_{pp}/(\rho^2 c^2)$ ). By comparing the methods used, the smaller values of the turbulence parameters are more plausible, since the PSD/autocorrelation methods integrate the acoustic pressure signals in the energy domain and are



based on relations specific to plane waves  $S_{uu}(f)$  can be used to obtain the turbulent kinetic energy. The calculation procedure is as follows: it starts from relation (29):

$$k = \frac{1}{2} u'^2 \rightarrow k/U^2 = \frac{1}{2} \left( \frac{u'}{U} \right)^2 \quad (\text{dimensionless}) \quad (29)$$

and the relationship between acoustic pressure and velocity can be written as:

$$S_{uu}(f) = \frac{S_{pp}(f)}{\rho_0^2 c_0^2} \rightarrow u'^2 = \int S_{uu}(f) df \rightarrow k = \frac{1}{2} \int \frac{S_{pp}(f)}{\rho_0^2 c_0^2} df \quad (30)$$

thus, for a known  $S_{pp}(f)$ ,  $k$  can be calculated directly. It should be noted that the values obtained are local, at the point where the microphone is located, and do not represent the total turbulent energy of the system. This quantity refers only to the longitudinal components (if the signal is considered to be aligned along a single direction). The spectrum  $S_{uu}(f)$  derived from the raw pressure signal assumes plane-wave propagation, which may be a reasonable approximation at large distances but is debatable in the near field close to the source.

## 6.2. Experimental results

The raw signals recorded by the 12 GRAS 40AE microphones via the Dewesoft acquisition system were processed (FFT) and subsequently exported in the form of sound pressure level values. For each spatial position, a single value was recorded and represented on the spherical cap shown in Figure 23, while the interpolated data allowed the creation of a much smoother distribution (Figure 24). The code included in the appendix attached to the in extenso work follows the logic described below: construction of the measurement field (knowing the measurement planes and the spacing between microphones), import of the results for each point, import of the nozzle geometry (represented by a large number of points), visualization of the markers corresponding to each measurement point using a color scale associated with the SPL value, selection of a single value for the fixed microphones (at 0 and 180 degrees), and interpolation of the results over the surface (spherical cap) using either triangulation (the “rough” option) or v4 interpolation (specific to Matlab/Octave and superior to cspline for the present case). This computational workflow was applied to all available datasets (combinations of blade geometries and upper plates used to set the installation angle), and the resulting distributions are presented below.

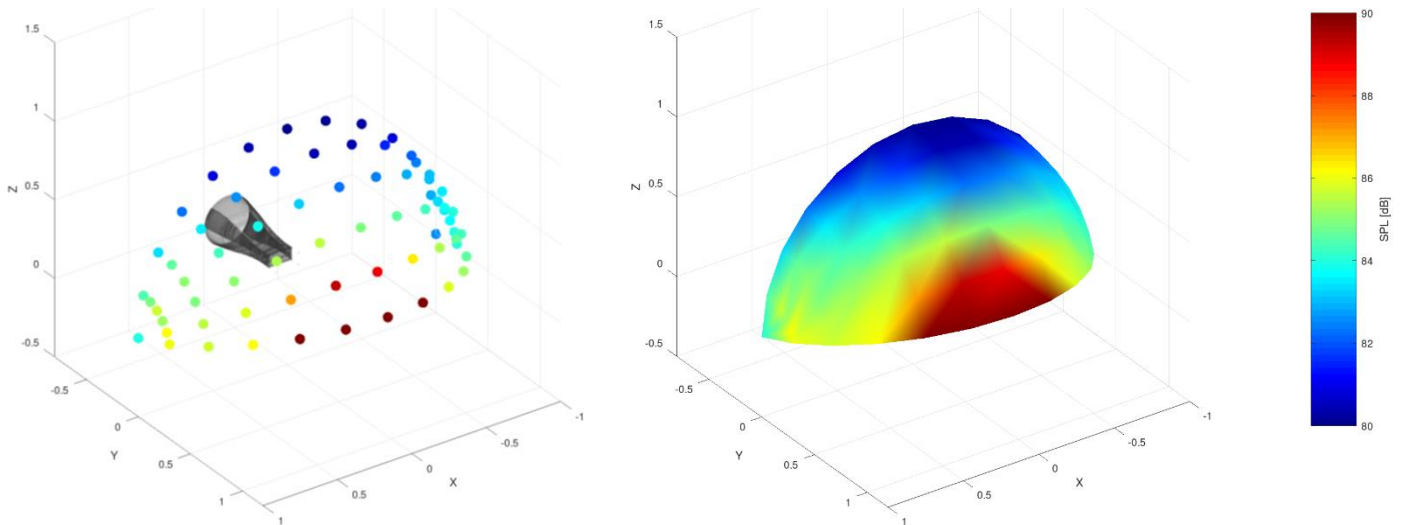


Figure 23. SPL representation: at the measurement points (left) and on the spherical cap (right, “trisurf” interpolation)

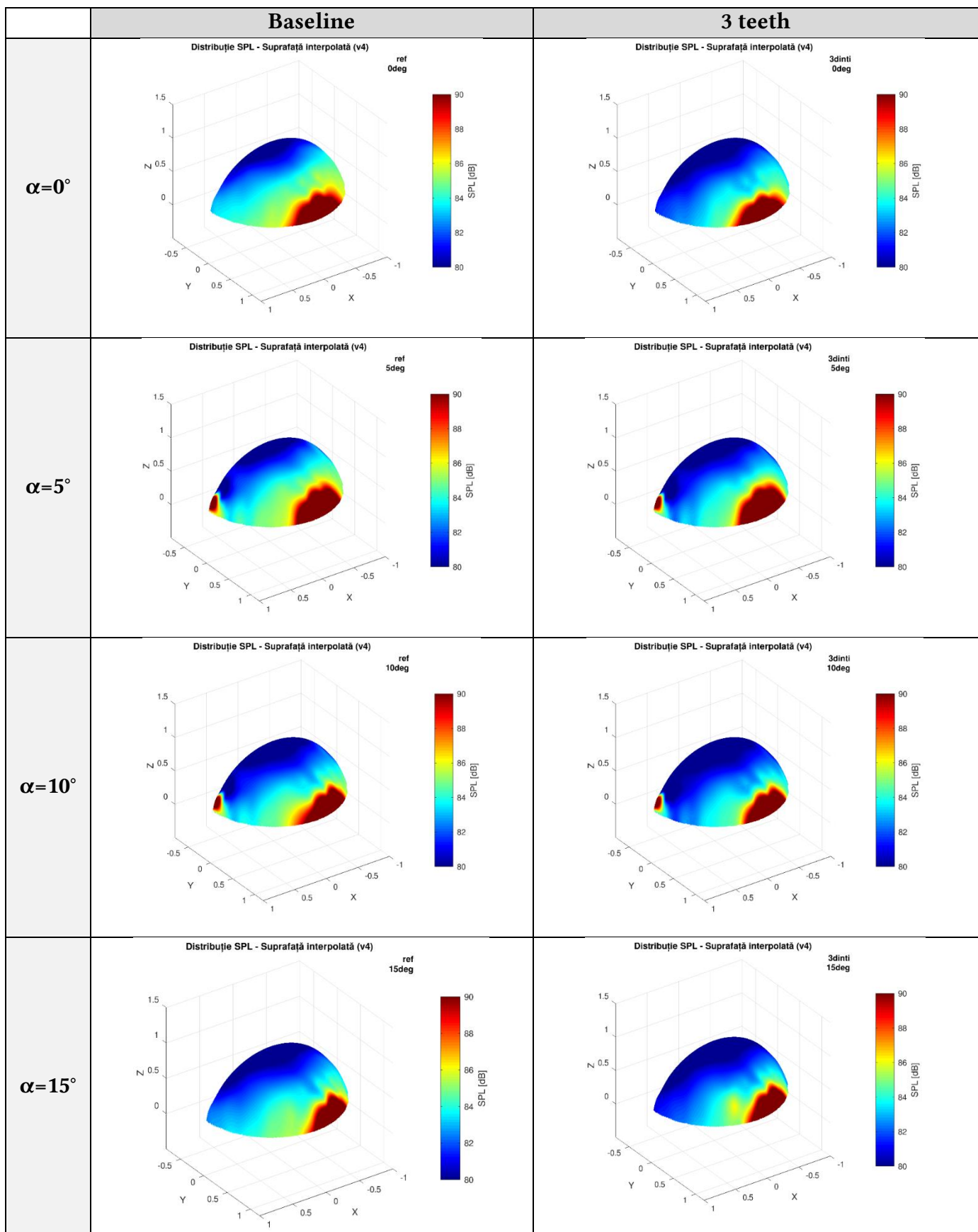


Figure 24. SPL representation on the spherical cap (“v4” interpolation, excerpt – “3 teeth” geometry)

In Figure 25, the results for all combinations of blades and installation angles are presented as differences in sound pressure level, expressed in dB (Z, rms). With the exception of the measurement planes at 15° and 30°, where the jet tends to interfere with the microphones around the sixth one (the

75° position and its vicinity), a global reduction is observed at all positions. This reduction increases in magnitude as the number of teeth increases (i.e., as the serration pitch decreases). Notable values are also obtained for the blade sectors with five teeth, which are comparable to those corresponding to the minimum pitch configuration (nine teeth).

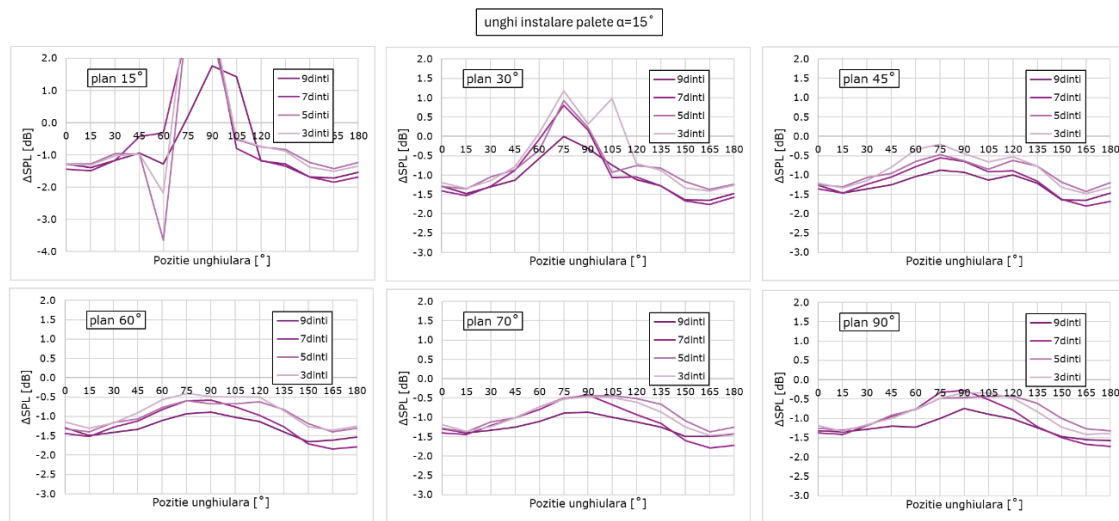


Figure 25. Representation of  $\Delta SPL$  for the tested combinations (sample,  $\alpha = 15^\circ$ )

If all microphones are averaged over all positions within the same measurement plane, Figure 26 is obtained. Two variants of results are presented here: both a simple (arithmetic) averaging and a logarithmic averaging (which is commonly applied when differences greater than 3 dB exist between microphones [147]).

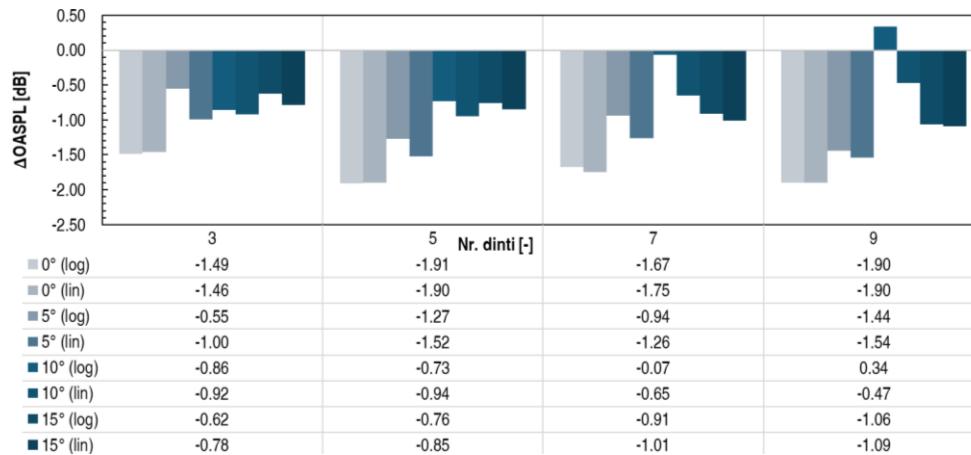


Figure 26. Global levels (comparison between arithmetic averaging and logarithmic averaging)

Acoustic beamforming is a spatial signal processing technique applied to data acquired from a microphone array, used for the localization and quantification of noise sources. In the study of noise generated by turbulent jets, this method enables the determination of the spatial distribution of the sound pressure level (SPL) within an observation plane, providing essential information regarding the intensity and the predominant direction of acoustic radiation. Acoustic beamforming was employed to characterize the spatial distribution of the noise generated by the turbulent jet and by its interaction with the analyzed blades. The method allows the identification of preferential radiation directions and the comparative evaluation of the effect of blade geometry on the acoustic field, based on signals recorded with a microphone array arranged on a semicircle and positioned in several inclined planes.

The analysis focused on a frequency range relevant to jet noise, selected according to the geometric and dynamic parameters of the flow. Signal processing led to the generation of two-dimensional maps of the sound pressure level, expressed relative to the local maximum, which

highlight the spatial modifications induced by the applied passive solutions. Since the data were acquired sequentially, the final acoustic distributions were obtained by averaging the individual results, providing a robust estimate of the mean acoustic field. The computational details and numerical implementation are presented in the in extenso work, and the dedicated codes are included in the corresponding appendices.

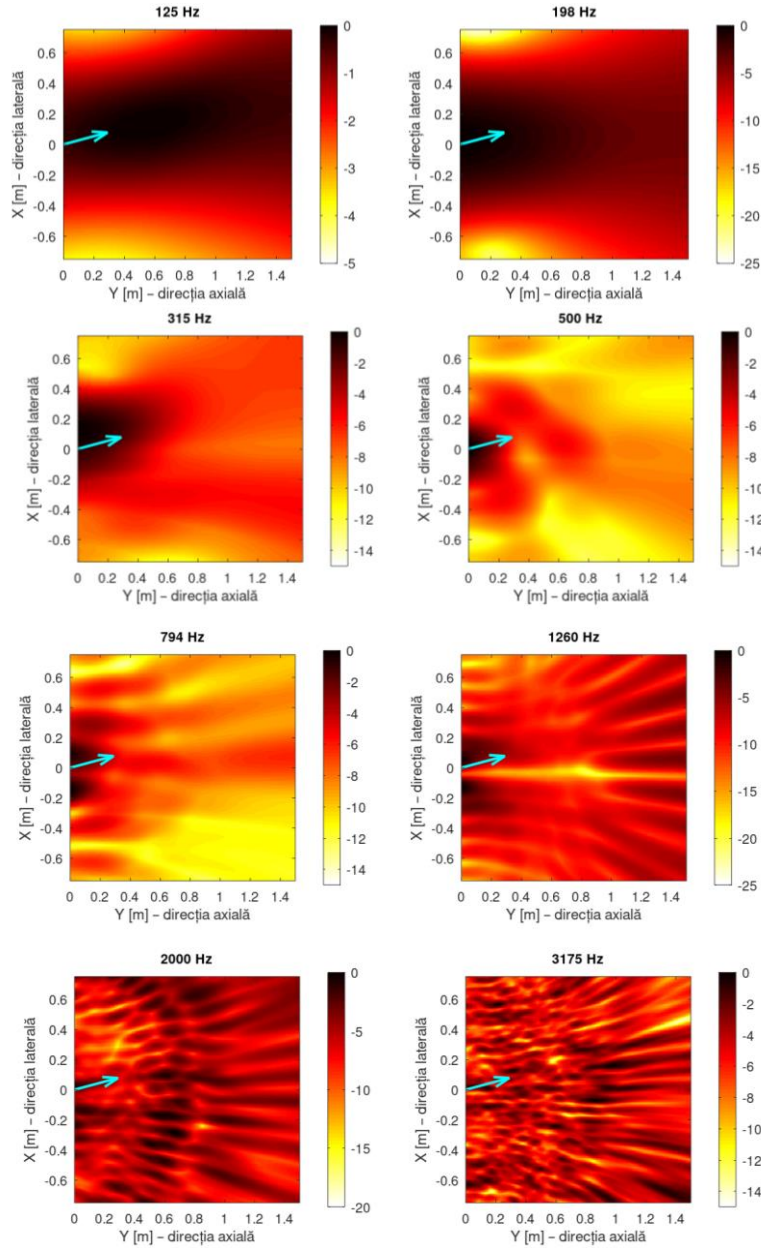


Figure 27. Baseline cascade beamforming (alfa 15 deg)

In the absence of an inverse transfer function (obtained through numerical modeling or experimental calibration), beamforming maps provide information on the relative distribution and directivity of acoustic energy, being suitable for comparisons between configurations and for the identification of dominant sources (Figure 27). In order to synthesize the two-dimensional distributions into a form that is easy to compare, the SPL maps in the XY plane were transformed into directivity curves by aggregating the values as a function of the polar angle associated with each observation point. This procedure leads to a variation of the sound level with direction, represented in the form of polar curves (“butterfly plots”). The resulting representations highlight the shape, width, and orientation of the acoustic lobes, as well as the position of the dominant directions relative to the jet axis, allowing the identification of the main noise reduction direction for each analyzed

configuration (Figure 28). The computational details and numerical implementation are presented in the in extenso work, and the dedicated code is included in the corresponding appendices.

In Figure 29, the 3D representation adds geometric context by reconstructing the shapes of the directional lobes in space, each plane being projected according to its inclination direction (15°–90°). Each curve is relatively scaled and placed within a common coordinate system, in which the nozzle geometry is also visible. This method allows the evaluation of the global orientation of the acoustic source and of possible asymmetries between planes, complementing the polar analysis with an intuitive visualization of spatial directivity.

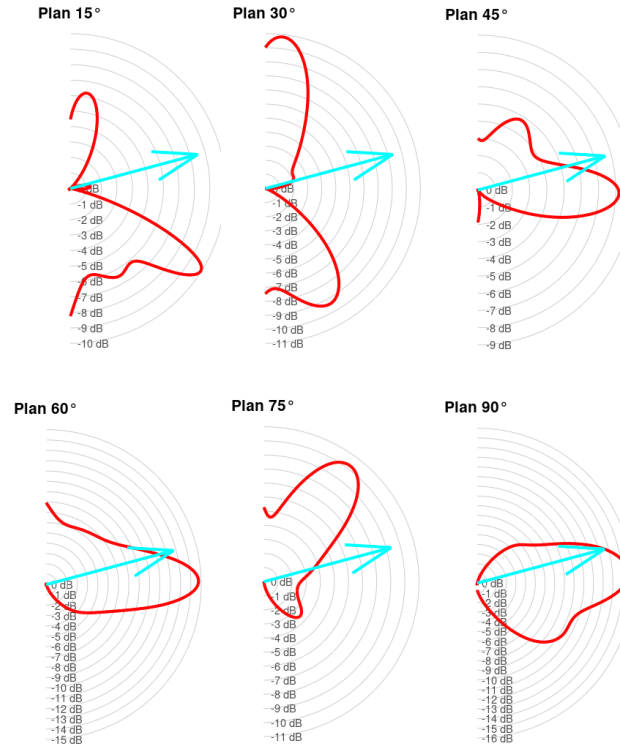


Figure 28. Baseline cascade directivity, 315Hz (alfa 15 deg)

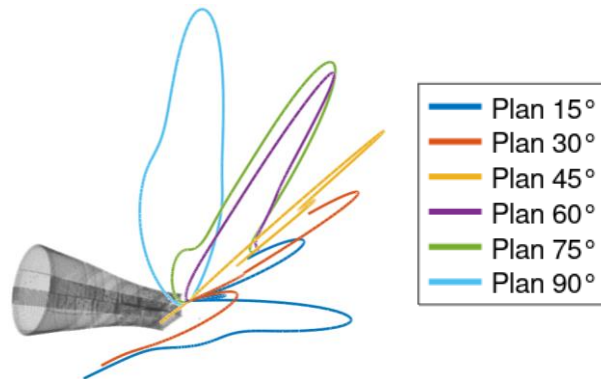


Figure 29. Plane directivity overlap (all computed planes, baseline)

### 6.3. Serrations impact

The beamforming maps (see Figure 30; only the representations in the 1–3 kHz range were selected, as they are the most relevant in the context of the significant influence of the BPF component) provide a first indication of how leading-edge serrations influence the spatial distribution of noise sources. The reference configuration, with a straight leading edge (0T), exhibits compact and well-defined maxima in the vicinity of the blade, with the energy concentrated along the axial direction.



The introduction of serrations progressively modifies this pattern: as the number of teeth increases, the sources appear to be distributed over a more extended region, and the maximum intensity decreases. The cases with five and seven teeth are particularly suggestive, highlighting a reduction in source coherence and a more fragmented structure at both 2000 Hz and 3175 Hz, in agreement with the hypothesis that serrations decorrelate (change the phase of) the incident turbulence and reduce the intensity of coherent scattering.

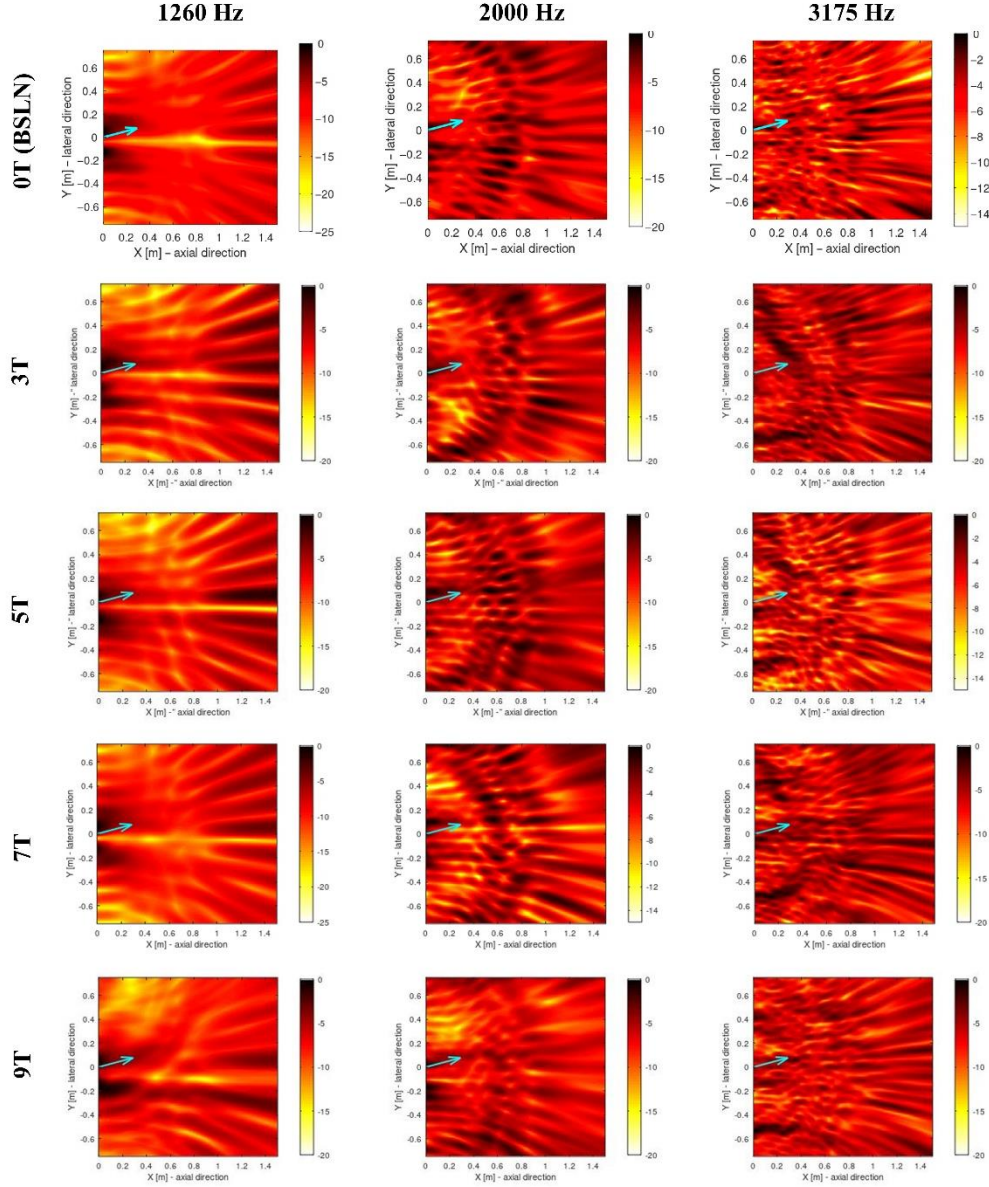


Figure 30. Beamforming (from straight LE, 0T, to 9 serrations per blade, 9T)

The polar directivity diagrams (see Figure 31) complement these observations by highlighting how the radiated energy is redistributed in the far field. At mid frequencies (approximately 1260–2000 Hz), the configurations with serrations generally exhibit smoother angular distributions and moderate reductions of the main lobes, whereas at higher frequencies (3175 Hz) the effect becomes more pronounced, manifesting through broader lobes and reduced maximum levels compared to the reference case. These results are consistent with the expectation that serrations act primarily by modifying phase coherence, a mechanism that becomes more effective as the acoustic wavelength approaches the characteristic size of the serrations. The combination of beamforming and directivity analyses thus confirms both the local modifications of the sources and their consequences on the far-field acoustic field.

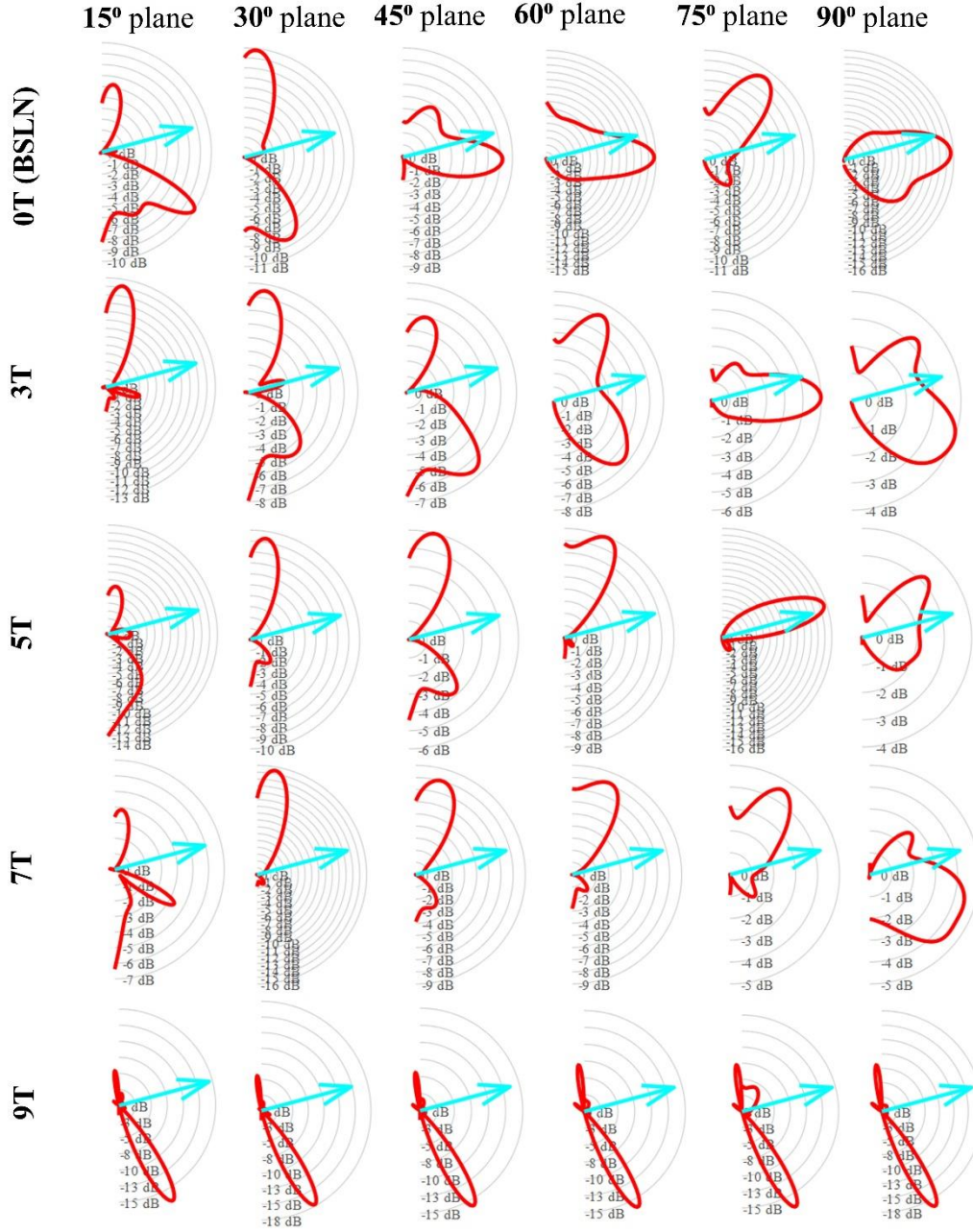


Figure 31. Directivity (from straight LE, 0T, to 9 serrations per blade, 9T)

#### 6.4. Serrations Effects on the Radiated Acoustic Energy

The acoustic pressures were measured using 13 microphones distributed over five inclined planes (30°–90°), arranged on a spherical cap. The 15° plane was excluded in order to avoid near-field effects. The working assumptions are: propagation in an unbounded medium, local isotropy, absence of reflections, and an equivalent point acoustic source located at the center of the array.

The total radiated power through the spherical cap was estimated based on the local acoustic intensity:

$$I_i = \frac{p_{rms,i}^2}{\rho c} \rightarrow P_{calotă} = \sum_{i=1}^N I_i \cdot d\Omega_{eff} \cdot r^2 \quad (31)$$



where  $d\Omega_{eff}$  is the effective solid angle associated with each microphone. This power was used as the initial value to estimate the far-field distribution, under the assumption of a spherical field:

$$I(r) = \frac{P_{calotă}}{4\pi r^2} \rightarrow SPL(r) = 20 \log_{10} \left( \frac{\sqrt{I(r)\rho c}}{p_0} \right) \quad (32)$$

For each configuration (reference and serrated), the cumulative acoustic energy emitted up to a distance  $r$  was calculated by integrating the acoustic intensity:

$$E(r) = \int_{r_0}^r I(r') \cdot 4\pi r'^2 dr' \rightarrow \Delta E(r) = E_{ref}(r) - E_{serrated}(r) \quad (33)$$

To evaluate the global impact of the passive treatments on noise propagation, the energetic differences between the reference configuration and the serrated configuration were normalized by the spherical propagation volume, yielding energy density indicators as a function of distance. These indicators were analyzed over the range 5–100 m, allowing the estimation of the cumulative effect of noise reduction not only in the near field of the source, but also on the dispersion of acoustic energy in the far field. The calculation methodology, propagation assumptions, and numerical implementation are presented in detail in the work in extenso and are accompanied by a dedicated code included in the appendices. Applying this procedure to the cases “ref\_15deg” and “7dinti\_15deg”, based on the raw pressure signals, leads to the trends shown in Figure 32, highlighting the differences in acoustic attenuation as a function of distance.

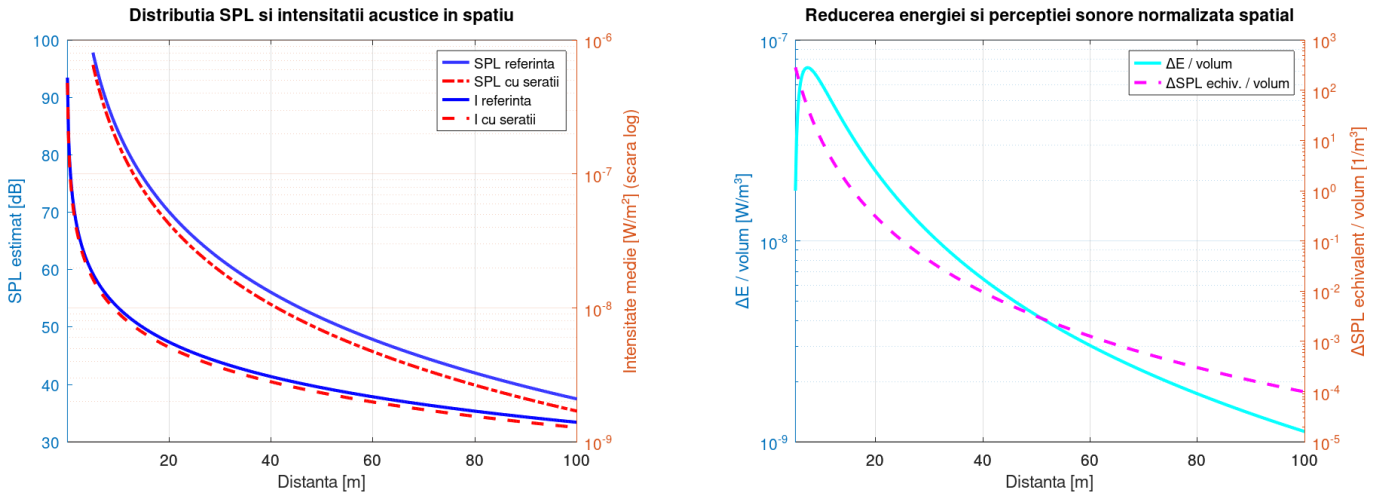


Figure 32. Evolution of relevant parameters with distance

## CHAPTER 7. DERIVATION OF SEMI-EMPIRICAL RELATIONS AND SIMULATION OF THE ACOUSTIC PERFORMANCE OF LEADING EDGE SERRATED CASCADES

### 7.1. Derivation of semi-empirical laws

Generation of aerodynamic noise associated with the interaction between turbulent structures and solid surfaces remains a major challenge in the design of aerodynamic components operating at low and moderate Mach numbers, particularly for applications such as open rotors, wind turbines, and unmanned aerial vehicles, where passive solutions are preferred due to constraints related to mass, energy consumption, and robustness [8] [12] [152] [153] [154] [155] [156] [157]. In this context, serrations applied at the leading or trailing edge have proven effective in reducing broadband noise,

by modifying the mechanisms of scattering of turbulent pressure fluctuations in the vicinity of geometric discontinuities [6] [14].

Classical theoretical foundations, such as the formulations proposed by Howe [23], Amiet [24], or the BPM empirical framework [13], have significantly contributed to the understanding of these mechanisms, but are frequently based on simplifying assumptions that limit their applicability to complex geometries and flow regimes [161] [166] [167]. Consequently, numerous recent studies have highlighted the need for complementary approaches, based on experimental data, capable of capturing the broadband attenuation trends observed in practice [152] [158] [168].

In this thesis, a semi-empirical strategy is adopted, based on functional regressions and ensemble-type methods, to directly correlate acoustic pressure levels with measurable geometric and aerodynamic parameters, without resorting to predefined nondimensional groups. This approach allows the formulation of compact and interpretable predictive models, useful both for analyzing the aeroacoustic mechanisms associated with serrations and for supporting the design process. Unlike established models, which are often calibrated locally and dependent on similarity assumptions, the proposed framework aims at a controlled generalization, validated on reduced-scale experimental datasets. The methodology focuses on modeling SPL differences relative to reference configurations, either resolved spectrally or integrated over third-octave bands, using variables with direct physical significance, such as serration amplitude and density, installation angles, and observation angles. By integrating physical concepts from classical theories with the flexibility of data-driven methods, the study contributes to the development of predictive tools with practical applicability in the design of low-noise aerodynamic components. The general equations are formulated as linear, polynomial, logarithmic, and exponential, and are used for regression of acoustic metrics ( $\Delta$ SPL, OASPL, PWL, PSD).

To investigate the relationship between acoustic response and geometric and angular control parameters, several types of regression models were analyzed, selected according to their ability to capture the trends observed in the SPL data. Linear models were used as a baseline reference, providing a simple description of proportional dependencies, but with limitations in the presence of pronounced nonlinear or directional behaviors. Higher-order polynomial regressions enabled the capture of curvature and local extrema, being suitable for modeling directivity and relevant geometric thresholds. Logarithmic models were introduced to describe diminishing-return effects, frequently observed in SPL variations, while exponential models were used to represent rapid decay or amplification behaviors associated with specific flow or orientation parameters. In addition to these analytical formulations, Random Forest regression was also explored, allowing the automatic identification of complex nonlinear interactions between variables without imposing a predefined functional form, albeit with reduced physical interpretability. All models used the same set of geometric and angular predictors, and performance evaluation was primarily based on the coefficient of determination  $R^2$ , complemented, for representative cases, by indicators such as RMSE and MAE, to quantify absolute prediction errors.

These functional forms are not purely theoretical: similar dependencies have been identified in experimental studies on leading-edge/trailing-edge serrations. Pereira et al. [163] reported a logarithmic relationship between  $\Delta$ SPL and the normalized wavelength parameter  $2h/\lambda$ , highlighting a saturation-type behavior beyond a certain threshold. Their model,  $\Delta\text{SPL}_{\max} = 10 \log_{10}[1 + 4(2h/\lambda)^2]$ , supports the use of such approximations in regression analyses. A more detailed logarithmic formulation for SPL is presented in [170]. In the case of acoustic power, the relationship between OASPL and directivity is described in [171] through a model including trigonometric-logarithmic terms. Additional formulations are mentioned in [172], particularly those related to trailing-edge noise associated with boundary-layer separation. Lee et al. [152] proposed a combined log-polynomial expression to describe narrowband SPL contributions in rotor experiments.

Experimental studies show that the acoustic response of serrated blades depends directly on flow parameters and serration geometry, with reported linear, polynomial, logarithmic, or exponential

dependencies depending on the normalized parameters used (such as  $h/\delta$ ,  $h/\lambda$ ,  $St$ ,  $Re$ , or  $Mach$ ). In particular, logarithmic and exponential formulations better describe the threshold and saturation behaviors observed experimentally, both for spectral SPL and for global indicators such as OASPL and PWL. These trends support the use of compact, regression-based models as efficient tools for describing the influence of geometric and aerodynamic variables on noise generation, in agreement with the analytical process illustrated in Figure 33.

To quantify the influence of each control parameter on SPL, a one-way analysis of variance (ANOVA) was applied, which allows the identification of variables with statistically significant impact and the evaluation of their contribution to the global variation of the acoustic response, through the associated effect size.

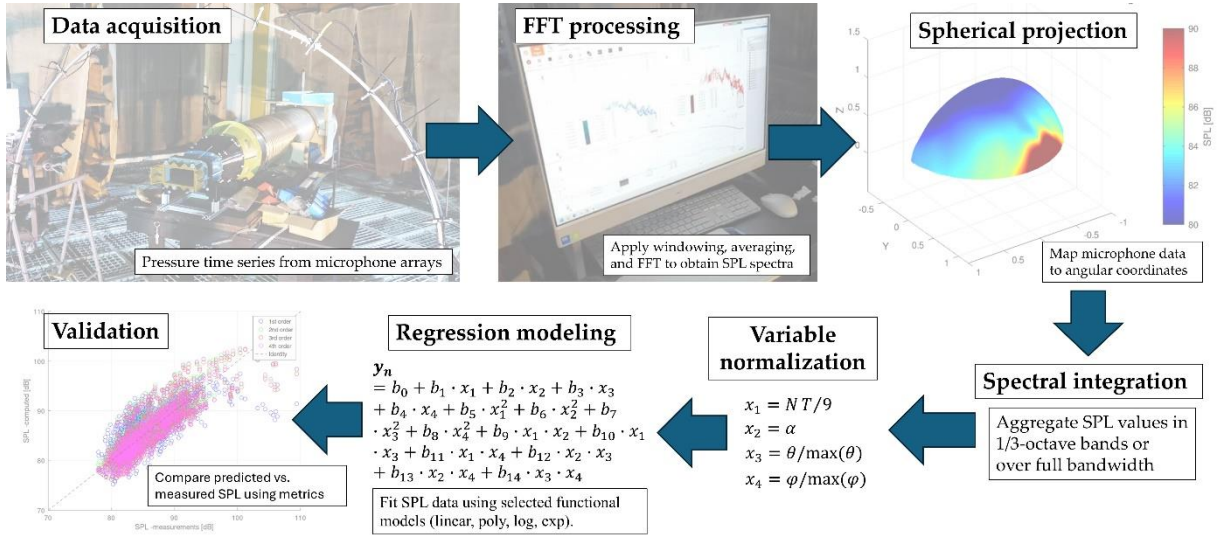


Figure 33. Logical diagram (from data acquisition to regression application and comparative plotting)

The SPL datasets were obtained from measurements using microphones arranged on circular arcs in multiple inclined planes, covering 13 discrete azimuthal positions ( $\theta$ ) and 6 elevation angles ( $\phi$ ), explicitly illustrated in Figure 34. The experimental campaign systematically varied two key geometric parameters: the serration configuration, defined by the number of teeth ( $NT = 0, 3, 5, 7, 9$ ), and the installation angle ( $\alpha = 0^\circ, 5^\circ, 10^\circ, 15^\circ$ ), resulting in 20 distinct test cases. Each configuration therefore captures the combined influence of serration geometry, angle of attack, and observation direction. The SPL values for each test case were organized into CSV matrices of size 6 (elevations)  $\times$  13 (azimuths).

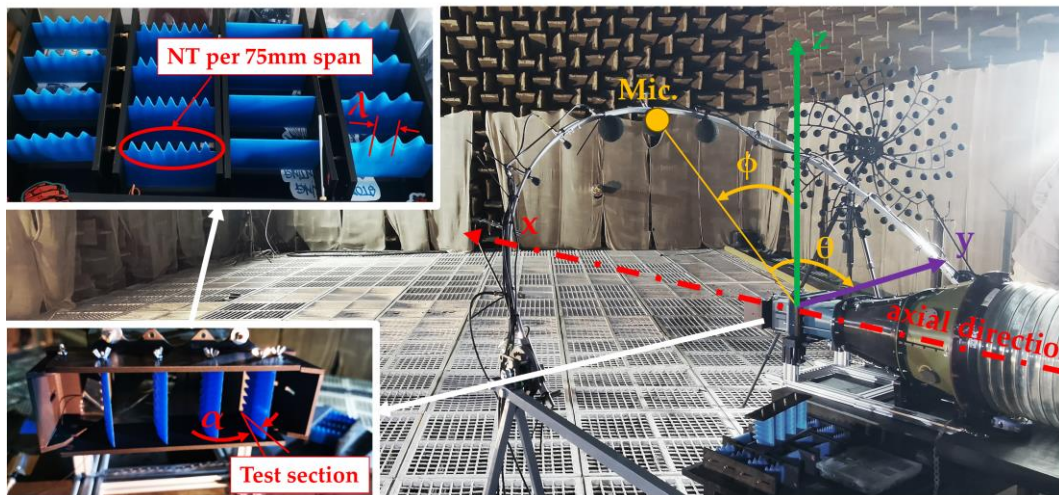


Figure 34. Relevant parameters

To eliminate influences associated with mechanical vibrations or structural coupling within the anechoic chamber, the microphone array was completely decoupled from the aeroacoustic test assembly. The microphones were mounted on an independent semicircular support, with no physical connections to the air supply system or to the load-bearing plate equipped with serrations, thus preventing vibration transmission to the measurement system. The microphones located in the vicinity of the jet were protected with porous foam to reduce local aerodynamic disturbances, without affecting the acoustic response. The analysis of the raw signals did not reveal tonal artefacts or parasitic noise that would require additional preprocessing.

During the preprocessing stage, the data were normalized with respect to the geometric and angular parameters (number of teeth, installation angle, and observation angles). The values corresponding to the low elevation planes (15° and 30°) were excluded, since these positions are strongly influenced by the jet near field and the turbulent shear layer, leading to larger SPL variations and a degradation of the statistical fitting quality. Higher elevation angles (45°–90°) provided more stable directivity patterns, representative of far-field radiation.

The final dataset included four normalized independent variables, and the robustness of the models was assessed using multiple predictor selection variants. Performance was quantified using the coefficient of determination  $R^2$ , and the contribution of each variable was estimated using permutation-based methods. All functional regression and ensemble-type models were implemented entirely in GNU Octave, using dedicated code, without the use of external libraries, ensuring transparency and full control over the modeling process. Complete details regarding the computational algorithms and numerical implementation are presented in the work in extenso, where a dedicated appendix with the corresponding code is also included. The polynomial approximations have the following structure (from first to fourth order), presented in equations (34)–(37).

$$y_{n1} = b_0 + b_1 \cdot x_1 + b_2 \cdot x_2 + b_3 \cdot x_3 + b_4 \cdot x_4 \quad (34)$$

$$y_{n2} = b_0 + b_1 \cdot x_1 + b_2 \cdot x_2 + b_3 \cdot x_3 + b_4 \cdot x_4 + b_5 \cdot x_1^2 + b_6 \cdot x_2^2 + b_7 \cdot x_3^2 + b_8 \cdot x_4^2 \\ + b_9 \cdot x_1 \cdot x_2 + b_{10} \cdot x_1 \cdot x_3 + b_{11} \cdot x_1 \cdot x_4 + b_{12} \cdot x_2 \cdot x_3 + b_{13} \cdot x_2 \cdot x_4 \\ + b_{14} \cdot x_3 \cdot x_4 \quad (35)$$

$$y_{n3} = [\text{all 2nd order terms}] + b_{15} \cdot x_1^3 + b_{16} \cdot x_2^3 + b_{17} \cdot x_3^3 + b_{18} \cdot x_4^3 \quad (36)$$

$$y_{n4} = [\text{all 3rd order terms}] + b_{19} \cdot x_1^4 + b_{20} \cdot x_2^4 + b_{21} \cdot x_3^4 + b_{22} \cdot x_4^4 \quad (37)$$

where  $y_{ni}$  represents the normalized SPL,  $b_0$  is the constant term (intercept), and  $b_1 - b_{22}$  are the regression coefficients. The independent variables are defined as follows:  $x_1 = NT/9$ ,  $x_2 = \alpha$ ,  $x_3 = \theta/\max(\theta)$ , and  $x_4 = \varphi/\max(\varphi)$ . The angle  $\theta$  used in the regressions lies in the  $[0, \pi]$  range, while  $\varphi$  ranges between 15° and 90°. The set angle  $\alpha$  (AoA) is used directly, with values of 0°, 5°, 10° or 15°.

The methods mentioned above, applied to the available datasets, led to the superpositions shown as an example in Figure 35, with the corresponding values of the  $R^2$  coefficient (and other quantitative indicators) listed (also as an example) in Table 1. The specific coefficients of the resulting polynomials are presented explicitly in the appendices of the work in extenso.

*Table 1.  $R^2$  values– all planes' data.*

	1st Degree	2nd Degree	3rd Degree	4th Degree
$\alpha = 0^\circ$	0.4151	0.6314	0.6453	0.6469
$\alpha = 5^\circ$	0.5398	0.7193	−1.9245	0.1198
$\alpha = 10^\circ$	0.4361	0.6660	0.6666	0.6753
$\alpha = 15^\circ$	0.3167	0.6387	0.6501	0.6573

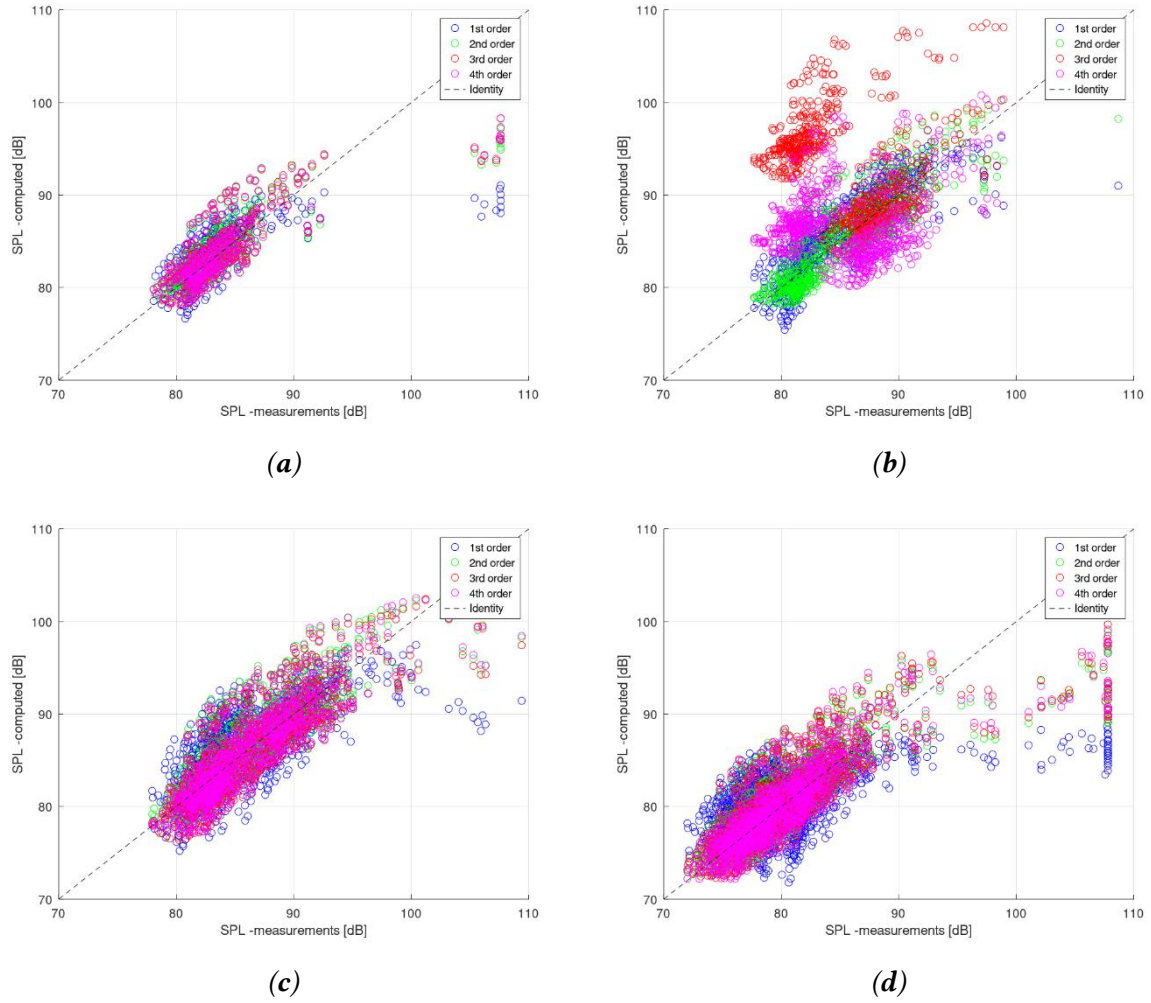


Figure 35. All data (15–90 deg planes): (a)  $\alpha = 0^\circ$ ; (b)  $\alpha = 5^\circ$ ; (c)  $\alpha = 10^\circ$ ; (d)  $\alpha = 15^\circ$ .

Other equations were also tested for fitting the experimental data, using as many independent variables as possible, in an attempt to obtain values as close as possible to the experimental ones. The verified laws are fairly general, being encountered in similar studies as well, and include logarithmic, sinusoidal, or exponential forms. As an example of the proximity of the numerical approximation to the exact data, Table 2 presents values of the  $R^2$  parameter.

Table 2.  $R^2$  values for various laws; 45–90 deg planes.

	Linier	Logaritmic	Sin	Exponential
$\alpha = 0^\circ$	0.6683	0.6750	0.6764	0.6697
$\alpha = 5^\circ$	0.5238	0.5439	0.5830	0.5849
$\alpha = 10^\circ$	0.2824	0.1055	−0.1296	0.2878
$\alpha = 15^\circ$	0.2583	0.1334	0.3064	0.3005

The one-way ANOVA analysis performed for the number of teeth, the angle of attack  $\alpha$ , the polar angle  $\theta$ , and the elevation angle  $\varphi$  indicates that all variables have a statistically significant influence on SPL ( $p < 10^{-8}$ ), as shown in Figure 36. The largest contribution is associated with the



elevation angle  $\varphi$  ( $\eta^2 = 0.219$ ), highlighting the dominant role of the observer position in acoustic directivity. This is followed by the angle of attack  $\alpha$  ( $\eta^2 = 0.169$ ) and the polar angle  $\theta$  ( $\eta^2 = 0.113$ ), while the number of teeth exhibits a smaller but statistically relevant effect ( $\eta^2 = 0.026$ ), confirming the secondary role of geometric parameters compared to flow conditions and observation geometry.

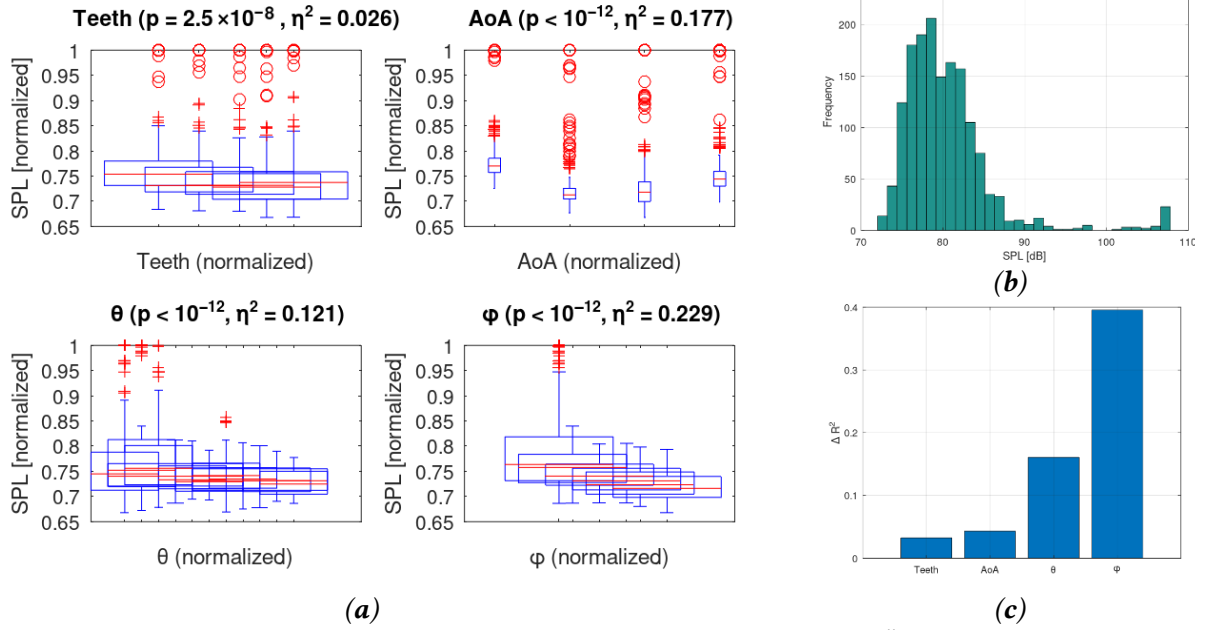


Figure 36. Full dataset analysis: (a) ANOVA boxplots; (b) SPL distribution; (c) “variable importance” (Random Forest).

Overall, the results confirm the multi-parametric nature of jet noise, which is sensitive to both aerodynamic and geometric parameters, supporting the use of multidimensional regression models for SPL prediction. The ANOVA analysis identified the elevation angle  $\varphi$  as the most influential predictor, in agreement with the physics of acoustic propagation and with the directivity of the radiation generated by the jet–serration interaction.

To assess predictive capability, several regression configurations were tested, corresponding to limited or selectively restricted data sets (variants A–H described in the work), by imposing conditions on the observation angles and geometric parameters. The results show that maximum performance was achieved only for very specific configurations, while for most variants the coefficient of determination remained moderate, indicating a complex and nonlinear interaction among the variables. Excessive restriction of the data set led, in some cases, to a significant degradation of performance due to the reduction in variability and sample size.

Although no configuration achieved excellent predictive performance ( $R^2 > 0.9$ ), valuable insights were obtained regarding the sensitivity of SPL to each parameter. The results confirm that multivariate and interaction effects dominate the SPL behavior in flows with serrated leading edges. Future modeling approaches could explore nonlinear methods or an expansion of the data set to increase the robustness of the predictions.

## 7.2. Leading edges serrated blades simulation in cascade configuration

The present chapter addresses the numerical–experimental validation of stages with modified leading edges. Small-scale experiments provide controlled conditions and high spatial resolution, while a range of turbulence modeling strategies—Spalart–Allmaras,  $k-\omega$  SST,  $k-\varepsilon$ , SAS, and LES (whose formulations are thoroughly documented in [213], [214], and [215])—are evaluated in transient simulations with variable temporal resolutions. The emphasis is placed on their ability to reproduce the measured spectra and to capture the dominant mechanisms of jet–blade interaction noise.



Comparisons with experiments indicate that interaction noise is negligible at low frequencies and well captured at high frequencies. While the Spalart–Allmaras and  $k-\omega$  SST models reproduce the low-frequency regime, SAS provides the best overall agreement in the mid-to-high frequency range, albeit with a slight overestimation, whereas LES satisfactorily reproduces the baseline response but at a significantly higher computational cost. These findings highlight the model-dependent trade-offs, clarify temporal resolution requirements, and confirm the relevance of numerical simulations as predictive tools for assessing the aeroacoustic benefits of bio-inspired leading-edge serrations.

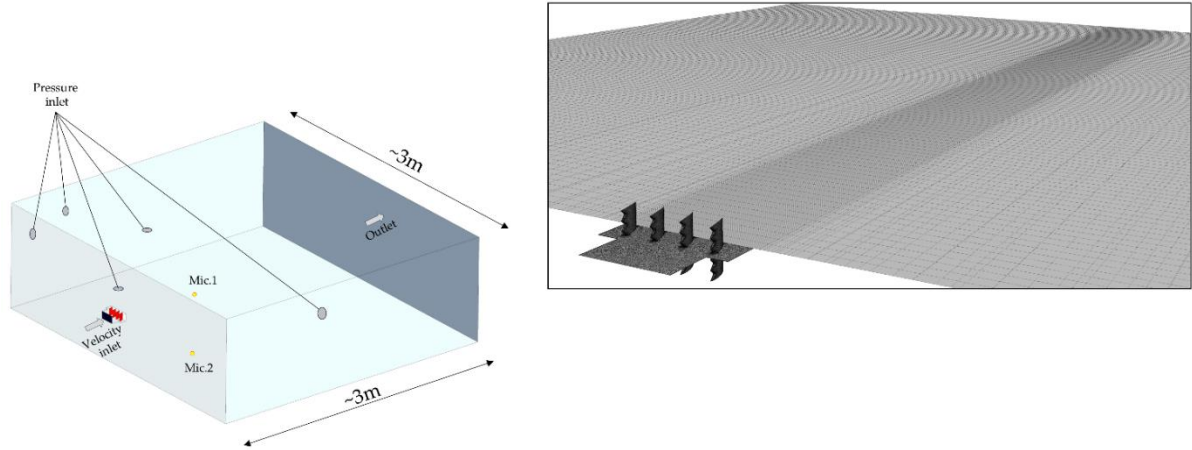


Figure 37. Computational domain and mesh.

The numerical simulations reproduced the experimental configuration and were divided into two regions. The near-field region resolved the interior of the cascade and the nozzle using a predominantly structured mesh (Figure 37) around the solid surfaces (blades and walls), with a wall spacing chosen to achieve  $y^+ \approx 1$ . The inlet boundary conditions prescribed a mean velocity of 50 m/s, a turbulence intensity  $Tu=10\%$ , and an integral length scale  $\Lambda=2.5\text{mm}$ , representing the interaction-noise condition generated experimentally by the physical grid. The outer region extended over approximately 3 m in length and width to include virtual microphone points coincident with the experimental sensor locations (radius of 1 m at  $10^\circ$  and  $90^\circ$ ). The far-field boundaries were set as non-reflecting to avoid acoustic contamination of the spectra. Five turbulence modeling strategies, commonly used in broadband aeroacoustics, were evaluated for both geometries: Spalart–Allmaras (SA),  $k-\omega$  SST,  $k-\epsilon$ , Scale-Adaptive Simulation (SAS), and Large-Eddy Simulation (LES).

The transient solutions were initialized from a statistically steady state obtained with a physical time step of 1 ms; stabilization was verified by monitoring the temporal evolution of  $p_{\text{rms}}$  and  $dp/dt$  until statistical stationarity was reached (Figure 38). The unsteady runs then continued with a time step  $\Delta t=10^{-5}\text{s}$ , for 1,800–2,000 steps and up to 20 inner iterations per step (to ensure that the spectral decay and peak locations were not artifacts of insufficient temporal resolution). For noise prediction using the FW–H equation, the formulation described in [197] was employed, starting from the general equation through to the Lighthill stress tensor ( $T_{ij}$ ) and the expressions for the compressive stress tensor ( $P_{ij}$ ).

A numerical grid convergence study was performed by analyzing several levels of discretization. An intermediate grid was selected for the comparison of turbulence models, providing an adequate compromise between spectral fidelity and computational cost. Figure 38 presents the comparison between the experimentally measured acoustic spectra and those obtained numerically, for both blade self-noise and jet–blade interaction noise, at the two microphone positions. The numerical prediction was carried out using the FW–H analogy and by extracting pressures at points collocated with the experimental microphones. The numerical signals were processed identically to the experimental ones, allowing a direct comparison, particularly in the frequency band dominated by interaction noise.

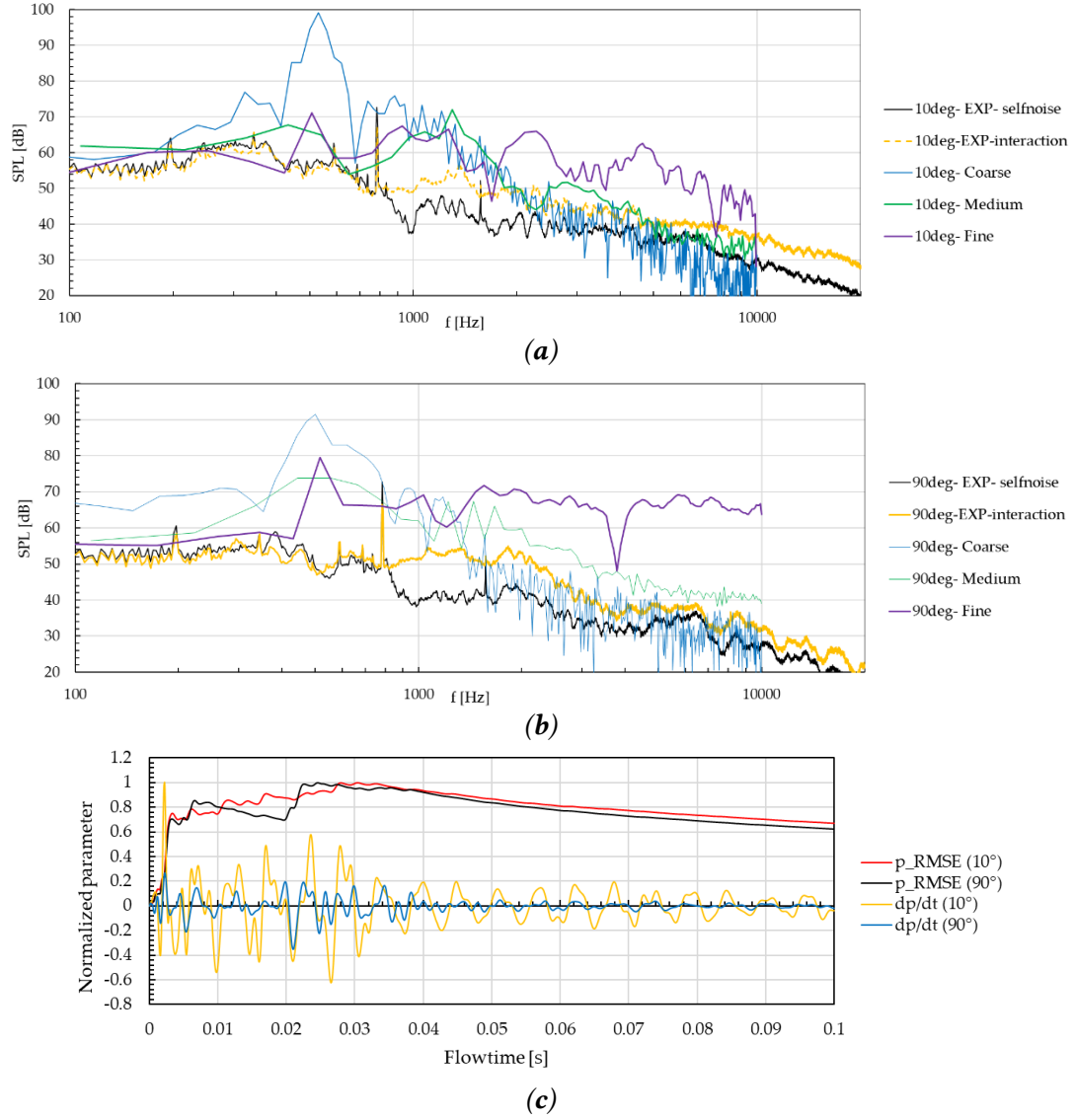


Figure 38. Stabilized solution and mesh stability analysis: (a) axial microphone (10°), blades with serrations; (b) lateral microphone (90°), blades with serrations; (c) stabilized solution (1 ms) prior to transient simulation.

For the quasi-axial microphone, the coarse grid overestimates the low-mid frequencies, exhibiting a broad hump that reaches a maximum around a few hundred hertz and remains elevated up to ~1 kHz. The intermediate grid follows more closely the experimental interaction-noise trend in the 1–5 kHz range, whereas the fine grid shows pronounced oscillations and local maxima (e.g., between 1.5–3 kHz) that are not observed in the measurements. For the lateral recording, the coarse-grid case again overestimates in the 0.5–1 kHz band; the intermediate variant is systematically closer to the interaction-noise spectrum over most of the band, while the fine variant remains higher and relatively flat over a wide frequency range, with a local drop around ~2 kHz.

Overall, Figures 38(a) and (b) indicate that a grid-independence plateau is reached at the intermediate resolution: the transition from the Coarse to the Medium grid clearly improves spectral agreement, whereas further refinement does not provide consistent benefits and may introduce artefacts if not supported by longer temporal histories and stricter temporal resolution. Comparative results for the reference configuration and the serrated configuration are presented in Figure 39. Unless otherwise stated, simulations were performed on the Medium grid, with stabilized initialization and a comparable number of time steps, the SPL being derived from the numerical PSD via FFT. The predictions are generally consistent across models, with more pronounced differences at low

frequencies ( $<1$  kHz) and good agreement in the frequency band of interest, 2–5 kHz, particularly for the SAS model, which offers a favorable compromise between accuracy and computational cost.

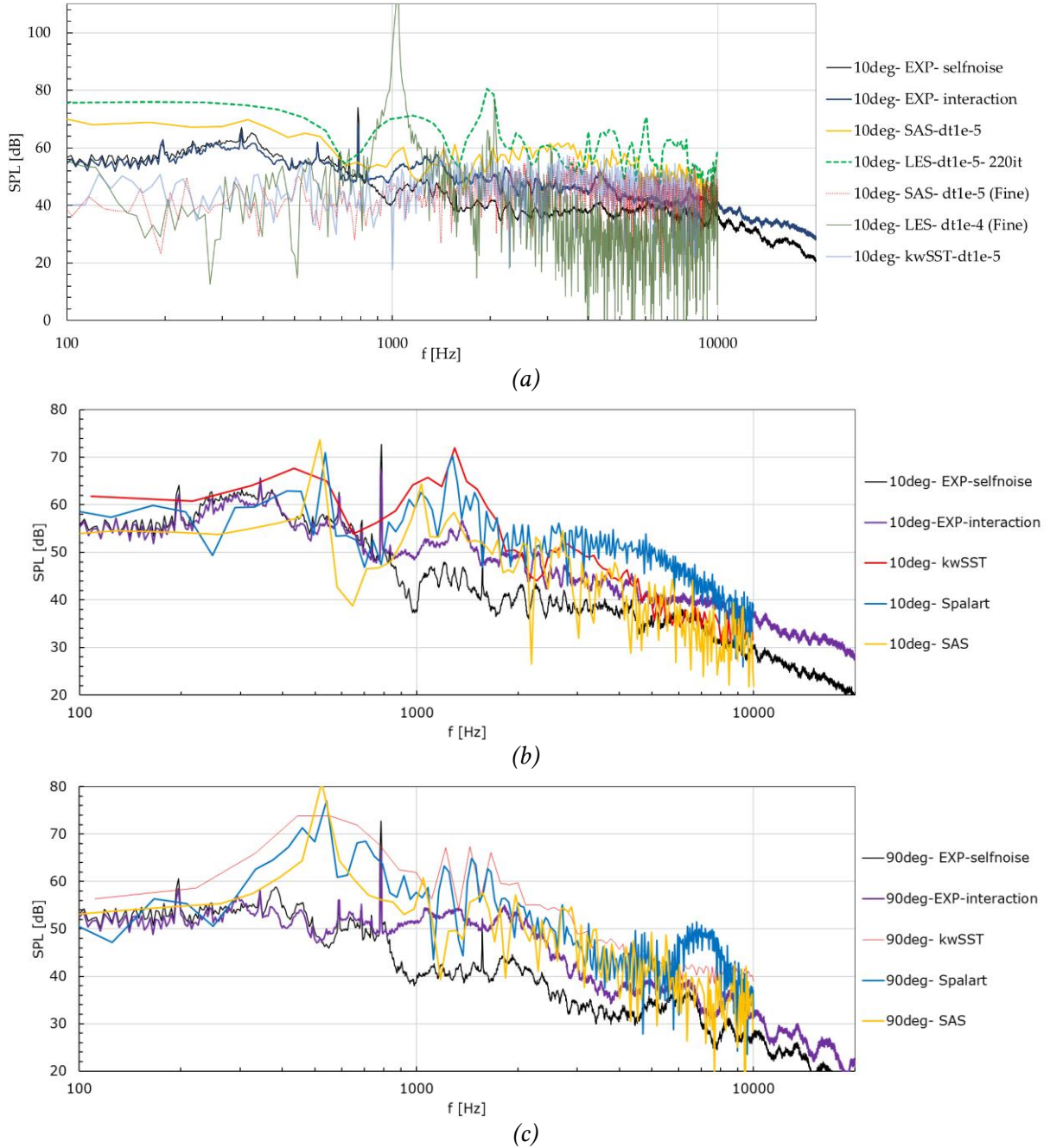


Figure 39. Overlaid spectra: (a) different models for the reference blade (straight leading edge,  $10^\circ$  direction); (b) different models for the reference blade (straight leading edge,  $10^\circ$  direction,  $\Delta t = 10^{-5}$  s); (c) different models for the serrated blade ( $90^\circ$  direction,  $\Delta t = 10^{-5}$  s).

The analysis for the microphone at  $10^\circ$  (Figure 39(a)) highlights the critical role of temporal resolution: LES requires very small time steps to avoid noisy spectra, whereas SAS and  $k-\omega$  SST more robustly reproduce the mid-frequency band, with slight local overestimations. For the serrated geometry (Figure 39(b)), no single model dominates across the entire band:  $k-\omega$  SST tends to overestimate low frequencies, SA follows the high-frequency slope more accurately, and SAS remains competitive in the central region.

For the lateral position (Figure 39(c)),  $k-\omega$  SST most coherently reproduces the experimental envelope up to approximately 2–3 kHz, while SA and SAS exhibit local maxima that are not observed experimentally. These results indicate that the hierarchy of turbulence models depends on the observation angle, underscoring the need for multi-angle validation for a robust assessment of

numerical performance. Figure 40 overlays the spectra computed for three acoustic source scenarios—the near-blade domain, the outer domain, and the combined case—sampled at the same receiver locations as in the previous figures. For this analysis, the  $k$ - $\omega$  SST model was used with a time step of  $\Delta t = 10^{-5}$  s, and the results were obtained after slightly more than 500 time steps.

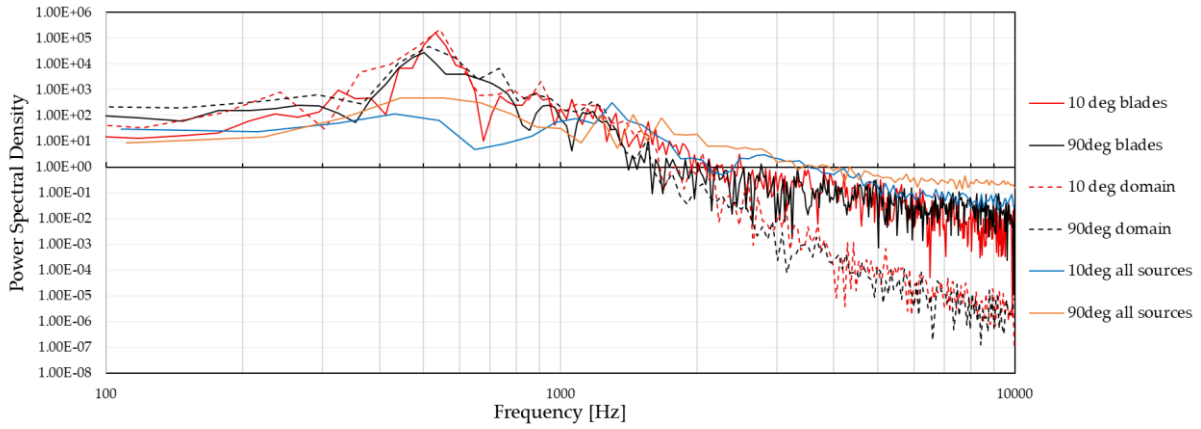


Figure 40. Blades vs free domain sources

### 7.3. Pressure fluctuations coherence (“spanwise coherence”) for the serrated leading-edge configuration. Unsteady statistics.

The methodology aims to evaluate the three-dimensional organization of the unsteady pressure field on the blade surface, with emphasis on the leading edge, by quantifying the spatial correlation of pressure fluctuations in the spanwise direction using magnitude-squared coherence. Data acquisition was performed only after a statistically stationary regime was reached, verified by the stabilization of the mean and RMS pressure values over several flow-through times. The analysis was based on pressure signals extracted at discrete points on the blade surface, distributed along the leading edge and selected so as to include both peak and valley regions of the serration relative to the mid-plane (Figure 41), allowing characterization of the spatial structure of the fluctuations and subsequent comparisons in the chordwise direction.

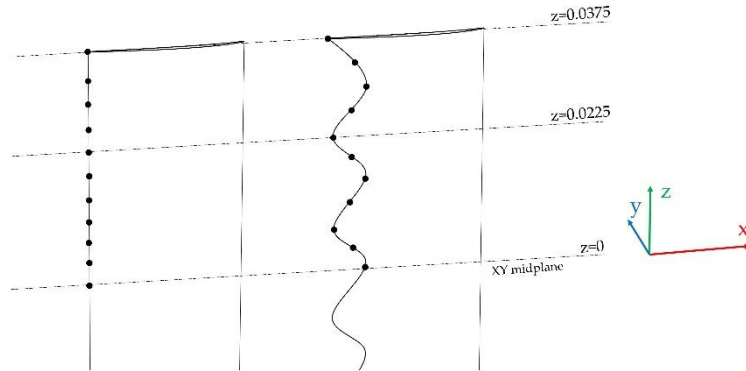


Figure 41. Simulation report points.

$$p'_{i(t)} = p_{i(t)} - \overline{p_{i(t)}} \quad (38)$$

In the analysis of the spatial coherence of pressure fluctuations, the numerical signals were first preprocessed to remove slow quasi-static variations and the initial transient portion, so that the evaluation was based exclusively on a statistically stable regime. The available data contain only the spanwise coordinate  $z$ ; therefore, the study addresses exclusively the decorrelation of fluctuations along the leading edge, as a function of the separation between points along the blade span. Coherence

was estimated in the frequency domain for all available pairs of points using a robust spectral method (Welch), and subsequently averaged both over frequency bands and over pairs with the same spanwise separation, in order to reduce sensitivity to numerical noise, narrowband spikes, and local bias. From these results, a characteristic coherence length was extracted, which synthesizes the rate of decay of correlation along the blade: large values indicate extended coherent structures, whereas small values suggest rapid decorrelation induced by geometry. The analysis focused on the frequency band relevant to interaction noise (kilohertz range), where serrations are expected to modify not only the SPL level but also the spatial organization of the acoustic source. The results, presented in Figure 42, were obtained using a dedicated code implemented in GNU Octave (with the dedicated code included in the work in extenso) and provide a complementary indicator to acoustic spectra, directly linked to the physical noise-reduction mechanisms.

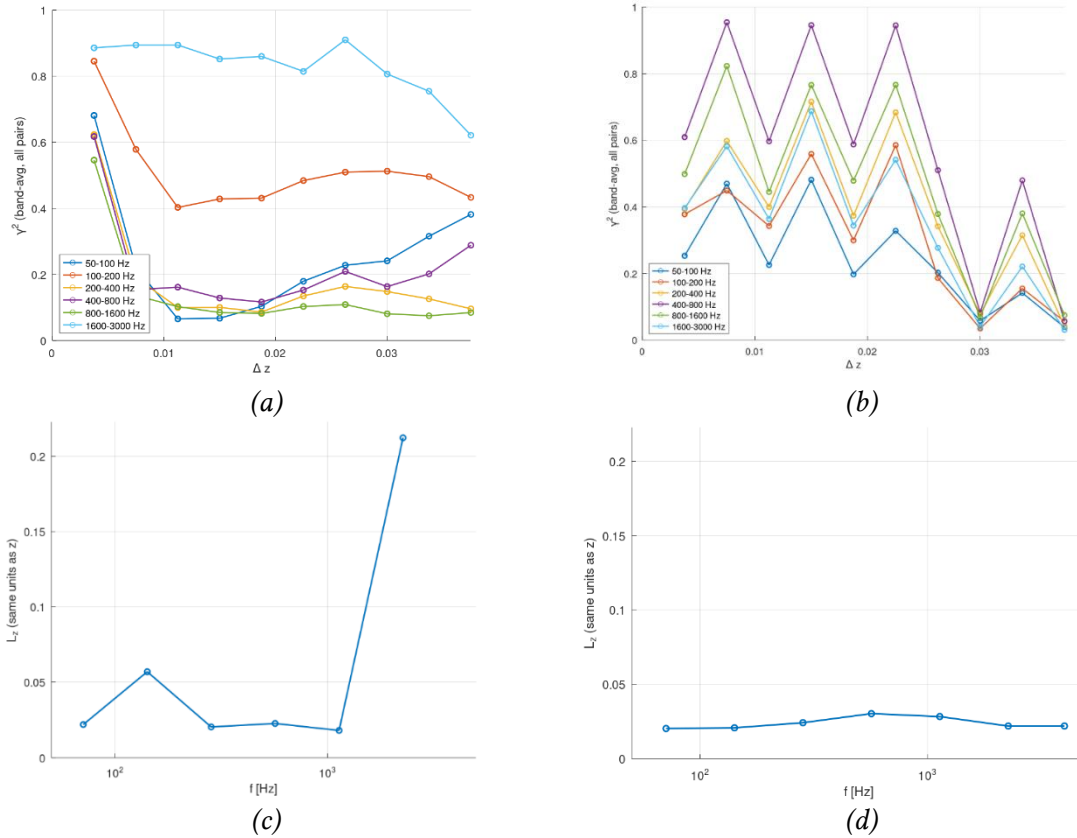


Figure 42. Spanwise coherence analysis along the blade: (a) coherence averaged over frequency bands, reference; (b) coherence averaged over frequency bands, serrations; (c) characteristic length  $L_z$  (result averaged over all values), reference; (d) characteristic length  $L_z$  (result averaged over all values), serrations.

The analysis of pressure unsteadiness on the blade surfaces is complemented by statistical representations that highlight the differences between turbulence models through the way they treat unsteady scales. The  $k-\omega$  SST model tends to maintain higher levels of modeled turbulence in the leading-edge region, which is reflected in a more pronounced content at low and mid frequencies. In contrast, SAS adaptively reduces the turbulent viscosity where unsteadiness is partially resolved, promoting a transfer of energy toward higher frequencies, while LES resolves an even larger portion of the turbulent spectrum, at a significantly higher computational cost. Figure 43(a–d) illustrates these differences through the pressure time-derivative indicator ( $dp/dt$ ): the surface maps and axial sections show that, relative to the reference configuration, blades with serrations exhibit reduced spanwise continuity and a faster downstream attenuation of the loadings. This spatial fragmentation is consistent with a phase modulation induced by the leading-edge serrations, which limits the coherent accumulation of unsteady forces and supports the spectral reductions observed in the frequency band of interest.



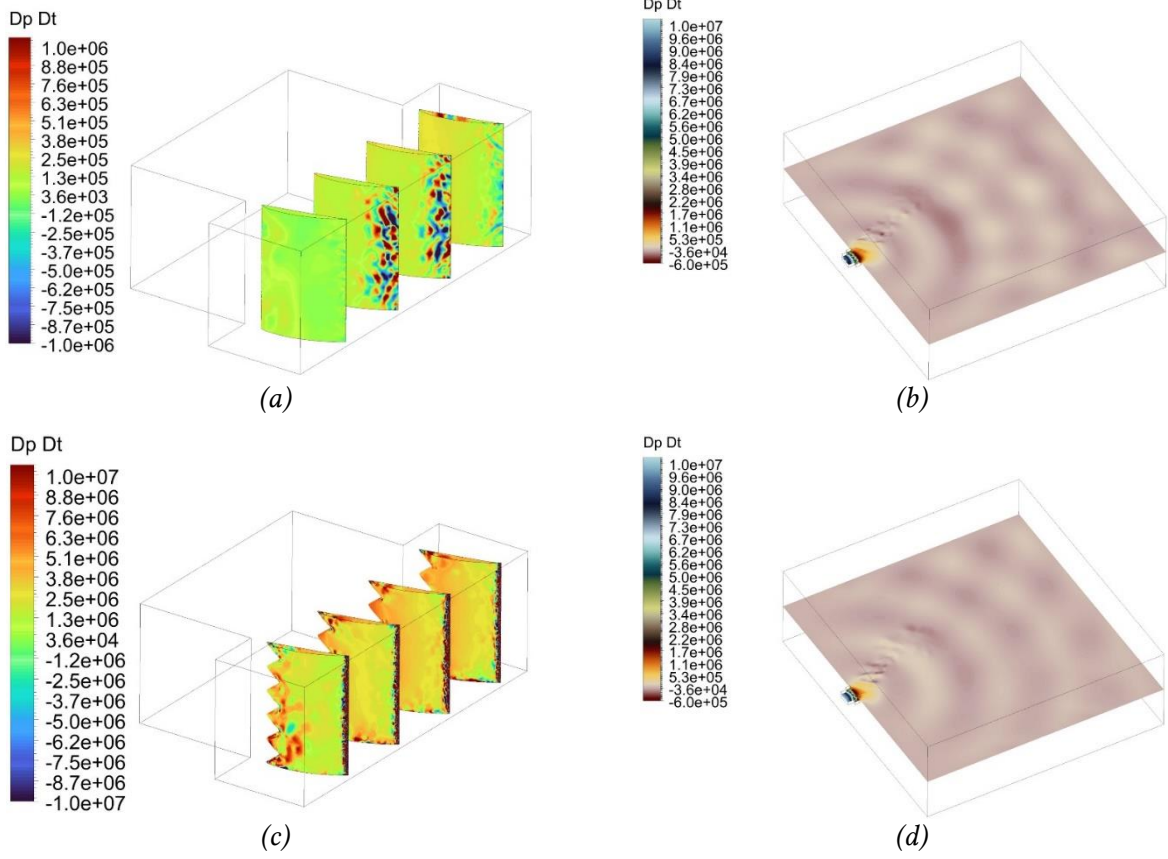


Figure 43. Comparison of  $dp/dt$ : straight leading edge vs. serrations, LES,  $dt = 10^{-4}$  s,  $t \approx 50$  ms: (a) reference (representation on the blade surface); (b) reference (representation in the axial plane); (c) serrations (representation on the blade surface); (d) serrations (representation in the axial plane).

The iso-surfaces in Figure 44 provide a three-dimensional perspective on the unsteady structures. In the case of the straight leading edge, the  $dp/dt$  field forms large lobes with continuity throughout the computational domain, suggesting a spanwise-correlated loading. In the serrated case, at the same threshold ( $dp/dt = 2 \times 10^{-4}$  Pa/s), the lobes become narrower and more fragmented, segmented by the serrated geometry, with a visibly reduced lateral/longitudinal continuity. This topological modification is consistent with a phase variation imposed by the serration geometry: the incident vortices/turbulence decorrelate laterally, limiting the constructive accumulation of unsteady forces and promoting a faster downstream attenuation.

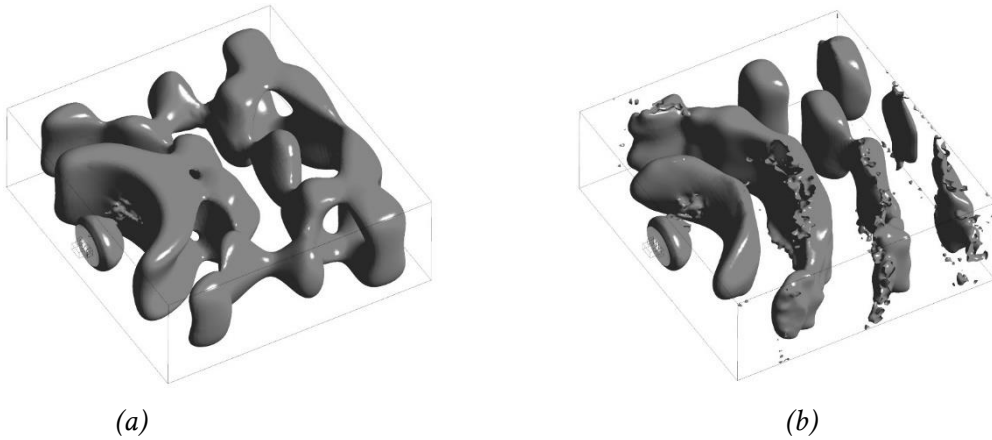


Figure 44. Iso-contours ( $dp/dt=2 \cdot 10^{-4}$  Pa/s, LES): (a) baseline; (b) serrations.



## 7.4. Further development of the directivity analysis

Noise generated by turbulence–airfoil interaction and by rotor–stator interaction mechanisms remains a central issue in the aeroacoustics of subsonic fans, propellers, and compressors. While incident turbulence produces broadband noise dependent on vortex intensity and scales, rotor–stator interactions introduce well-defined tonal components. In this context, leading-edge serrations represent a promising passive solution, as they modify the local receptivity to incident turbulence, reduce the coherence of pressure fluctuations, and promote the redistribution of acoustic energy in the far field. Analytical models and experimental studies show that the efficiency of this mechanism depends critically on the serration geometry and on the ratio between turbulence scales and the serration wavelength; however, scaling to real rotor–stator configurations remain incompletely understood. The present study focuses strictly on turbulence–blade interaction and analyzes the influence of serration geometric parameters on SPL levels and on the angular redistribution of noise, using beamforming and polar directivity diagrams.

The experiments are conducted on a compact blade cascade exposed to a controlled subsonic flow, with 3D-printed serrated inserts and upstream turbulence grids for controlling the flow scales. Measurements are performed in an anechoic environment, using a semicircular microphone array arranged in multiple inclined planes, enabling the capture of the three-dimensional distribution of acoustic radiation within a single campaign. The signals are processed using standard spectral analysis and beamforming techniques, complemented by deconvolution methods to improve source contrast and by polar representations for directivity assessment.

The beamforming maps (Figure 45) indicate that the reference blade, with a straight leading edge, generates compact and coherent sources concentrated near the leading edge. The introduction of serrations leads to a progressive fragmentation of these sources and to a reduction in the maximum intensity, an effect that is more evident for configurations with a larger number of teeth, in agreement with the hypothesis of incident-turbulence decorrelation. The polar diagrams (detailed in the full manuscript) show that these local modifications translate into an angular redistribution of acoustic energy: at medium and high frequencies, the serrated configurations exhibit broader lobes and reduced peak levels compared to the baseline case. The results confirm that serrations act primarily by modifying the phase coherence of the sources, with more pronounced effects when the acoustic wavelength is comparable to the geometric scale of the serrations. The data presented correspond to the maximum installation angle tested ( $15^\circ$ ), where the turbulence–leading-edge interaction is most intense, thus providing a robust framework for validating the experimental methodology and the processing workflow. The analysis of additional cases at lower incidences will complete the picture and allow the evaluation of angular dependence, contributing to a systematic interpretation of how serration geometry and flow conditions govern the spatial and angular characteristics of the radiated noise.

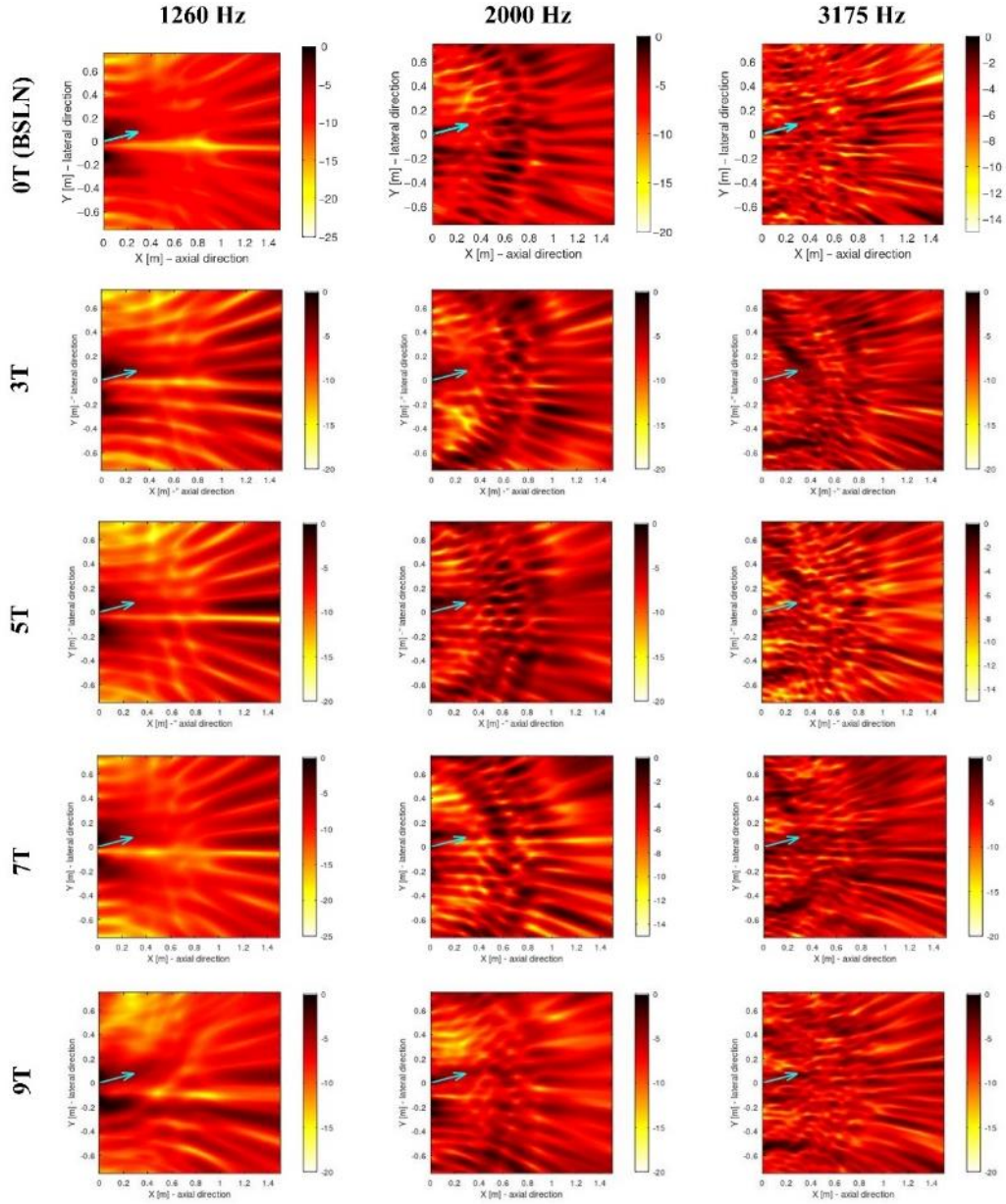


Figure 45. Beamforming (straight LE, 0T, vs various serrations).

## CHAPTER 8. CONCLUSIONS

### 8.1. General conclusions

The present thesis had as its main objective the investigation of the mechanisms of aerodynamic noise generation associated with turbomachinery blades and the evaluation of the efficiency of passive serration-type solutions, through an integrated experimental and numerical approach. The study highlighted the deeply interdependent nature of aerodynamic and acoustic phenomena, confirming that the noise generated by blades is the direct result of the interaction between the structure of the turbulent flow and the airfoil geometry, particularly in the leading-edge region.

The results obtained show that serration-type solutions can lead to significant reductions in the overall sound pressure level; however, their efficiency is strongly conditioned by geometric parameters, by the characteristics of the incident turbulence, and by the blade installation

configuration. In this sense, the thesis demonstrated that the hypotheses and conclusions formulated for isolated blades cannot be automatically transferred to blades arranged in cascades, where additional aerodynamic and acoustic interaction mechanisms arise.

Through the development of a dedicated experimental facility and the comparative analysis of multiple geometric configurations, it was possible to identify clear trends regarding the aeroacoustic behavior of serrated blades. These results contribute to a better understanding of the phenomenon and provide a basis for the controlled use of serrations in real turbomachinery applications and beyond.

## **8.2. Thesis novelty**

The main novelty of the thesis lies in the systematic investigation of the aeroacoustic behavior of serrated blades not only in an isolated airfoil configuration, but also in a cascade configuration, an approach that is relatively rarely encountered in the specialized literature despite its obvious practical relevance. This direction made it possible to highlight specific features of blades operating in cascades, which cannot be captured through classical studies on isolated airfoils.

Another element of originality is the direct correlation established between the geometric parameters of the serrations, the characteristics of the incident turbulence, and the global acoustic response (sound pressure level as well as the phase shift of pressure fluctuations along the blade), based on a coherent set of controlled experiments (installation angles, various serration parameters). Through this approach, the thesis goes beyond the level of qualitative analysis and provides quantifiable results, useful for the comparative evaluation of constructive solutions.

Furthermore, the formulation of experimental and semi-empirical relations derived from real data, tailored to the configurations investigated, represents an original contribution, considering the limitations of classical analytical models in fully describing aeroacoustic phenomena under real operating conditions.

## **8.3. Personal contributions**

The original contributions of the thesis are embedded in a coherent framework that integrates a critical analysis of the specialized literature, experimental development, and numerical modeling, with the aim of deepening the understanding of aeroacoustic mechanisms associated with turbomachine blades equipped with passive serration-based solutions. A first significant contribution consists in a critical synthesis of existing passive solutions for the reduction of aerodynamic noise, with a particular focus on applications relevant to turbomachinery and aeronautical engines. This analysis made it possible to identify the limitations of existing approaches and highlighted the insufficiently explored nature of studies dedicated to blades operating in cascade configurations, thereby clarifying the research directions subsequently addressed in the thesis.

A major contribution is represented by the design, development, and validation of a miniaturized experimental facility dedicated to the study of the interaction between a turbulent jet and blades with or without serrations. The experimental rig, largely manufactured using additive manufacturing techniques (3D printing with different materials), was conceived to allow precise control of the global flow parameters and of the incident turbulence characteristics, such as turbulence intensity and integral length scale. This was achieved through prior dimensional design and numerical simulation of the flow path and of the elements introduced into the convergent channel. In this context, numerical analyses of the flow-path aerodynamics were carried out, together with analytical calculations of the turbulence spectra generated by grids (initially proposed in several variants to target frequency bands relevant to the BPF region), followed by their experimental validation. This

ensured consistency between theoretical assumptions, numerical simulations, and experimental measurements.

The thesis also provides original contributions through the experimental investigation of blades with leading-edge modifications (referred to throughout the thesis as serrations) arranged in cascade configurations. A comparative analysis of blades with a constant aerodynamic profile along the span, with serrations applied at the leading edge and/or trailing edge, enabled the identification of specific spectral and spatial features of the generated noise, depending on geometry, microphone positioning, and the analyzed frequency band. These results complement the existing literature by providing original experimental data for configurations that have been rarely investigated to date. The order of magnitude of the reductions in sound pressure level obtained during the experimental campaigns is comparable to those reported in the literature, while in certain frequency bands improved performance was identified, attributable to the occurrence of destructive interference phenomena, as expected for cascade-type configurations.

An important contribution of the work consists in extending the acoustic analysis toward the evaluation of the acoustic field over an extended spatial region, by using a mobile arc equipped with an array of 13 microphones. Adapting the experimental setup for measurements on a spherical cap enabled the acquisition of a detailed representation of the spatial distribution of sound pressure levels. Dedicated processing, interpolation, and visualization methods were developed (with the corresponding codes attached to the thesis), including representations in the form of acoustic lobes (supported by CFD-based numerical simulations), which facilitated direct comparison between different blade configurations and the identification of directional noise characteristics.

The contributions of the thesis also extend into the domain of experimental data modeling and processing, through the formulation of semi-empirical laws for estimating sound pressure levels as functions of geometric and operational parameters. Based on extensive experimental datasets, functional regression techniques and ensemble learning methods were applied and further developed, yielding polynomial, exponential, logarithmic, and sinusoidal relationships capable of capturing the global trends of the generated noise. Statistical analyses based on ANOVA and the application of Random Forest regression algorithms allowed the quantification of the contribution of each parameter to the global noise and the assessment of the robustness of the proposed models—an analysis of such depth and complexity not previously identified in the specialized literature on this topic.

Complementing the experimental approach, the thesis further contributes through an advanced numerical analysis of serrated blades in cascade configurations, by comparing predictions obtained with various turbulence models against experimental results. The numerical studies highlighted the role of different blade regions in noise generation and enabled the identification of frequency bands in which satisfactory agreement between simulations and measurements can be achieved, including through the use of computationally less expensive RANS-based models. This approach provides a realistic perspective on the use of numerical methods in aeroacoustic design, emphasizing both their potential and their inherent limitations.

## **8.4. Future perspectives**

The results obtained within this thesis open several directions for future research. A first perspective concerns extending the study toward a broader range of operating parameters, including variations in flow velocity, turbulence intensity, and angle of incidence, in order to assess the robustness of serration-based solutions.

In addition, the integration of advanced numerical approaches, such as fully coupled CFD–aeroacoustic simulations, could enable a more detailed analysis of the local noise generation mechanisms and provide further validation of the proposed experimental relationships. Another promising research direction involves the investigation of three-dimensional serrations with more

complex geometries (not limited to sinusoidal shapes), as well as combinations of passive control solutions, with the objective of achieving enhanced acoustic reductions without significant aerodynamic penalties.

Finally, the methodology developed in this thesis can be extended and adapted to other engineering applications, such as wind turbines, cogeneration turbines, industrial fans, or ventilation systems, thereby facilitating the transfer of the results to related fields and contributing to the consolidation of applied aeroacoustic research.

## PUBLICATIONS AND PROJECTS

### I. Publications in WOS journals in the field of PhD thesis

- **Totu, A.-G.**, Cican, G., & Crunțeanu, D.-E. (2024). Serrations as a Passive Solution for Turbomachinery Noise Reduction. *Aerospace*, 11(4), 292. <https://doi.org/10.3390/aerospace11040292> (*Aerospace*, Q2)
- **Totu, A.-G.**, Olariu, C.-T., Trifu, A.-T., Totu, A.-C., & Cican, G. (2024). Development and Assessment of a Miniaturized Test Rig for Evaluating Noise Reduction in Serrated Blades Under Turbulent Flow Conditions. *Acoustics*, 6(4), 978-996. <https://doi.org/10.3390/acoustics6040054> (*Acoustics*, Q3)
- **Totu, Andrei-George**, Marius Deaconu, Laurențiu Cristea, Alina Bogoi, Daniel-Eugeniu Crunțeanu, and Grigore Cican. 2024. "Experimental Analysis of Acoustic Spectra for Leading/Trailing-Edge Serrated Blades in Cascade Configuration" *Processes* 12, no. 11: 2613. <https://doi.org/10.3390/pr12112613> (*Processes*, Q2)
- **Totu, A.-G.**; Crunțeanu, D.-E.; Deaconu, M.; Cican, G.; Cristea, L.; Levențiu, C. Application of Passive Serration Technologies for Aero-Engine Noise Control in Turbulent Inflow Environments. *Technologies* 2025, 13, 363. <https://doi.org/10.3390/technologies13080363> (*Technologies*, Q1)
- **Totu, A.-G.**; Crunțeanu, D.-E.; Drăgășanu, L.; Cican, G.; Levențiu, C. SPL-Based Modeling of Serrated Airfoil Noise via Functional Regression and Ensemble Learning. *Computation* 2025, 13, 203. <https://doi.org/10.3390/computation13090203> (*Computation*, Q2)
- **Totu, A.-G.**; Crunțeanu, D.-E.; Isvoranu D.; Bio-Inspired Blade Cascades: Numerical Predictions versus Experimental Measurements, *Biomimetics* 2026, 11(3), 199; <https://doi.org/10.3390/biomimetics11030199> (*Biomimetics*, Q1)

### II. Participation in conferences with papers on the topic of the PhD thesis

- **Totu, A.-G.**; Crunțeanu, D.-E.; Cican, G.; *Aeroacoustic Directivity of Serrated Blades under Turbulent Jet Interaction*, CEAS/AIDAA 2025 Conference, 1-4 December 2025

## REFERENCES

- [1] Azimi, Mohammadreza & Ommi, Fathollah. (2014). Fan Noise Sources and Passive Reduction Methodologies in High Bypass Turbofan Engines. *Noise & Vibration Worldwide*. 45. 18-22. 10.1260/0957-4565.45.5.18.
- [2] Paruchuri, Chaitanya. (2017). Aerofoil geometry effects on turbulence interaction noise, University of Southampton, PhD thesis
- [3] Weger M, Wagner H (2016) Morphological Variations of Leading-Edge Serrations in Owls (Strigiformes). *PLoS ONE* 11(3): e0149236. doi:10.1371/journal.pone.0149236

- [4] Fish, Frank & Weber, Paul & Murray, M. & Howle, Laurens. (2011). The Tubercles on Humpback Whales' Flippers: Application of Bio-Inspired Technology. *Integrative and comparative biology*. 51. 203-13. 10.1093/icb/icr016.
- [5] B. Lyu, M. Azarpeyvand, On the noise prediction for serrated leading edges, *Journal of Fluid Mechanics* 826, DOI: 10.1017/jfm.2017.429
- [6] M. Gruber, Airfoil noise reduction by edge treatments, University of Southampton, PhD thesis, 2012
- [7] T. M. Biedermann, F. Kameier, C. O. Paschereit, Statistical–Empirical Modeling of Airfoil Noise Subjected to Leading-Edge Serrations, *AIAA JOURNAL*, DOI: 10.2514/1.J055633
- [8] J. Ryi, J. Choi, Estimation Method to Achieve a Noise Reduction Effect of Airfoil with a Serrated Trailing Edge for Wind Turbine Rotor, <http://dx.doi.org/10.5772/intechopen.73608>
- [9] B. Lyu, Mahdi Azarpeyvand, Samuel Sinayoko, Prediction of noise from serrated trailing edges, *Journal of Fluid Mechanics*, 2016
- [10] Yuan Tian, Benjamin Cotté, Antoine Chaigne. Wind Turbine Noise Modelling Based on Amiet's Theory. 5th International Meeting on Wind Turbine Noise, Aug 2013, Denver, CO, United States. CD-ROM proceedings. fhal-00975237f
- [11] Stefan Oerlemans, Peter Fuglsang, Low-noise wind turbine design, SIEMENS AG 2012
- [12] Paruchuri, Chaitanya & Subramanian, Narayanan & Joseph, Phillip & Kim, Jae. (2016). Leading edge serration geometries for significantly enhanced leading edge noise reductions. 10.2514/6.2016-2736.
- [13] Brooks T. F., Pope D.S., Marcolini M.A., Airfoil Self-Noise and Prediction, NTRS, Document ID 19890016302, <https://ntrs.nasa.gov/citations/19890016302>
- [14] Al Tlua B., Experimental Wind Tunnel Testing and Numerical Optimization Studies for Airfoil Trailing Edge Noise Reduction, Ottawa-Carleton Institute for Mechanical and Aerospace Engineering, PhD thesis, 2021
- [15] Alex Siu Hong Lau, Xun Huang, The control of aerodynamic sound due to boundary layer pressure gust scattering by trailing edge serrations, *Journal of Sound and Vibration*, Volume 432, 2018, Pages 133-154, ISSN 0022-460X, <https://doi.org/10.1016/j.jsv.2018.06.026>.
- [16] Alex S.H. Lau, Sina Haeri, Jae Wook Kim, The effect of wavy leading edges on aerofoil–gust interaction noise, *Journal of Sound and Vibration*, Volume 332, Issue 24, 2013, Pages 6234-6253, ISSN 0022-460X, <https://doi.org/10.1016/j.jsv.2013.06.031>.
- [17] Cyril Polacsek, Vincent Clair, Gabriel Reboul, Hugues Deniau. Turbulence-airfoil interaction noise reduction using wavy leading edge: an experimental and numerical study. Institute of Noise Control Engineering/Japan & Acoustical Society of Japan, Sep 2011, Osaka, Japan. pp.170-180. fhal02086677
- [18] NASA@SC15, Computational Aeroacoustic Open-Rotor Simulations for Green Aviation, Available at <https://www.nas.nasa.gov/SC15/demos/demo8.html#prettyPhoto>
- [19] Shyam, Vikram & Ameri, Ali & Poinatte, Philip & Thurman, Douglas & Wroblewski, Adam & Snyder, Christopher. (2015). Application of Pinniped Vibrissae to Aeropropulsion. V02AT38A023. 10.1115/GT2015-43055.
- [20] Ito S., Aerodynamic Influence of Leading-Edge Serrations on an Airfoil in a Low Reynolds Number – A Study of an Owl Wing with Leading Edge Serrations-, *Journal of Biomechanical Science and Engineering*, Vol.4, No.1, 2009, DOI:10.1299/jbse.4.117
- [21] Paruchuri, Chaitanya, Joseph, Phillip, Narayanan, Subramanyam, Vanderwel, Christina, Turner, Jacob, Kim, Jae and Ganapathisubramani, Bharathram (2017) Performance and mechanism of sinusoidal leading edge serrations for the reduction of turbulence-aerofoil interaction noise. University of Southampton doi:10.5258/SOTON/405263
- [22] Carlos Arce León, Daniele Ragni, Stefan Pröbsting, Fulvio Scarano, Jesper Madsen, Flow topology and acoustic emissions of trailing edge serrations at incidence, *Exp Fluids* (2016) 57:91, DOI 10.1007/s00348-016-2181-1
- [23] M.S. Howe, Noise Produced by a Sawtooth Trailing Edge, *The Journal of the Acoustical Society of America* 90, 482 (1991)
- [24] Paterson W, Amiet R. K., Acoustic radiation and surface pressure response of an airfoil due to incident turbulence, NASA CR-2733
- [25] R. K. Amiet, Acoustic Radiation from an Airfoil in a Turbulent Stream, *Journal of Sound and Vibration* (1975) 41(4), 407--420



- [26] R. K. Amiet, Airfoil Gust Response and The Sound Produced By Airfoil-Vortex Interaction, United Technologies Research Center East Hartford, Connecticut
- [27] Curle, N. "The Influence of Solid Boundaries upon Aerodynamic Sound." Proceedings of the Royal Society of London. Series A, Mathematical and Physical Sciences 231, no. 1187 (1955): 505–14. <http://www.jstor.org/stable/99804>.
- [28] Lighthill, M. J. „On Sound Generated Aerodynamically. I. General Theory”, Proceedings of the Royal Society of London. Series A, Mathematical and Physical Sciences, Vol. 211, No. 1107 (Mar. 20, 1952), pp. 564-587, <http://www.jstor.org/stable/98943>.
- [29] Liu, X. , Kamliya Jawahar, H., & Azarpeyvand, M. (2016). Wake Development of Airfoils with Serrated Trailing Edges. In 22nd AIAA CEAS Aeroacoustics Conference [AIAA 2016-2817] American Institute of Aeronautics and Astronautics Inc. (AIAA). <https://doi.org/10.2514/6.2016-2817>
- [30] Woodhead, P.C., Chong, T.P., Joseph, P.F. et al. Aerofoil self-noise radiations subjected to serration flap angles. *Exp Fluids* 62, 152 (2021). <https://doi.org/10.1007/s00348-021-03239-y>
- [31] Dvorak P., Siemens low noise wind turbine blades inspired by silent flight of the owl, September 28, 2016, Available at <https://www.windpowerengineering.com/siemens-low-noise-wind-turbine-blades-inspired-silent-flight-owl/>
- [32] Sears, W. R., 1941, Some aspects of non-stationary airfoil theory and its practical application. *Journal of the Aeronautical Sciences* 8, 104–108.
- [33] Benshuai Lyu, Lorna J. Ayton, Rapid noise prediction models for serrated leading and trailing edges, <https://doi.org/10.48550/arXiv.1906.02645>
- [34] F. Tong, W. Qiao, W. Chen, H. Cheng, R. Wei, X. Wang, Numerical analysis of broadband noise reduction with wavy leading edge, *Chinese Journal of Aeronautics*, 2018, <https://doi.org/10.1016/j.cja.2018.03.020>
- [35] Liu, Xiao & Kamliya Jawahar, Hasan & Azarpeyvand, Mahdi & Theunissen, R.. (2015). Aerodynamic and Aeroacoustic Performance of Serrated Airfoils. 21st AIAA/CEAS Aeroacoustics Conference. 10.2514/6.2015-2201.
- [36] Soderman, P.T. 1972 Aerodynamic effects of leading-edge serrations on a two- dimensional airfoil. Tech. Rep.. NASA TM X-2643.
- [37] Hersh, A.S., Soderman, P.T. & Hayden, R.E. 1974 Investigation of acoustic effects of leading edge serrations on airfoils. *Journal of Aircraft* 11(4), 197–202
- [38] D. J. Moreau, On the noise reduction mechanism of a flats plate serrated trailing edge at low-to-moderate Reynolds number, 18th AIAA/CEAS Aeroacoustics Conference (33rd AIAA Aeroacoustics Conference) 04 - 06 June 2012, Colorado Springs, CO
- [39] Lianjie Liu, Liangliang Zhang, Bo Wu and Ben Chen, Numerical and Experimental Studies on Grid-Generated Turbulence in Wind Tunnel, *Journal of Engineering Science and Technology Review* 10 (3) (2017) 159-169
- [40] S. Narayanan, Airfoil noise reductions through leading edge serrations, University of Southampton, Highfield, Southampton-SO17 1BJ, UK
- [41] Subramanian, Narayanan & Joseph, Phillip & Haeri, Sina & Kim, Jae & Paruchuri, Chaitanya & Polacsek, C.. (2014). Noise Reduction Studies from the Leading Edge of Serrated Flat Plates. 20th AIAA/CEAS Aeroacoustics Conference, Atlanta, USA. 10.2514/6.2014-2320.
- [42] Clair, Vincent & Polacsek, C. & Garrec, Le & Reboul, Gabriel. (2012). CAA methodology to simulate turbulence-airfoil noise. 18th AIAA/CEAS Aeroacoustics Conference (33rd AIAA Aeroacoustics Conference). 10.2514/6.2012-2189.
- [43] Christopher Teruna, Francesco Avallone, Damiano Casalino, Daniele Ragni, Numerical investigation of leading edge noise reduction on a rod-airfoil configuration using porous materials and serrations, *Journal of Sound and Vibration*, Volume 494, 2021, 115880, ISSN 0022-460X, <https://doi.org/10.1016/j.jsv.2020.115880>.
- [44] Agrawal, Bharat Raj, "Modeling fan broadband noise from jet engines and rod-airfoil benchmark case for broadband noise prediction" (2015). Graduate Theses and Dissertations. 14326. <https://lib.dr.iastate.edu/etd/14326>
- [45] A. Aravind Raghavan Sreenivasan and B. Kannan Iyer , "Enhanced wall turbulence model for flow over cylinder at high Reynolds number", *AIP Advances* 9, 095012 (2019) <https://doi.org/10.1063/1.5118421>
- [46] Turner, J., & Kim, J. (2022). Quadrupole noise generated from a low-speed aerofoil in near- and full-stall conditions. *Journal of Fluid Mechanics*, 936, A34. doi:10.1017/jfm.2022.75

- [47] Weger M, Wagner H (2016) Morphological Variations of Leading-Edge Serrations in Owls(Strigiformes). PLoS ONE 11(3): e0149236. doi:10.1371/journal.pone.0149236
- [48] Cyril Polacsek, Vincent Clair, Gabriel Reboul, Hugues Deniau. Turbulence-airfoil interaction noise reduction using wavy leading edge: an experimental and numerical study. Institute of Noise Control Engineering/Japan & Acoustical Society of Japan, Sep 2011, Osaka, Japan. pp.170-180. fflhal02086677
- [49] Jiang, Min & Li, Xiaodong & Zhou, Jia-jian. (2011). Experimental and numerical investigation on sound generation from airfoil-flow interaction. Applied Mathematics and Mechanics (English Edition). 32. 765-776. 10.1007/s10483-011-1456-7.
- [50] Greschner, Björn & Peth, S. & Moon, Young & Seo, Jung Hee & Jacob, Marc & Thiele, Frank. (2007). Three-dimensional predictions of the rod wake-airfoil interaction noise by hybrid methods. 14th International Congress on Sound and Vibration 2007, ICSV 2007. 2. 1599-1610.
- [51] Lianjie Liu, Liangliang Zhang, Bo Wu and Ben Chen, Numerical and Experimental Studies on Grid-Generated Turbulence in Wind Tunnel, Journal of Engineering Science and Technology Review 10 (3) (2017) 159-169
- [52] Hales ADG, Ayton LJ, Wills AO, et al. A mathematical model for the interaction of anisotropic turbulence with porous surfaces. *Journal of Fluid Mechanics*. 2024;1001:A16. doi:10.1017/jfm.2024.1067
- [53] Ito S., Aerodynamic Influence of Leading-Edge Serrations on an Airfoil in a Low Reynolds Number – A Study of an Owl Wing with Leading Edge Serrations-, Journal of Biomechanical Science and Engineering, Vol.4, No.1, 2009, DOI:10.1299/jbse.4.117
- [54] Kim, J., Haeri, S., & Joseph, P. (2016). On the reduction of aerofoil-turbulence interaction noise associated with wavy leading edges. *Journal of Fluid Mechanics*, 792, 526-552. doi:10.1017/jfm.2016.95
- [55] Lacagnina, Giovanni & Paruchuri, Chaitanya & Kim, Jung-Hoon & Berk, Tim & Joseph, Phillip & Choi, Kwing-So & Ganapathisubramani, Bharathram & Hasheminejad, Seyed Mohammad & Chong, Tze & Stalnov, Oksana & Shahab, Muhammad & Omidyeganeh, Mohammad & Pinelli, Alfredo. (2020). Leading edge serrations for the reduction of aerofoil self-noise at low angle of attack, pre-stall and post-stall conditions. *International Journal of Aeroacoustics*. 20. 10.1177/1475472X20978379.
- [56] Salama, Yehia. "Experimental and Numerical Investigation of Bio-Inspired Airfoil Trailing-Edge Designs for Noise Reduction." .
- [57] Rajeshwaran, M.S. & Kushari, Abhijit. (2015). Experimental Study on the Flow Past Sinusoidal Leading Edge Serrations in a Compressor Cascade. V001T01A017. 10.1115/GTINDIA2015-1334.
- [58] Smith, E.G., Sowers, H.D., Cascade tests of serrated leading edge blading at high subsonic speeds, 1974, NASA CR-2472
- [59] Qiao, W & Ji, L & Tong, W & Xu, K & Chen, W. (2014). Application of Phased Array in the Study of Linear Cascade Noise Reduction on the Indoor Test Bed.
- [60] Craig, Mary E.. "Trailing-Edge Blowing of Model Fan Blades for Wake Management." (2005).
- [61] Geiger, Derek. (2005). Comparative Analysis of Serrated Trailing Edge Designs on Idealized Aircraft Engine Fan Blades for Noise Reduction.
- [62] Ye, Xuemin & Zheng, Nan & Zhang, Ruixing & Li, Chunxi. (2022). Effect of serrated trailing-edge blades on aerodynamic noise of an axial fan. *Journal of Mechanical Science and Technology*. 36. 2937-2948. 10.1007/s12206-022-0526-7.
- [63] Teruna, Christopher & Ragni, Daniele & Avallone, Francesco & Casalino, Damiano. (2019). A rod-linear cascade model for emulating rotor-stator interaction noise in turbofans: A numerical study. *Aerospace Science and Technology*. 90. 10.1016/j.ast.2019.04.047.
- [64] Liu, X. , Zang, B., & Azarpeyvand, M. (2022). Wake-aerofoil interaction noise control with trailing-edge serrations. *Experimental Thermal and Fluid Science*, 130, [110510]. <https://doi.org/10.1016/j.expthermflusci.2021.110510>
- [65] Alkhalifa, A.S.; Uddin, M.N.; Atkinson, M. Aerodynamic Performance Analysis of Trailing Edge Serrations on a Wells Turbine. *Energies* 2022, 15, 9075. <https://doi.org/10.3390/en15239075>
- [66] Cyril Polacsek, Adil Cader, Martin Buszyk, Raphaël Barrier, Fernando Gea-Aguilera, et al.. Aeroacoustic Design and Broadband Noise Predictions of a Fan Stage with Serrated Outlet Guide Vanes. *Physics of Fluids*, 2020, 32 (10), ffl0.1063/5.0020190ff. fflhal-02968328v2f
- [67] Filamentive Limited, PLA/rPLA, Fișă de material, Available at <https://www.farnell.com/datasheets/2913593.pdf>
- [68] C. Polacsek, R Barrier, M. Kohlhaas, T. Carolus, P. Kausche, et al.. Turbofan Interaction Noise Reduction Using Trailing Edge Blowing: Numerical Design and Assessment and Comparison with Experiments.V2. Aerospace Lab, 2014, 7, p. 1-9. ffl0.12762/2014.AL07-03ff. fflhal-01184670f

- [69] Westley, R., & Lilley, G.M. (1952). An Investigation of the Noise Field from a Small Jet and Methods for its Reduction. College of Aeronautics Report.
- [70] Biedermann, T.M.; Czeckay, P.; Hintzen, N.; Kameier, F.; Paschereit, C.O. Applicability of Aeroacoustic Scaling Laws of Leading Edge Serrations for Rotating Applications. *Acoustics* 2020, 2, 579–594. <https://doi.org/10.3390/acoustics2030030>
- [71] Lee, H.M., Lim, K.M., Xie, J., & Lee, H.P., Experimental Study on the Half Flat Tip Serrated Trailing Edge for Stand Fan. *Archives of Acoustics*. 45, 2, pp. 359–365, 2020, DOI: 10.24425/aoa.2020.133156
- [72] Becker, S. & Riedel, Jörg & Kaltenbacher, Manfred & Schoder, Stefan & Czwielong, Felix. (2022). ON THE FLUID MECHANICAL AND ACOUSTIC MECHANISMS OF SERRATED LEADING EDGES. 10.26083/tuprints-00021712.
- [73] Chen, L.; Yang, P.; Zhang, B.; Chen, L. Aerodynamic Enhancement of Vertical-Axis Wind Turbines Using Plain and Serrated Gurney Flaps. *Appl. Sci.* 2023, 13, 12643. <https://doi.org/10.3390/app132312643>
- [74] Qaissi, K.; Elsayed, O.; Faqir, M.; Essadiqi, E. Aerodynamic Optimization of Trailing-Edge Serrations for a Wind Turbine Blade Using Taguchi Modified Additive Model. *Energies* 2023, 16, 1099. <https://doi.org/10.3390/en16031099>
- [75] Tay, Wb., Lu, Z., Ramesh, S.S., Khoo, Bc. (2020). Numerical Simulations of Serrated Propellers to Reduce Noise. In: Panda, D. (eds) *Supercomputing Frontiers. SCFA 2020. Lecture Notes in Computer Science()*, vol 12082. Springer, Cham. [https://doi.org/10.1007/978-3-030-48842-0\\_6](https://doi.org/10.1007/978-3-030-48842-0_6); Accessed on 09.07.2024
- [76] Hsiao Mun Lee, Zhenbo Lu, Kian Meng Lim, Jinlong Xie, Heow Pueh Lee, Quieter propeller with serrated trailing edge, *Applied Acoustics*, Volume 146, 2019, Pages 227–236, ISSN 0003-682X, <https://doi.org/10.1016/j.apacoust.2018.11.020>.
- [77] Tam C.K.W, Viswanathan K, Ahuja K.K., Panda J. The sources of jet noise: experimental evidence. *Journal of Fluid Mechanics*. 2008; 615:253–292. doi:10.1017/S0022112008003704
- [78] Auris Juknevičius, Tze Pei Chong, On the leading edge noise and aerodynamics of thin aerofoil subjected to the straight and curved serrations, *Journal of Sound and Vibration*, Volume 425, 2018, <https://doi.org/10.1016/j.jsv.2018.02.038>; Accessed on 09.07.2024
- [79] Leandro Rego, Francesco Avallone, Daniele Ragni, Damiano Casalino, On the mechanisms of jet-installation noise reduction with flow-permeable trailing edges, *Journal of Sound and Vibration*, Volume 520, 2022, <https://doi.org/10.1016/j.jsv.2021.116582>; Accessed on 09.07.2024
- [80] Vieira, A. E., von den Hoff, B., Snellen, M., & Simons, D. G. (2022). Comparison of Semi-Empirical Noise Models with Flyover Measurements of Operating Aircraft. *Journal of Aircraft*, 59(6), 1574–1587. <https://doi.org/10.2514/1.C036387>
- [81] Brenda S. Henderson, Dennis L. Huff, Jeffrey J. Berton, Jet Noise Prediction Comparisons with Scale Model Tests and Learjet Flyover Data, Book Chapter, 25th AIAA/CEAS Aeroacoustics Conference, 10.2514/6.2019-2768
- [82] Danny Lewis, Jérôme de Laborderie, Marlène Sanjosé, Stéphane Moreau, Marc C. Jacob, Vianney Masson, Parametric study on state-of-the-art analytical models for fan broadband interaction noise predictions, *Journal of Sound and Vibration*, Volume 514, 2021, <https://doi.org/10.1016/j.jsv.2021.116423>; Accessed on 09.07.2024
- [83] Raposo, Henrique & Azarpeyvand, Mahdi. (2024). Turbulence ingestion noise generation in rotating blades. *Journal of Fluid Mechanics*. 980. 10.1017/jfm.2024.7.
- [84] Zorumski, W. E., Weir, D. S., Empirical source noise prediction method with application to subsonic coaxial jet mixing noise, NASA TP 2084 c.1, Available at <https://ntrs.nasa.gov/citations/19830007878>
- [85] Powell, Alan. “On the Generation of Noise by Turbulent Jets.”, The American Society of Mechanical Engineers, AD-A286 649, 1959
- [86] Seoud, Rich E. E. and John Christos Vassilicos. “Dissipation and decay of fractal-generated turbulence.” *Physics of Fluids* 19 (2007): 105108.
- [87] Trevor A. Stout, Kent L. Gee, Tracianne B. Neilsen, Alan T. Wall, Michael M. James; Intensity analysis of the dominant frequencies of military jet aircraft noise. *Proc. Mtgs. Acoust.* 2 December 2013; 20 (1): 040010. <https://doi.org/10.1121/1.4895772>
- [88] Cyril Polacsek, Martin Buszyk, Raphaël Barrier, Vincent Clair, Edouard Salze. Aeroacoustic performances of a low-noise airfoil cascade with serrated leading edges: predictions and measurements. ICAS 2022, Sep 2022, STOCKHOLM, Sweden. hal-03938107

- [89] Abbas, M.; Riggins, D.W. Analysis of Energy Utilization and Losses for Jet-Propelled Vehicles. *Aerospace* 2021, 8, 342. <https://doi.org/10.3390/aerospace8110342>
- [90] Foggi Rota, G., Monti, A., Rosti, M.E. et al. Saving energy in turbulent flows with unsteady pumping. *Sci Rep* 13, 1299 (2023). <https://doi.org/10.1038/s41598-023-28519-x>
- [91] Mahmoudi, Mahsa & Banihashemi, Mohammad. (2023). Turbulence effect on total mechanical energy budget and energy loss of turbulent flows with different hydraulic regimes in open-channel transitions. *ISH Journal of Hydraulic Engineering*. 30. 10.1080/09715010.2023.2276924.
- [92] Wilson, David K., Three-Dimensional Correlation and Spectral Functions for Turbulent Velocities in Homogeneous and Surface-Blocked Boundary Layers, ARMY RESEARCH LAB ADELPHI MD, ADA327709, Available at <https://apps.dtic.mil/sti/citations/tr/ADA327709>
- [93] Ragni, D., Fisaletti, D. & Baars, W.J. Jet noise predictions by time marching of single-snapshot tomographic PIV fields. *Exp Fluids* 63, 84 (2022). <https://doi.org/10.1007/s00348-022-03436-3>; Accessed on 09.07.2024
- [94] Riccardo da Soghe, Luca Innocenti, Antonio Andreini, Sébastien Poncet. Numerical Benchmark of Turbulence modelling in Gas Turbine Rotor-Stator System. ASME TURBO EXPO 2010: Power for Land, Sea & Air (GT2010), Jun 2010, Glasgow, United Kingdom. <https://hal.science/hal-00679123>
- [95] Maxime Fiore, Nicolas Gourdain. Reynolds, Mach, and Freestream Turbulence Effects on the Flow in a Low-Pressure Turbine. *Journal of Turbomachinery*, 2021, 143 (10), pp.101009-1010022. <https://hal.science/hal-03238795>
- [96] Michel, Ulf & Ahuja, Krishan, On the Scaling of Jet Noise with Helmholtz Number Close to the Jet Axis., 20th AIAA/CEAS Aeroacoustics Conference, 2014, DOI:10.2514/6.2014-2338.
- [97] Rajeshwaran, M.S. & Kushari, Abhijit. (2015). Experimental Study on the Flow Past Sinusoidal Leading Edge Serrations in a Compressor Cascade. V001T01A017. 10.1115/GTINDIA2015-1334.
- [98] Salehian, S.; Mankbadi, R. Jet Noise in Airframe Integration and Shielding. *Appl. Sci.* 2020, 10, 511. <https://doi.org/10.3390/app10020511>
- [99] Gabriele Grasso, P. Jaiswal, Hao Wu, Stéphane Moreau, Michel Roger. Analytical models of the wall-pressure spectrum under a turbulent boundary layer with adverse pressure gradient. *Journal of Fluid Mechanics*, 2019, 877, pp.1007-1062., Available at <https://hal.science/hal-03158378>
- [100] Shahzad, H., Hickel, S. & Modesti, D. Permeability and Turbulence Over Perforated Plates. *Flow Turbulence Combust* 109, 1241–1254 (2022). <https://doi.org/10.1007/s10494-022-00337-7>; Accessed on 09.07.2024
- [101] Sravani Vemulapalli, Santhosh Krishnan Venkata, Parametric analysis of orifice plates on measurement of flow: A review, *Ain Shams Engineering Journal*, Volume 13, Issue 3, 2022, <https://doi.org/10.1016/j.asej.2021.11.008>; Accessed on 09.07.2024
- [102] Yulian Pramiyanti, Suzairin Md Seri, Azwan Sapit, Incompressible Turbulent Swirling Flow through Circle Grid Perforated Plate, *Journal of Complex Flow*, Vol. 2 No. 1 (2020) p. 11-16
- [103] Larssen, Jon V., Devenport, William J., On the generation of large-scale homogeneous turbulence, *Experiments in Fluids*, 2011, <https://doi.org/10.1007/s00348-010-0974-1>; Accessed on 09.07.2024
- [104] Christopher Teruna, Daniele Ragni, Francesco Avallone, Damiano Casalino, A rod-linear cascade model for emulating rotor-stator interaction noise in turbofans: A numerical study, *Aerospace Science and Technology*, Volume 90, 2019, Pages 275-288, <https://doi.org/10.1016/j.ast.2019.04.047>.
- [105] Prince, Simon & Khodagolian, V. & Gai, R. (2012). An experimental study of a pulsed air jet and an acoustic synthetic jet on a low speed turbulent boundary layer. 28th Congress of the International Council of the Aeronautical Sciences 2012, ICAS 2012. 2. 1005-1014.
- [106] Blake, J.D.; Sescu, A.; Thompson, D.; Hattori, Y. A Coupled LES-Synthetic Turbulence Method for Jet Noise Prediction. *Aerospace* 2022, 9, 171. <https://doi.org/10.3390/aerospace9030171>
- [107] Dieste, M., Gabard, G., Broadband Interaction Noise Simulations Using Synthetic Turbulence, The Sixteenth International Congress on Sound and Vibration, Krakow, Iulie 2009
- [108] dos Santos, Fernanda Leticia & Botero Bolivar, Laura & Venner, C. & Santana, Leandro. (2021). Modelling the Dissipation Range of von Kármán Turbulence Spectrum. 10.2514/6.2021-2292.
- [109] Philips, C., Bandyopadhyay, R., McComas, D.J., Taylor Microscale and Effective Reynolds Number near the Sun from PSP, *The Astrophysical Journal*, Volume 933, Number 1, DOI 10.3847/1538-4357/ac713f
- [110] Wang, Bing & Manhart, Michael. (2012). Two-phase micro- and macro-time scales in particle-laden turbulent channel flows. *Acta Mechanica Sinica*. 28. 10.1007/s10409-012-0034-6.

- [111] Li D, Salesky ST, Banerjee T. Connections between the Ozmidov scale and mean velocity profile in stably stratified atmospheric surface layers. *Journal of Fluid Mechanics*. 2016;797:R3. doi:10.1017/jfm.2016.311
- [112] Wang, G-H, Clemens, N.T., Barlow, R.S., Varghese, P.L., A system model for assessing scalar dissipation measurement accuracy in turbulent flows, *Measurement Science and Technology*, Volume 18, Number 15, DOI 10.1088/0957-0233/18/5/015
- [113] Essa, K.S.M. (2000). Estimation of MONIN-OBUKHOV length using richardson and bulk richardson number. In Hanna, K.M. (Ed.). *Proceedings of the Second Conference on Nuclear and Particle Physics (NUPPAC-99)*, (p. 711). Egypt
- [114] Dong S, Huang Y, Yuan X, Lozano-Durán A. The coherent structure of the kinetic energy transfer in shear turbulence. *Journal of Fluid Mechanics*. 2020;892:A22. doi:10.1017/jfm.2020.195
- [115] Kim, Sehoon & Jung, & Kong, & Lee, Kunwoo & An, Yun-Kyu. (2019). In-Situ Data-Driven Buffeting Response Analysis of a Cable-Stayed Bridge. *Sensors*. 19. 3048. 10.3390/s19143048.
- [116] Suresh Palani, Chaitanya C. Paruchuri, Phillip Joseph, Sergey A. Karabasov, Annabel Markesteijn, Hussain Abid, Tze Pei Chong and Sergey Utyuzhnikov. "Modified TNO-Blake model for aerofoil surface pressure prediction with canopies," *AIAA 2023-3203. AIAA AVIATION 2023 Forum*. Iunie 2023.
- [117] Goldstein, Marvin E., The 90 deg Acoustic Spectrum of a High Speed Air Jet, NASA E-14396, Available at <https://ntrs.nasa.gov/citations/20050196696>
- [118] McLaughlin, Dennis & Kuo, Ching-Wen & Papamoschou, Dimitri. (2008). Experiments on the Effect of Ground Reflections on Supersonic Jet Noise. 10.2514/6.2008-22.
- [119] Lianjie Liu, Liangliang Zhang, Bo Wu and Ben Chen, Numerical and Experimental Studies on Grid Generated Turbulence in Wind Tunnel, *Journal of Engineering Science and Technology Review* 10 (3) (2017) 159-169
- [120] Rutherford, Dan. 2025. "The International Civil Aviation Organization's CAEP/13 Aircraft Noise Standards." Available at <https://theicct.org/wp-content/uploads/2025/05/ID-358-%E2%80%93-Noise-standard-ICAO-final.pdf>.
- [121] "EASA Certification Noise Levels." n.d. EASA. Available at <https://www.easa.europa.eu/en/domains/environment/easa-certification-noise-levels>.
- [122] Zaporozhets, Oleksandr. (2022). Balanced Approach to Aircraft Noise Management. 10.1007/978-3-030-91194-2\_3.
- [123] "ICAO ENVIRONMENTAL REPORT." n.d., Available at [https://www.icao.int/environmental-protection/Documents/EnvironmentalReports/2016/ENVReport2016\\_pg38-41.pdf](https://www.icao.int/environmental-protection/Documents/EnvironmentalReports/2016/ENVReport2016_pg38-41.pdf).
- [124] Chaitanya, Paruchuri, Phillip Joseph, Tze Pei Chong, Matthew Priddin, and Lorna Ayton. 2020. "On the Noise Reduction Mechanisms of Porous Aerofoil Leading Edges." *Journal of Sound and Vibration* 485 (October): 115574. <https://doi.org/10.1016/j.jsv.2020.115574>.
- [125] Pollok, Alexander, and Andreas Schröffer. n.d. "AST 2017 SIMULATION of HELMHOLTZ RESONANCE EFFECTS in AIRCRAFT ECS." Accessed Iunie 4, 2025. [https://elib.dlr.de/111334/1/AST2017\\_Paper117\\_Pollok.pdf](https://elib.dlr.de/111334/1/AST2017_Paper117_Pollok.pdf).
- [126] Zhang, Chengchun, Wen Cheng, Tianyu Du, Xiaowei Sun, Chun Shen, Zhengwu Chen, and Dong Liang. 2022. "Experimental and Numerical Study on Noise Reduction of Airfoil with the Bioinspired Ridge-like Structure." *Applied Acoustics* 203 (December): 109190. <https://doi.org/10.1016/j.apacoust.2022.109190>.
- [127] Lu, Yu, Ziyang Li, Xin Chang, Zhenju Chuang, and Junhua Xing. 2021. "An Aerodynamic Optimization Design Study on the Bio-Inspired Airfoil with Leading-Edge Tubercles." *Engineering Applications of Computational Fluid Mechanics* 15 (1): 292–312. <https://doi.org/10.1080/19942060.2020.1856723>.
- [128] Andrei-George Totu, Grigore Cican, and Daniel-Eugeniu Crunțeanu. 2024. "Serrations as a Passive Solution for Turbomachinery Noise Reduction." *Aerospace* 11 (4): 292–92. <https://doi.org/10.3390/aerospace11040292>.
- [129] Andrei-George Totu, Marius Deaconu, Laurențiu Cristea, Alina Bogoi, Daniel-Eugeniu Crunțeanu, and Grigore Cican. 2024. "Experimental Analysis of Acoustic Spectra for Leading/Trailing-Edge Serrated Blades in Cascade Configuration." *Processes* 12 (11): 2613–13. <https://doi.org/10.3390/pr12112613>.
- [130] Yu, Xishuai, Jianxi Zhou, and Yong Li. 2025. "Noise Control in Tandem Airfoil Configurations Using Leading-Edge Serrations on the Front Airfoil." *Experiments in Fluids* 66 (5): 1–17. <https://doi.org/10.1007/s00348-025-04033-w>.

- [131] Piccolo, A, R. Zamponi, F Avallone, and D Ragni. 2024. "Turbulence Distortion and Leading-Edge Noise." *Physics of Fluids* 36 (12): 125183. <https://doi.org/10.1063/5.0244627>.
- [132] Geyer, Thomas, Sahan Wasala, and Ennes Sarradj. 2020. "Experimental Study of Airfoil Leading Edge Combs for Turbulence Interaction Noise Reduction." *Acoustics* 2 (2): 207–23. <https://doi.org/10.3390/acoustics2020014>.
- [133] Goldstein, M.E. "Aeroacoustics", McGraw-Hill International. Book Company, 1976. Available at <https://archive.org/details/Aeroacoustics/page/52/mode/2up>.
- [134] "Computational Aeroacoustics-Issues and Methods-Tam1995 - AIAA JOURNAL Vol. 33, No. 10, October 1995 - Studocu." 2019. Studocu. 2019. <https://www.studocu.com/gr/document/eoniko-metsobio-polytexneio/aeroakoystikh/computational-aeroacoustics-issues-and-methods-tam1995/30207542>.
- [135] Steve Cawser, MEng CEng MIOA, Acoustic measurements in airflow, AECOM, Available at [https://www.ioa.org.uk/sites/default/files/Acoustic%20measurements%20in%20airflow%20Mar\\_Apr%202019.pdf](https://www.ioa.org.uk/sites/default/files/Acoustic%20measurements%20in%20airflow%20Mar_Apr%202019.pdf)
- [136] "Welch's Power Spectral Density Estimate - MATLAB Pwelch." n.d. [Www.mathworks.com](https://www.mathworks.com/help/signal/ref/pwelch.html). <https://www.mathworks.com/help/signal/ref/pwelch.html>.
- [137] "Siemens PLM." 2019. Siemens.com. 2019. <https://community.sw.siemens.com/s/article/window-types-hanning-flattop-uniform-tukey-and-exponential>.
- [138] "Fourier Analysis and Power Spectral Density 4.1 Fourier Series and Transforms." n.d. Accessed Iunie 4, 2025. <https://www.fccdecastro.com.br/pdf/FAPSD.pdf>.
- [139] Chan, Stanley. n.d. "ECE 302: Lecture 10.6 Power Spectral Density." Accessed Iunie 4, 2025. [https://engineering.purdue.edu/ChanGroup/ECE302/files/Slide\\_10\\_06.pdf](https://engineering.purdue.edu/ChanGroup/ECE302/files/Slide_10_06.pdf).
- [140] "Chapter 7 Basic Turbulence." n.d. <https://www.astronomy.ohio-state.edu/ryden.1/ast825/ch7.pdf>.
- [141] Agrawal, Bharat R, and Anupam Sharma. 2014. "Aerodynamic Noise Prediction for a Rod-Airfoil Configuration Using Large Eddy Simulations." 28th AIAA/CEAS Aeroacoustics 2022 Conference, Iunie. <https://doi.org/10.2514/6.2014-3295>.
- [142] Zamponi, R., S. Satcunanathan, S. Moreau, D. Ragni, M. Meinke, W. Schröder, and C. Schram. 2020. "On the Role of Turbulence Distortion on Leading-Edge Noise Reduction by Means of Porosity." *Journal of Sound and Vibration* 485 (October): 115561. <https://doi.org/10.1016/j.jsv.2020.115561>.
- [143] Carley, Michael. n.d. "Turbulence and Noise." <https://people.bath.ac.uk/ensmjc/Notes/tnoise.pdf>.
- [144] Lau, Y.L, R.M.C So, and R.C.K Leung. 2004. "Flow-Induced Vibration of Elastic Slender Structures in a Cylinder Wake." *Journal of Fluids and Structures* Vol. 19 (November): 1061–83. <https://doi.org/10.1016/j.jfluidstructs.2004.06.007>.
- [145] Troolin, D. R., E. K. Longmire, and W. T. Lai. 2006. "Time Resolved PIV Analysis of Flow over a NACA 0015 Airfoil with Gurney Flap." *Experiments in Fluids* 41 (2): 241–54. <https://doi.org/10.1007/s00348-006-0143-8>.
- [146] Fischer, A. (2012). Hot Wire Anemometer Turbulence Measurements in the wind Tunnel of LM Wind Power. Wind Energy Department, Technical University of Denmark. DTU Wind Energy E No. 0006
- [147] "Understanding the 3dB Rule - Pulsar Instruments." n.d. Available at <https://pulsarinstruments.com/news/understanding-3db-rule/>.
- [148] Castellini, Paolo, and Milena Martarelli. 2007. "Acoustic Beamforming: Analysis of Uncertainty and Metrological Performances." *Mechanical Systems and Signal Processing* 22 (3): 672–92. <https://doi.org/10.1016/j.ymssp.2007.09.017>.
- [149] Silva, Ikaro. 2023. "Mathematics of Beam Forming - Ikaro Silva - Medium." Medium. Iulie 25, 2023. <https://medium.com/@ikarosilva/mathematics-of-beam-forming-a518e59542ad>.
- [150] Barry Van Veen, et. Al. "Beamforming Techniques for Spatial Filtering." 2000 CRC Press LLC., Available at <https://dsp-book.narod.ru/DSPMW/61.PDF>
- [151] Chu, Zhigang, Shuyi Zhao, Yang Yang, and Yongxin Yang. 2018. "Deconvolution Using CLEAN-SC for Acoustic Source Identification with Spherical Microphone Arrays." *Journal of Sound and Vibration* 440 (October): 161–73. <https://doi.org/10.1016/j.jsv.2018.10.030>.
- [152] Lee, S. Trailing-Edge Noise and its Applications to Urban Air Mobility Noise. 2024. disponibil online: [https://www.nas.nasa.gov/assets/nas/pdf/ams/2024/AMS\\_20240314\\_Lee.pdf](https://www.nas.nasa.gov/assets/nas/pdf/ams/2024/AMS_20240314_Lee.pdf) (accesed on 26 Iulie 2025).



- [153] Shen, Y.; Bai, Y.; Liu, X.; Zang, B. Drone Noise Reduction Using Serration–Finlet Blade Design and Its Psychoacoustic and Social Impacts. *Sustainability* 2025, 17, 3451. <https://doi.org/10.3390/su17083451>.
- [154] Candeloro, P.; Ragni, D.; Pagliaroli, T. Unconventional Application of Serrated Trailing Edges for Quieter Propeller Drones. In Proceedings of the 30th AIAA/CEAS Aeroacoustics Conference, Rome, Italy, 4–7 June 2024. <https://doi.org/10.2514/6.2024-3107>.
- [155] Robert, J.; Antoine, M.; Sébastien, G.; Rainer, S. Optimization of Trailing-Edge Serrations to Reduce Open-Rotor Tonal Interaction Noise. In Proceedings of the 16th International Symposium on Transport Phenomena and Dynamics of Rotating Machinery, Honolulu, HI, USA, 10–15 April 2016. ffh1-01884252.
- [156] Hansen, C.; Hansen, K. Recent Advances in Wind Turbine Noise Research. *Acoustics* 2020, 2, 171–206. <https://doi.org/10.3390/acoustics2010013>.
- [157] Deaconu, M.; Cican, G.; Toma, A.-C.; Drăgășanu, L.I. Helicopter Inside Cabin Acoustic Evaluation: A Case Study—IAR PUMA 330. *Int. J. Environ. Res. Public. Health* 2021, 18, 9716. <https://doi.org/10.3390/ijerph18189716>.
- [158] Ragni, D.; Avallone, F.; van der Velden, W.C.P.; Casalino, D. Measurements of near-wall pressure fluctuations for trailing-edge serrations and slits. *Exp. Fluids* 2018, 60, 6. <https://doi.org/10.1007/s00348-018-2654-5> (accessed on 21 Iulie 2025).
- [159] Chaitanya, P.; Joseph, P. Slitted leading edge profiles for the reduction of turbulence-aerofoil interaction noise. *J. Acoust. Soc. Am.* 2018, 143, 3494–3504. <https://doi.org/10.1121/1.5040972>.
- [160] Singh, S.M.; Garg, M.; Narayanan, S.; Ayton, L.J.; Paruchuri, C.C. On the Reductions of Airfoil Broadband Noise through Sinusoidal Trailing-Edge Serrations. *J. Aerosp. Eng.* 2022, 35, 04022003. [https://doi.org/10.1061/\(asce\)as.1943-5525.0001386](https://doi.org/10.1061/(asce)as.1943-5525.0001386).
- [161] Cao, H.; Zhang, M.; Zhang, Y.; Zhou, T. A general model for trailing edge serrations simulation on wind turbine airfoils. *Theor. Appl. Mech. Lett.* 2021, 11, 100284. <https://doi.org/10.1016/j.taml.2021.100284> (accessed on 18 Iulie 2025).
- [162] Xue, W.; Jia, S.; Wang, H.; Chen, Z.; Yang, B. An Experimental Study of Noise Reduction in Wind Turbine Airfoils with Serrated Trailing Edges. 2025. disponibil online: <https://arxiv.org/pdf/2307.12188> (accessed on 18 Iulie 2025).
- [163] Pereira, L.T.L.; Avallone, F.; Ragni, D.; Scarano, F. A parametric study of serration design for trailing-edge broadband noise reduction. *Appl. Acoust.* 2023, 211, 109470. <https://doi.org/10.1016/j.apacoust.2023.109470> (accessed on 21 Iulie 2025).
- [164] Chong, T.P.; Dubois, E. Optimization of the poro-serrated trailing edges for airfoil broadband noise reduction. *J. Acoust. Soc. Am.* 2016, 140, 1361–1373. <https://doi.org/10.1121/1.4961362> (accessed on 21 Iulie 2025).
- [165] Mayer, Y.D.; Lyu, B.; Jawahar, H.K.; Azarpeyvand, M. A semi-analytical noise prediction model for airfoils with serrated trailing edges. *Renew. Energy* 2019, 143, 679–691, ISSN 0960-1481. <https://doi.org/10.1016/j.renene.2019.04.132>. (accessed on 21 Iulie 2025).
- [166] Tian, C.; Liu, X.; Wang, L.; Li, Y.; Wu, Y. Analytical Solution and Analysis of Aerodynamic Noise Induced by the Turbulent Flow Interaction of a Plate with Double-Wavelength Bionic Serration Leading Edges. *Biomimetics* 2025, 10, 193. <https://doi.org/10.3390/biomimetics10040193>.
- [167] Lee, S. The Effect of Airfoil Shape on Trailing Edge Noise. *J. Theor. Comput. Acoustics*. 2018, 27, 1850020. <https://doi.org/10.1142/S2591728518500202>.
- [168] Chong, T.P.; Joseph, P.F. An experimental study of airfoil instability tonal noise with trailing edge serrations. *J. Sound. Vib.* 2013, 332, 6335–6358, ISSN 0022-460X. <https://doi.org/10.1016/j.jsv.2013.06.033> (accessed on 21 Iulie 2025).
- [169] Ayton, L.J.; Kim, J.W. An analytic solution for the noise generated by gust–aerofoil interaction for plates with serrated leading edges. *J. Fluid. Mech.* 2018, 853, 515–536. <https://doi.org/10.1017/jfm.2018.583>. disponibil online: <https://arxiv.org/pdf/1805.05118> (accessed on 21 Iulie 2025).
- [170] Schlegel, R.; King, R.; Mull, H. Helicopter rotor noise generation and propagation. In US Army Aviation Materiel Laboratories; US Army Garrisons: Fort Eustis, VA, USA, 1966. disponibil online: <https://apps.dtic.mil/sti/tr/pdf/AD0645884.pdf> (accessed on 21 Iulie 2025).
- [171] Stuckey, T.J.; Goddard, J.O. Investigation and prediction of helicopter rotor noise part I. Wessex whirl tower results. *J. Sound. Vib.* 1967, 5, 50–80.
- [172] Hua, J.; Mankbadi, R.R. Prediction and Control of Broadband Noise Associated with Advanced Air Mobility—A Review. *Appl. Sci.* 2024, 14, 8455. <https://doi.org/10.3390/app14188455>.

- [173] Greenberg, M.; Kushnir, U.; Frid, V. Innovative Regression Model for Frequency-Dependent Acoustic Source Strength in the Aquatic Environment: Bridging Scientific Insight and Practical Applications. *Sensors* 2025, 25, 1560. <https://doi.org/10.3390/s25051560>.
- [174] D.S.; Jumper, S.J.; Burley, C.L. Rotorcraft System Noise Prediction System (ROTONET), Aircraft Noise Prediction Theo-retical Manual, NASA Technical Memorandum 83199, Part 4. disponibil online: <https://ntrs.nasa.gov/api/citations/19950019972/downloads/19950019972.pdf> (accesed on 25 Iulie 2025).
- [175] Küçükosman, Y.C.; Christophe, J.; Schram, C. Trailing edge noise prediction based on wall pressure spectrum models for NACA0012 airfoil. *J. Wind. Eng. Ind. Aerodyn.* 2018, 175, 305–316. <https://doi.org/10.1016/j.jweia.2018.01.030>. (accesed on 21 Iulie 2025).
- [176] ISO 3745:2012; Acoustics—Determination of Sound Power Levels and Sound Energy Levels of Noise Sources Using Sound Pressure—Precision Methods for Anechoic Rooms and Hemi-Anechoic Rooms. ISO: Geneva, Switzerland, 2012. disponibil online: <https://www.iso.org/standard/45362.html> (accesed on 2 Iulie 2025).
- [177] Akiwate, Deepak & Parry, Anthony & Joseph, Phillip & Paruchuri, Chaitanya. (2021). On the balance between the tonal and broadband noise of uninstalled propellers. 10.2514/6.2021-2308.
- [178] Peeters B., Nusselder R., Overview of critical noise values in the European Region, M+P report revision 4, prepared for EPA Network Interest Group on Noise Abatement (IGNA) (2019). [https://epanet.eea.europa.eu/reports-letters/reports-and-letters/ig-noise\\_critical-noise-values-in-eu.pdf](https://epanet.eea.europa.eu/reports-letters/reports-and-letters/ig-noise_critical-noise-values-in-eu.pdf) (accesed on 25 August 2025)
- [179] Edouard Salze, A. Pereira, Christoph Brandstetter, Vincent Clair, Fernando Gea-Aguilera, et al.. Noise Reduction of Aero-Engines Using Innovative Stators With Leading Edge Features. 30th AIAA/CEAS Aeroacoustics Conference, Jun 2024, Rome, Italy. 10.2514/6.2024-3159
- [180] Du, H.; Jiang, H.; Yang, Z.; Xia, H.; Chen, S.; Wu, J. Experimental Investigation of the Effect of Bio-Inspired Wavy Leading-Edges on Aerodynamic Performance and Flow Topologies of the Airfoil. *Aerospace* 2024, 11, 194. <https://doi.org/10.3390/aerospace11030194>
- [181] Yaroslav Pochkin, Yuri Khaletskiy, Aircraft Fan Noise Reduction Technology Using Leaned Stator Blades, *Procedia Engineering*, Volume 106, 2015, Pages 368-376, ISSN 1877-7058, <https://doi.org/10.1016/j.proeng.2015.06.047> (accesed on 25 August 2025).
- [182] Wei, Z., Wang, S., Farris, S., Chennuri, N., Wang, N., Shinsato, S., Demir, K., Horii, M., & Gu, G. X. (2023, August 17). Nature-inspired three-dimensional surface serration topologies enable silent flight by suppressing airfoil-turbulence interaction noise. *arXiv.org*. <https://arxiv.org/abs/2308.08788> (accesed on 25 August 2025)
- [183] Moreau, S.; Roger, M. Turbomachinery Noise Review. *Int. J. Turbomach. Propuls. Power* 2024, 9, 11. <https://doi.org/10.3390/ijtp9010011>
- [184] Kholodov, P.; Moreau, S. Identification of Noise Sources in a Realistic Turbofan Rotor Using Large Eddy Simulation. *Acoustics* 2020, 2, 691-706. <https://doi.org/10.3390/acoustics2030037>
- [185] Cican, G.; Frigioescu, T.-F.; Crunteanu, D.-E.; Cristea, L. Micro Turbojet Engine Nozzle Ejector Impact on the Acoustic Emission, Thrust Force and Fuel Consumption Analysis. *Aerospace* 2023, 10, 162. <https://doi.org/10.3390/aerospace10020162>
- [186] Tongwei Lu, Chun Liu, Nengyin Wang, Chen Shao, Yong Li, Ultra-broadband acoustic metaliner for fan noise reduction, *International Journal of Mechanical Sciences*, Volume 293, 2025, 110173, ISSN 0020-7403, <https://doi.org/10.1016/j.ijmecsci.2025.110173> (accesed on 25 August 2025)
- [187] Andrea Cattanei, Fabio Mazzocut Zecchin, Alessandro Di Pasquali, Andrea Lazari, Effect of the uneven blade spacing on the noise an-noyance of axial-flow fans and side channel blowers, *Applied Acoustics*, Volume 177, 2021, 107924, ISSN 0003-682X, <https://doi.org/10.1016/j.apacoust.2021.107924> (accesed on 25 August 2025)
- [188] Wang, Y.; Zhao, K.; Lu, X.-Y.; Song, Y.-B.; Bennett, G.J. Bio-Inspired Aerodynamic Noise Control: A Bibliographic Review. *Appl. Sci.* 2019, 9, 2224. <https://doi.org/10.3390/app9112224>
- [189] Qiao, C.; Ye, X.; Wu, Y.; Li, C. Insight into the Impact of Blade Perforation on the Aerodynamics and Acoustics of a Two-Stage Varia-ble-Pitch Axial Fan. *Energies* 2025, 18, 1966. <https://doi.org/10.3390/en18081966>
- [190] Lahoz, M.; Nabhani, A.; Saemian, M.; Bergada, J.M. Wind Turbine Enhancement via Active Flow Control Implementation. *Appl. Sci.* 2024, 14, 11404. <https://doi.org/10.3390/app142311404>
- [191] Parra, H.G.; Ceron, H.D.; Gomez, W.; Gaona, E.E. Experimental Analysis of Bio-Inspired Vortex Generators on a Blade with S822 Airfoil. *Energies* 2023, 16, 4538. <https://doi.org/10.3390/en16124538>

- [192] Wang, J.; Nakata, T.; Liu, H. Development of Mixed Flow Fans with Bio-Inspired Grooves. *Biomimetics* 2019, 4, 72. <https://doi.org/10.3390/biomimetics4040072>
- [193] Juangphanich, Paht. Bio-inspired Design of a Turbine Stage. Purdue University Graduate School. Thesis, 2019. <https://doi.org/10.25394/PGS.10055423.v1> (accessed on 25 August 2025)
- [194] Tan, J., Dong, P., Gao, J., Wang, C. and Zhang, L. (2023). Coupling Bionic Design and Numerical Simulation of the Wavy Leading-Edge and Seagull Airfoil of Axial Flow Blade for Air-conditioner. *Journal of Applied Fluid Mechanics*, 16(7), 1316-1330. doi: 10.47176/jafm.16.07.1634 (accessed on 25 August 2025)
- [195] Jiaxin Rong, Hao Liu; Effects of owl-inspired leading-edge serrations on tandem wing aeroacoustics. *AIP Advances* 1 November 2022; 12 (11): 115103. <https://doi.org/10.1063/5.0128543> (accessed on 25 August 2025)
- [196] Lei Wang, Xiaomin Liu, Liming Wu, Dian Li, Effect of the asymmetric bio-inspired trailing-edge serrations on sound suppression in a coupled owl-based airfoil, *Applied Acoustics*, Volume 191, 2022, 108667, ISSN 0003-682X, <https://doi.org/10.1016/j.apacoust.2022.108667>.(accessed on 25 August 2025)
- [197] Xing, Y.; Chen, W.; Wang, X.; Tong, F.; Qiao, W. Effect of Wavy Leading Edges on Airfoil Trailing-Edge Bluntness Noise. *Aerospace* 2023, 10, 353. <https://doi.org/10.3390/aerospace10040353>
- [198] Li, J.; Liu, C.; Li, X. Effects of Wavy Leading-Edge Protuberance on Hydrofoil Performance and Its Flow Mechanism. *J. Mar. Sci. Eng.* 2021, 9, 1138. <https://doi.org/10.3390/jmse9101138>
- [199] Wang, D.; Cai, C.; Zha, R.; Peng, C.; Feng, X.; Liang, P.; Meng, K.; Kou, J.; Maeda, T.; Li, Q. Impact of Leading-Edge Tubercles on Airfoil Aerodynamic Performance and Flow Patterns at Different Reynolds Numbers. *Energies* 2024, 17, 5518. <https://doi.org/10.3390/en17215518>
- [200] Pal A, Ghoshal R. Acoustic radiation characteristics of shark skin inspired surface modified plates. *Sci Rep.* 2024 Oct 9;14(1):23639. doi: 10.1038/s41598-024-72489-7. <https://pmc.ncbi.nlm.nih.gov/articles/PMC11464837> (accessed on 25 August 2025).
- [201] Cheng, M.; Zhu, Z.; Wu, B.; Ye, L.; Song, K. Simulation and Experimental Study of the Suppression of Low-Frequency Flow Noise Signals by a Placoid-Scale Skin. *Appl. Sci.* 2024, 14, 3855. <https://doi.org/10.3390/app14093855>
- [202] Lloyd, C. J., Peakall, J., Burns, A. D., Keevil, G. M., Dorrell, R. M., Wignall, P. B., & Fletcher, T. M. (2021). Hydrodynamic efficiency in sharks: the combined role of riblets and denticles. *Bioinspiration & Biomimetics*, 16(4), 046008. <https://doi.org/10.1088/1748-3190/abf3b1> (accessed on 25 August 2025).
- [203] Powerful owl. (n.d.). Adaptations in the Grampians. <https://biology-adaptations-telkington.weebly.com/powerful-owl.html> (accessed on 25 August 2025).
- [204] Arrondeau, B.; Rana, Z.A. Computational Aerodynamics Analysis of Non-Symmetric Multi-Element Wing in Ground Effect with Humpback Whale Flipper Tubercles. *Fluids* 2020, 5, 247. <https://doi.org/10.3390/fluids5040247>
- [205] Day, L. (2023, August 31). Sharkskin coating reduces airliner fuel use, emissions. *Hackaday*. <https://hackaday.com/2023/08/23/sharkskin-coating-reduces-airliner-fuel-use-emissions/> (accessed on 25 August 2025).
- [206] Vathylakis, Alexandros, Reduction of broadband trailing edge noise by serrations, Brunel University London, Doctoral Thesis, <https://bura.brunel.ac.uk/handle/2438/11554> (accessed on 25 August 2025).
- [207] Thompson, C., Biler, H., Symon, S., & Ganapathisubramani, B. (2023). Effects of integral length scale variations on the stall characteristics of a wing at high free-stream turbulence conditions. *Journal of Fluid Mechanics*, 974, A9. doi:10.1017/jfm.2023.789 (accessed on 25 August 2025).
- [208] Sivakumar, Aravind & Porteous, Ric & Mimani, Akhilesh & Doolan, Con. (2015). AN EXPERIMENTAL INVESTIGATION OF TURBULENT BOUNDARY- LAYER INTERACTION WITH DIFFERENT SERRATED TRAILING-EDGE CONFIGURATIONS. *ACOUSTICS 2015*, Annual Conference of the Australian Acoustical Society, Australia
- [209] Tian, H., & Lyu, B. (2024). The impact of non-frozen turbulence on the modelling of the noise from serrated trailing edges. *Journal of Fluid Mechanics*, 990, A4. doi:10.1017/jfm.2024.495 (accessed on 25 August 2025).
- [210] Stephane Moreau, Georgios Bampanis, Michel Roger. Analytical and experimental investigation of leading-edge noise reduction on a flat plate with serrations. *AIAA AVIATION 2020 FORUM*, AIAA, Jun 2020, VIRTUAL EVENT, United States. DOI:10.2514/6.2020-2542, <https://hal.science/hal-04929001v1> (accessed on 25 August 2025).

- [211] Huang, X. A theoretical study of serrated leading edges in aerofoil and vortical gust interaction noise. *Adv. Aerodyn.* 1, 6 (2019). <https://doi.org/10.1186/s42774-019-0010-y> (accessed on 25 August 2025).
- [212] Kaya, M.N.; Satcunanathan, S.; Meinke, M.; Schröder, W. Leading-Edge Noise Mitigation on a Rod–Airfoil Configuration Using Regular and Irregular Leading-Edge Serrations. *Appl. Sci.* 2025, 15, 7822. <https://doi.org/10.3390/app15147822>
- [213] Oluseyi O. Ajayi, Logan Unser, Joseph O. Ojo, Implicit rule for the application of the 2-parameters RANS turbulence models to solve flow problems around wind turbine rotor profiles, *Cleaner Engineering and Technology*, Volume 13, 2023, 100609, ISSN 2666-7908, <https://doi.org/10.1016/j.clet.2023.100609> (accessed on 25 August 2025).
- [214] Intizar Ali, Tanweer Hussain, Imran Nazir Unar, Laveet Kumar, Inam Ul Ahad, Turbulence model study for aerodynamic analysis of the leading edge tubercle wing for low Reynolds number flows, *Heliyon*, Volume 10, Issue 11, 2024, e32148, ISSN 2405-8440, <https://doi.org/10.1016/j.heliyon.2024.e32148> (accessed on 25 August 2025).
- [215] Muhammed, M.; Virk, M.S. On the Fidelity of RANS-Based Turbulence Models in Modeling the Laminar Separation Bubble and Ice-Induced Separation Bubble at Low Reynolds Numbers on Unmanned Aerial Vehicle Airfoil. *Drones* 2024, 8, 148. <https://doi.org/10.3390/drones8040148>
- [216] Amiet, R. K. “Noise Due to Turbulence–Airfoil Interaction.” NASA Technical Report (1975). <https://ntrs.nasa.gov/api/citations/19780024880/downloads/19780024880.pdf>
- [217] Tyler, J. M., and T. G. Sofrin. “Axial Flow Compressor Noise Studies.” SAE Transactions (1962). [https://ae.metu.edu.tr/~ae548/ref\\_papers/Axial\\_Flow\\_Compressor\\_Noise\\_Studies.pdf](https://ae.metu.edu.tr/~ae548/ref_papers/Axial_Flow_Compressor_Noise_Studies.pdf)
- [218] Ayton, L. J., and J. W. Kim. “An Analytic Solution for Gust–Airfoil Interaction with Serrated Leading Edges.” arXiv preprint arXiv:1805.05118 (2018). <https://arxiv.org/abs/1805.05118>
- [219] Lyu, B., L. J. Ayton, and P. Chaitanya. “On the Acoustic Optimality of Leading-Edge Serration Profiles.” *Journal of Sound and Vibration* (2019). Author OA PDF: [https://eprints.soton.ac.uk/433818/1/1\\_s2.0\\_S0022460X19304857\\_main.pdf](https://eprints.soton.ac.uk/433818/1/1_s2.0_S0022460X19304857_main.pdf)
- [220] Mayer, Y. D., B. Zang, and M. Azarpeyvand. “On the Effects of Leading-Edge Serrations on Aeroacoustic Properties during Stall.” University of Bristol Report (2019). [https://research-information.bris.ac.uk/files/209220556/Full\\_text\\_PDF\\_final\\_published\\_version.pdf](https://research-information.bris.ac.uk/files/209220556/Full_text_PDF_final_published_version.pdf)
- [221] Al-Okbi, Y., et al. “Noise Reduction Using Leading-Edge Serrations with Blowing.” *Applied Sciences* 11, no. 6 (2021): 2593. <https://doi.org/10.3390/app11062593>
- [222] Totu, A.-G.; Crunțeanu, D.-E.; Drăgășanu, L.; Cican, G.; Leventiu, C. SPL-Based Modeling of Serrated Airfoil Noise via Functional Regression and Ensemble Learning. *Computation* 2025, 13, 203. <https://doi.org/10.3390/computation13090203>
- [223] Totu, A.-G.; Crunțeanu, D.-E.; Deaconu, M.; Cican, G.; Cristea, L.; Leventiu, C. Application of Passive Serration Technologies for Aero-Engine Noise Control in Turbulent Inflow Environments. *Technologies* 2025, 13, 363. <https://doi.org/10.3390/technologies13080363>
- [224] Merino-Martínez, R., S. Luesutthiviboon, R. Zamponi, et al. “Assessment of the Accuracy of Microphone Array Methods for Aeroacoustic Measurements.” *JSV* 470 (2020): 115176. [https://research.tudelft.nl/files/71596148/1\\_s2.0\\_S0022460X20300079\\_main\\_1.pdf](https://research.tudelft.nl/files/71596148/1_s2.0_S0022460X20300079_main_1.pdf)
- [225] Sijtsma, P. “High-Resolution CLEAN-SC: Theory and Experimental Validation.” *International Journal of Aeroacoustics* 16, no. 4–5 (2017): 274–298. <https://research.tudelft.nl/files/23308367/1475472X17713034.pdf>
- [226] Brooks, T. F., and W. M. Humphreys Jr. “A Deconvolution Approach for the Mapping of Acoustic Sources (DAMAS) Determined from Phased Microphone Arrays.” AIAA/CEAS Aeroacoustics Conference (2004). <https://ntrs.nasa.gov/api/citations/20050209957/downloads/20050209957.pdf>
- [227] VanDercreek, C., R. Merino-Martínez, M. Snellen, D. Ragni, and D. G. Simons. “Comparison of Cavity Geometries for a Microphone Array in an Open-Jet Wind-Tunnel Experiment.” Berlin Beamforming Conference (BeBeC-2020). <https://www.bebec.eu/fileadmin/bebec/downloads/bebec-2020/papers/BeBeC-2020-D07.pdf>
- [228] Casagrande Hirono, F., P. F. Joseph, and F. M. Fazi. “An Open-Source Implementation of Analytical Turbulence–Airfoil Interaction Noise Model.” AIAA Aviation Forum (2020). [https://eprints.soton.ac.uk/441573/1/Hirono\\_Joseph\\_Fazi\\_Open\\_Source\\_Implementation\\_of\\_Airfoil\\_Noise.pdf](https://eprints.soton.ac.uk/441573/1/Hirono_Joseph_Fazi_Open_Source_Implementation_of_Airfoil_Noise.pdf)
- [229] Merino-Martínez, R. Microphone Arrays for Imaging of Aerospace Noise Sources. PhD thesis, Delft University of Technology, 2018. [https://research.tudelft.nl/files/47465472/PhD\\_Thesis\\_RobertoMerinoMart](https://research.tudelft.nl/files/47465472/PhD_Thesis_RobertoMerinoMart)

